NASA Technical Paper 2737

June 1987

New Methods and Results for Quantification of Lightning-Aircraft Electrodynamics

Felix L. Pitts,
Larry D. Lee,
Rodney A. Perala, and
Terence H. Rudolph

NASA

NASA Technical Paper 2737

1987

New Methods and Results for Quantification of Lightning-Aircraft Electrodynamics

Felix L. Pitts
Langley Research Center
Hampton, Virginia

Larry D. Lee
Old Dominion University
Norfolk, Virginia

Rodney A. Perala and
Terence H. Rudolph
Electro Magnetic Applications, Inc.
Lakewood, Colorado

National Aeronautics
and Space Administration

**Scientific and Technical
Information Office**

Contents

Abstract

The NASA F-106 has acquired considerable data on the rates of change of electromagnetic parameters on the aircraft surface during over 700 direct lightning strikes while penetrating thunderstorms at altitudes from 15 000 to 40 000 ft (4570 to 12 190 m). These in situ measurements have provided the basis for the first statistical quantification of the lightning electromagnetic threat to aircraft appropriate for determining indirect lightning effects on aircraft. The data are presently being used in updating previous lightning criteria and standards developed over the years from ground-based measurements. The proposed lightning standards will be the first which reflect actual aircraft responses measured at flight altitudes. Nonparametric maximum likelihood estimates of the distribution of the peak electromagnetic rates of change for consideration in the new standards are obtained based on peak recorder data for flights which have multiple strikes. The linear and nonlinear modeling techniques developed provide means to interpret and understand the direct-strike electromagnetic data acquired on the F-106. The reasonable results obtained with the models, compared with measured responses, provide increased confidence that the models may be credibly applied to other aircraft types and used in the prediction of internal coupling effects in the design of lightning protection for new aircraft.

Introduction

The advent and projected application of composite structures with flight-critical digital electronics compound lightning problems in advanced civil and military aircraft. The application of these technologies motivates the need to quantify the lightning-generated environment affecting such aircraft since composite structures do not provide shielding equivalent to that of metal aircraft, and digital systems are potentially more susceptible to "upset" by electrical transients than previous analog electronic systems. The term upset refers to the propensity for digital electronic systems to malfunction as a result of electronic transients which cause no permanent damage to the electronic hardware. Upsets which significantly affect system functional performance cannot be tolerated in flight-critical applications. In order to achieve the full performance potential of advanced transports or the mission potential of advanced military aircraft employing flight-critical digital controls and composite structures, credible design and assessment techniques are required which optimally address the design of protection against lightning damage and upset.

The in-flight direct-strike lightning electromagnetic threat criteria presently used for aircraft have evolved over a number of years and have generally been inferred from ground-based measurements of lightning strikes to instrumented towers. Protection of present generation metallic transport aircraft against potential catastrophic effects of lightning through use of these criteria has been satisfactory, with only nuisance outages of electronic subsystems reported in 87 of 783 strikes (ref. 1). Application of composite structures, coupled with the more sensitive digital electronic subsystems, will increase the vulnerability of the total system function to electrical transients. The design and assessment techniques for future aircraft should be based on a realistic, statistically significant definition of the lightning threat concerning its potential to generate interfering electrical transients.

The NASA Langley Research Center has conducted direct-strike lightning characterization research using a specially instrumented F-106 aircraft since 1980. During these tests, the F-106 has acquired direct-strike lightning data on over 700 strikes at altitudes between 15 000 and 40 000 ft (4570 to 12 190 m). The research has emphasized the rates of change associated with the lightning external interaction with the aircraft; this emphasis was motivated by the technical community's interest in indirect effects. The acquired electromagnetic data include the rate of change of current to the nose boom; the rates of change of electric and magnetic flux density at a number of locations on the aircraft; currents to the nose boom and vertical fin cap; and induced voltages recorded on a few internal wires. A photograph showing the sensor locations on the F-106 aircraft used in the Langley direct-strike lightning research is shown in figure 1.

This paper includes a brief summary of the direct-strike data and acquisition, a description of lightning-aircraft interaction mathematical modeling along with some typical modeling results, a discussion of in-flight strike phenomenology, and the development of the statistical method used to estimate the peak rates of change of currents and fields. The paper closes with a discussion of the impact of the F-106 data on lightning test criteria and a discussion of the relationship of the data to existing criteria.

The numerical analysis presented consists of both linear and nonlinear finite-difference modeling. The analysis was performed to determine the lightning environment (ambient electric field, lightning current, channel properties, etc.) associated with each lightning strike to the F-106. Linear modeling makes several simplifying assumptions about the lightning-aircraft interaction to derive lightning currents. The

nonlinear model allows the lightning-aircraft interaction to be examined in more detail, but at the expense of far greater complexity in the model. Although the numerical models described herein deal with metallic aircraft only, they can be extended to composite structures. The effect of a composite is to redistribute lightning currents at later times (generally >1 μs after the beginning of an event) and to allow electromagnetic energy to diffuse through the aircraft skin. Therefore, models of aircraft having composite materials must be altered to account for these phenomena for simulations extending beyond the initial stage of a lightning event. Details of the models and results are presented in a subsequent section.

A statistical method is proposed for estimating the distributions $H(x)$ of peak rates of change of currents and fields on the basis of data provided by the F-106 peak recording instruments. Peak recorder data consist of pairs (z_i, w_i) for $i = 1, 2, ..., n$, where w_i is the largest of the individual peak readings generated by z_i strikes during the ith flight. Since the individually generated peak readings are not observable (because there is generally more than one strike on a given flight), inference concerning the form of $H(x)$ must be made on the basis of a model which links (z_i, w_i) $(i = 1, 2, ..., n)$ to $H(x)$. The classic way to deal with maxima of random variables is to consider the three possible limit laws of extreme-value theory (refs. 2 and 3), attempt to determine which of the laws is applicable to the data, and then perform estimation in a parametric setting. This method, however, requires that the number of observations contributing to the maxima be quite large and introduces the difficulty of discriminating between the three possible models. Herein a nonparametric approach is developed in which a likelihood function is derived from the assumption that the individually generated peak rates of change are statistically independent and have a common distribution. This is the first known attempt to estimate a general form of underlying distribution based on the observation of only the maxima of random variables. A computationally feasible form of the estimating equations is obtained and asymptotic properties $(n \rightarrow \infty)$ of the maximum likelihood estimators are established. Details concerning the model, the method, and its application to the peak recorder data are presented in a later section.

The goal of this research has been to study the lightning threat by establishing a credible lightning-aircraft interaction data base, obtained in situ during direct-strike flight tests, and by developing models of lightning-aircraft interaction based on the actual strike data obtained. This research has provided the first statistically significant data base on the peak rates of change of currents and fields on an aircraft when struck by lightning. The peak rates of change of currents on aircraft struck by lightning are about two times those of previously accepted airworthiness criteria. Since there are at present no criteria on the rate of change of electric flux density, the new data can be used as the basis for new criteria on the electric characteristics of lightning-aircraft electrodynamics. The findings are at present being included in new criteria concerning protection of aircraft electrical and electronic systems against lightning. The new lightning-aircraft interaction modeling techniques, developed to understand and interpret the direct-strike measurements, can provide the basis for prediction of lightning-aircraft electrodynamics of generic aircraft types.

Symbols

$a_0, a_1, ..., a_k$	grouping limits for the observed largest peak rates ($k + 1$ is the number of grouping intervals)
$\mathbf{B}$	matrix with elements defined by $B_{rs}(\theta) = \partial\psi_s/\partial\theta_r$ $(r, s = 1, 2, ..., k)$
B-dot	time derivative of magnetic flux density
CFC	carbon fiber composite
$\mathbf{D}$	diagonal matrix with the reciprocal of the diagonal elements being the variances of the limiting distribution of $n^{1/2}(\hat{\boldsymbol{\psi}} - \boldsymbol{\psi}_o)$
D-dot	time derivative of electric displacement
d	thickness
$\mathbf{E}$	electric intensity
$E(\ )$	mathematical expectation
E_b	air breakdown field strength
E_{mag}	electric field magnitude
E_r	electric field radial component
E_{rel}	relative electric field intensity
E_s	surface electric field (tangential to surface)
$f_i(v\|z, \theta)$	joint density of $\mathbf{V}_i$ conditional on $Z_i = z$
G	avalanche rate
H	magnetic field

$H(x)$	cumulative distribution function of individually generated peak rates of change of currents and fields
$\hat{H}(x)$	maximum likelihood estimator of $H(x)$
$h(x)$	density function of $H(x)$
I	electric current
I-dot	time derivative of electric current
I_1	transmission line current
I_s	current source
I_t	vertical fin cap current
$\mathbf{J}$	matrix $(J_{rs}(\psi))$ of second derivatives of the negative of the log likelihood function
J_s	surface current density
k	propagation constant
L	inductance
n	number of flights of the F-106 airplane
n_+	positive ion density
n_-	negative ion density
n_e	electron density
P	percent water vapor
$p_i(z)$	probability that $Z_i = z$
Q	ambient ionization rate
Q_m	maximum charge an aircraft may hold
q	electric charge
R	resistance; response function
R_m	measured response function
r	radial distance coordinate
r_{trig}	radial distance at which aircraft lightning triggering occurs
T	transfer function
$\mathbf{V}_i$	vector $\left(V_{1i}, V_{2i}, ..., V_{(k+1)i}\right)$ of indicator variables defined by $V_{ji} = 1$ if $a_{j-1} \leq W_i < a_j$ and $V_{ji} = 0$ otherwise $(j = 1, 2, ..., k+1)$
V_s	voltage source
$\mathbf{v}_s$	drift velocity of species s
V_1	transmission line voltage
W_i	random variable which represents the largest peak rate generated during the ith flight
Z_i	random variable which represents the number of strikes to the F-106 during the ith flight
Z_t	transfer impedance
Z_0	characteristic impedance
$Z_1,\ Z_2$	termination impedances
α_e	electron attachment rate
β	electron-ion recombination coefficient
δ	negative-positive ion recombination coefficient
ε_o	permittivity of free space
η	intrinsic impedance
$\boldsymbol{\theta}$	parameters vector $(\theta_1,\ \theta_2, ...,\ \theta_{k+1})$
$\hat{\boldsymbol{\theta}}$	maximum likelihood estimator of $\boldsymbol{\theta}$
θ_j	$= H(a_j) - H(a_{j-1})(j = 1, 2, ..., k)$
$\boldsymbol{\Lambda}^{-1}$	covariance matrix of the limiting distribution of $n^{1/2}(\hat{\boldsymbol{\theta}} - \boldsymbol{\theta}_o)$
λ	electric charge per unit length
μ_e	electron mobility
μ_i	ion mobility
μ_s	mobility of species s
ρ_r	relative air density
σ	electrical conductivity
ϕ	$= \prod_{i=1}^{n} f_i(\mathbf{v}_i \mid z_i, \boldsymbol{\theta})$
$\boldsymbol{\psi}$	parameters vector $(\psi_1,\ \psi_2, ...,\ \psi_k)$ defined by $\theta_1 + \theta_2 + ... + \theta_j = \exp\left(-\sum_{l=j}^{k} \psi_l\right)$ for $j = 1, 2, ..., k$
$\hat{\boldsymbol{\psi}}$	maximum likelihood estimator of $\boldsymbol{\psi}$
$\boldsymbol{\psi}_o$	true value of $\boldsymbol{\psi}$
ω	angular frequency

Capital letters refer to random variables and lower-case letters refer to the realizations of these variables.

Direct-Strike Data Summary

The measurements made on the F-106 are electromagnetic parameters at the aircraft surface and induced voltages on a few internal wires. Several electromagnetic parameters have been studied: current and rate of change of current in the nose boom; current in the vertical fin cap; rate of change of electric flux density under the forward fuselage, at the base of the vertical fin, and under the outboard section of each wing; and rate of change of magnetic flux density on opposing sides of the aft fuselage and under each wing at about midspan. The lightning measurements and design of the F-106 experiment are described in detail in references 4 and 5, and the instrumentation is described in reference 6. The sensors, which are generally based on designs developed for nuclear electromagnetic pulse measurements, are described in reference 7.

The data are recorded in a shielded, self-contained instrumentation package which is mounted in the aircraft weapons bay. Power for the instrumentation is obtained from a motor generator set which decouples any lightning-induced transients in the aircraft power system to guard against spurious instrumentation system response. The electromagnetic sensors are electrically connected to the instrumentation package with foam-filled heliax cable. Control and diagnostics for the instrumentation are accomplished through the use of fiber-optic data links.

The direct-strike lightning process may last about 1 s and consists of a complex interaction of extremely fast electromagnetic pulses with the aircraft structure (refs. 8 to 10). Three basic recording techniques have evolved during the research as appropriate and complementary for investigating in-flight direct-strike lightning. The instruments used in these techniques are continuous analog recorders, digital transient recorders, and peak recorders. The continuous analog recorders yield temporal information on the overall lightning process; they do not, however, have sufficient bandwidth to record the fast pulses with suitable fidelity. The digital transient recorders have a sufficiently wide bandwidth but can record only during a small interval of the lightning event, and thus they yield information only on typical pulses which exceed their trigger threshold. The peak recorders supplement both the analog and digital transient recorders by obtaining information on the maximum parameter value attained during a strike.

The continuous analog recorders have a nominal bandwidth of 400 Hz to 100 kHz and, for current sensors with dc response, have been frequency-division multiplexed with subcarrier oscillators to obtain dc response to record the continuing current during strikes. The digital transient recorders, which have a Nyquist bandwidth of dc to 100 MHz when operating at the maximum selectable rate of one data sample every 5 ns, are central to the data acquisition system for obtaining time domain information appropriate for development of lightning interaction models. These recorders have 12 channels with 65 536 8-bit words each, yielding a data window of 327 μs at the maximum sample rate and have replaced the 2-channel, 131 072 6-bit word units used during the first several years of the research (ref. 11). The peak recorders sort the maximum voltage attained by the sensor connected to its input during a flight and are specified for operation over a bandwidth equivalent to half sine wave pulses with baseline widths between 5 ns and 10 μs.

Approximately 2500 individual time domain waveforms have been obtained from the various sensors during the strikes, and 130 peak recorder readings have been obtained during about 400 of the strikes. The maximum value recorded to date on the peak recorder monitoring the rate of change of the nose boom current is 380 kA/μs; the largest rate of change of electric flux density under the forward fuselage has exceeded the full-scale range of 97 A/m^2; and the largest peak vertical fin cap current recorded is 54 kA.

Figures 2 to 6 show examples of the types of time domain waveforms that have been recorded. These waveforms illustrate the overall lightning process, the triggering time of the transient recorder, and some of the wide-bandwidth transient recorder data. Figure 2 shows the current for three different strikes flowing in the tip of the vertical fin cap. The strikes were recorded from a current sensor with dc response on a frequency-division multiplexed analog recording system, which also had a dc response. Note the unipolar dc continuing current on the order of 80 A lasting 0.3 s or so with a number of pulses superimposed on it. As mentioned previously, the recording channel upper frequency response limit of 400 Hz does not allow sufficient fidelity to determine the peak values of the individual pulses, and thus the channel provides information useful only for studying the overall character and temporal nature of the lightning currents.

Figure 3 shows the temporal character of a typical lightning strike obtained from a number of different sensors recorded with a continuous analog recorder with a bandwidth of 400 Hz to 100 kHz. (The fin cap current was also recorded with a dc-to-400-Hz bandwidth channel.) This figure shows pulses from a light sensor which are concurrent with pulses from other sensors measuring the lightning external interaction with the aircraft. (The pulsing nature of

the light from lightning attached to the aircraft has also been noted in data from cockpit-mounted video cameras.)

Figure 4 shows details of the fin cap current of figure 3 recorded at a 40-ns sample interval with a digital transient recorder at the time of the transient recorder trigger. The trigger time is shown as the discrete event at the bottom trace of figure 3. The current in figure 4 has a high repetition rate, with about 50 μs between the two 12-kA pulses.

Figures 5 and 6 are typical simultaneous digital transient recorder waveforms (recorded at a 10-ns sample interval) of rates of change of electric and magnetic flux density from sensors located under the forward fuselage and on the side of the aft fuselage.

A multitude of time domain waveforms have been published which include all the transients recorded through the 1984 tests for 627 strikes (refs. 12 to 16). Photographs of lightning attachments taken from onboard motion picture cameras during 156 strikes in 1982 are in reference 17. Strike conditions, attachment photographs, and lightning patterns on the aircraft structure are discussed in reference 18. An overview of the acquired data including selected waveforms is given in reference 19.

Modeling and Phenomenology of Lightning Strikes to Aircraft

Lightning-Aircraft Interaction Modeling

In order to understand the lightning data collected from the F-106 thunderstorm penetrations and to extend that understanding to the lightning environment, it is necessary to model the lightning-aircraft interaction. Several distinct models have been developed in the course of this investigation. These include both nonlinear models for analyzing the physics of a lightning event and linear models (ref. 19) which can analyze the interaction in a simplified, or engineering, sense. All these models are based on the finite-difference methodology first developed by Yee (ref. 20).

In this section, the methodology of the finite-difference modeling is discussed briefly, followed by specific descriptions of the linear and nonlinear modeling techniques and selected results from these models. Comparisons with measured flight data are included.

Three-Dimensional Finite-Difference Modeling

The main analytical tool used in the analysis of the lightning-aircraft interaction is the computer code T3DFD, which stands for time domain 3-dimensional finite-difference code (ref. 21). The code solves Maxwell's equations in three dimensions and is capable of modeling complex geometries, space- and time-varying permittivity, permeability, and conductivity. It has been enhanced with an air chemistry model to allow the calculation of air conductivities which occur in the vicinity of large electric fields.

The particular problem space used in the F-106 program is a Cartesian mesh enclosing a space approximately twice the size of the aircraft itself. The spatial resolution is 1 m in the direction along the fuselage and 0.5 m in the wing-wing and vertical directions. The temporal resolution of the model is 1 ns. The nominal frequency resolution of the mesh, if we assume a minimum of five cells per wavelength, is therefore 60 MHz. The F-106 is placed within the problem space with all electric fields tangential to the surface set at zero at all times. Hence, the aircraft is assumed to be perfectly conductive, with no significant apertures which would alter the external response. This is a good approximation except for the immediate vicinity of the cockpit.

The F-106 as it appears in the finite-difference code is shown in figure 7. The coordinate system is also indicated, as are the locations of the external sensors which are modeled. One thing to notice about figure 7 is the blocky nature of the F-106 model. The large-scale structure of the aircraft is well resolved, but it is clear that details, such as the nose boom, are not resolved. This can cause difficulty when field distributions around such points are desired. In most cases, however, the model as shown is adequate to predict the response of the sensor system to a given lightning event. This is because the sensors have been placed away from those portions of the plane that are not well resolved by the finite-difference code.

Nonlinear Modeling

The development of a lightning strike to an aircraft certainly involves nonlinear processes. In particular, the initiation of a triggered lightning event by an aircraft immersed in a high electric field must include the development of a corona and associated conductivity around the aircraft, which is a function of the surrounding electric field. In order to correctly predict nonlinear aircraft responses to triggered lightning, any nonlinear model must be able to adequately model the corona growth.

The model described herein for an electrical corona solves for the air conductivity. It does this by calculating the densities of positive ions, negative

ions, and electrons as a function of space and time through the use of detailed balancing. Physical processes included are electron avalanching, electron attachment to neutral molecules to form negative ions, electron-positive ion recombination, and negative-positive ion recombination.

The air conductivity for the model is a nonlinear function of the electric field magnitude and can be written as

$$\sigma = q\left(n_e \mu_e + \left(n_+ + n_-\right)\mu_i\right) \tag{1}$$

Here, q is the electric charge, n_e is the free electron density, n_- is the negative ion density, n_+ is the positive ion density, μ_e is electron mobility, and μ_i is the ion mobility.

The electron and ion densities are calculated from a rate equation for each species:

$$\frac{\partial n_e}{\partial t} + \nabla \cdot (n_e \mathbf{v}_e) + [\beta n_+ + \alpha_e - G]\, n_e = \frac{\partial Q(t)}{\partial t} \tag{2}$$

$$\frac{\partial n_-}{\partial t} + \nabla \cdot (n_- \mathbf{v}_-) + \delta n_+ n_- = \alpha_e n_e \tag{3}$$

$$\frac{\partial n_+}{\partial t} + \nabla \cdot (n_+ \mathbf{v}+) + \beta n_e n_+ + \delta n_- n_+ = \frac{\partial Q(t)}{\partial t} + G n_e \tag{4}$$

where $\frac{\partial Q(t)}{\partial t}$ is the ambient ionization rate, α_e is the electron attachment rate, β is the electron-ion recombination coefficient, and δ is the negative-positive ion recombination coefficient. The velocity $\mathbf{v}_s$ of each species s is determined from the mobility μ_s and the electric intensity $\mathbf{E}$: $\mathbf{v}_s = \mu_s \mathbf{E}$. The actual rates used in the model are analytical fits to experimental data and are given in appendix A.

The closure of the rate equations for each species with the mobility equation for the velocities is a step which ultimately limits the model to low-temperature phenomena. Ideally, the set of equations should be supplemented by momentum and energy conservation equations and closed by an appropriate equation of state. This would allow the model to follow the development of a lightning event for a much longer time.

The integration of the nonlinear corona model with T3DFD is accomplished through the use of the $\sigma\mathbf{E}$ term in Maxwell's equations (refs. 22 to 25). The T3DFD code provides an electric field magnitude at each point in space; from the magnitude the air chemistry model calculates a conductivity which is then fed back into Maxwell's equations through the $\sigma\mathbf{E}$ term. The air chemistry equations are also solved with a finite-difference method, although somewhat differently than Maxwell's equations are solved. Maxwell's equations are central differenced in time and space for maximum stability. The air chemistry equations, because of their nonlinear character, cannot be efficiently central differenced and therefore one-sided differencing is used. Numerical tests with varying space and time steps have shown that for these equations, one-sided differencing is sufficiently accurate and does not affect overall stability of the model.

One of the uses of the calculated responses from the parameter study is for comparison with measured responses. If one can find an element of the parameter study that matches the measured data for a particular lightning event, then there is reasonable confidence that the ambient environment responsible for the event was similar to that of the parameter study element. Because of the nonlinear character of the parameter study, no scaling of calculated response amplitudes can be done, which implies that comparisons can be done in a general sense only, without detailed matching of amplitudes. The comparisons presented in this section were chosen mostly on the basis of waveform comparison without regard to amplitude, although in some cases the amplitudes also match quite closely. Examples of comparisons are shown in figures 8 to 11.

Of particular interest in the comparisons is the double pulse character shown in figures 8, 9, and 11. This double pulse corresponds to an air breakdown at two different places on the F-106 at separate times. The first breakdown raised the electric field at the second location enough to cause a breakdown there also. This type of comparison is strong evidence that the triggered lightning events on the F-106 are well modeled by the nonlinear air breakdown model.

Linear Modeling

Nonlinear lightning modeling, although more physically complete than linear methods, is costly and time-consuming. It is therefore quite useful to develop linear modeling techniques which allow one to investigate certain aspects of the lightning event without resorting to the complexity of a nonlinear model. One such technique is the use of transfer functions to determine the lightning current which caused a given set of measured electromagnetic responses on the F-106 aircraft. The transfer function is a functional relationship in the frequency domain between a source function and a response function. The use of a transfer function requires that the system under consideration be linear. This requirement is satisfied by a linear finite-difference code, but of course it is not satisfied by a real lightning-aircraft system. The justification for using the transfer function technique is that the nonlinearity in the real system is confined

mostly to the lightning channel itself. The electromagnetic responses on the aircraft are often approximately linear functions of the lightning current which flows onto the aircraft at the lightning attachment point. That is, although the formation of the lightning channel, its evolution, and the lightning current are complicated nonlinear functions of geometry and initial conditions, the aircraft responses usually depend, in a linear fashion, only on the current at the attachment point.

There are a number of assumptions which must be made when the transfer function technique is used. These assumptions are discussed individually below.

1. Lightning attachment points must be known. These attachment points constitute part of the initial conditions and as such are necessary to define the problem. In addition, the attachment points cannot change with time because time-dependent geometry is not presently allowed in the code. Also, if there are multiple channel attachments, only one of these can act as a source while the others just drain charge from the aircraft. Although having more than one source does not violate linear constraints, the problem no longer has a unique solution if more than one source is involved.

2. Relative formation times of multiple channels must be known. Because it is likely that exit channels for lightning currents form later than entry channels, it is necessary to know their formation times. In a sense, these channels which appear during the course of a problem constitute boundary conditions which change with time. This does not violate the linearity requirement as long as the formation times are fixed and do not vary with the time evolution of the problem.

3. Lightning channel geometry should be known. Although less important than the first two requirements, it is desirable to know the orientation of the lightning channel with respect to the aircraft. This geometry also constitutes boundary conditions which can affect aircraft responses to some extent. The responses are affected because electromagnetic radiation from current in the channel also produces some response on the aircraft, in addition to the current which flows onto the aircraft. The contribution of the current is much larger, however, so the channel radiation can be considered as a perturbation.

4. Lightning channel impedance should be known. Again, this is less important than the first two requirements, but it can affect the linear relationship between source and response somewhat. The reason for this is that the back effect of the aircraft on the lightning current is different depending on the channel impedance. For example, a channel with infinite impedance is completely unaffected by the presence of the aircraft. In this case, whatever current is flowing in the channel is the current which is transferred onto the aircraft, and reflections and responses on the aircraft behave as if the channel were nonexistent. For any other impedance, the response of the aircraft can affect the current in the channel, especially for lower impedances. The lower impedance slightly alters the electromagnetic responses of the aircraft. Hence, it is desirable to know the channel impedance as a boundary condition of the problem. It is possible to handle a time-varying impedance, as long as the variation is specified in advance and does not depend on the evolution of the problem.

The transfer function technique can be used for either triggered or natural lightning. The distinction between the two types of lightning is that triggered lightning begins at the aircraft and moves away, whereas natural lightning begins away from the aircraft and moves toward it. Typical geometries for both of these cases are shown in figure 12. The case for natural lightning is shown in figure 12(a). A current channel having a specified impedance and velocity of propagation is attached to the nose of the F-106. The impedance and velocity of propagation are determined from the inductance per unit length and the capacitance per unit length of the channel, which are determined from the physical diameter of the channel. Therefore, in the linear model, all the electrical properties of the channel are determined from the size of the channel. The attachment to the nose depicted in figure 12 is simply an example of the point at which many lightning strikes attach to the F-106. The model allows attachment at any point on the aircraft and allows multiple channels as long as there is only one current source in the problem. The difference between figures 12(a) and 12(b) is in the location of the current source. For natural lightning, the current source propagates toward the aircraft and is located at the edge of the problem space, in order to model initiation and driving forces for a natural lightning strike removed from the aircraft. The current source in figure 12(b) is located near the point where the channel attaches to the F-106 in order to model the phenomenon of initiation at the surface of the aircraft with propagation outward.

The mathematics of the model are handled identically in the two cases. A transfer function is determined from the Fourier transforms of the current source and the response waveforms:

$$T(\omega) = R(\omega)/I(\omega) \tag{5}$$

where $T(\omega)$ is the transfer function in the frequency domain, $R(\omega)$ is the Fourier transform of the calculated response waveform, and $I(\omega)$ is the Fourier

transform of the current source waveform. Since the model is linear, $T(\omega)$ is source independent; that is, changing I changes R in such a way as to keep T the same.

To determine the current source necessary to produce a given measured response, the measured response waveform must be Fourier transformed. Then the transfer function for the particular sensor is used to calculate the Fourier transform of the current source necessary to produce the measured response with equation (6).

$$I(\omega) = R_m(\omega)/T(\omega) \tag{6}$$

The current is then transformed into the time domain where it can be used in the linear model as a check to ensure the measured response is reproduced.

The transfer function technique is most useful in the events for which multiple simultaneous sensor responses have been recorded. Several current sources can then be derived, one for each of the multiple responses. In principle, if the model geometry chosen is correct, all the current sources should be the same.

An example of results from the linear model is presented in figure 13. The model used is of a triggered lightning strike to the nose of the F-106 with an exit channel also forming at the tip of the vertical stabilizer. The transfer function used to derive the source current is that appropriate to the B-dot longitudinal sensor. Agreement between predicted and measured results for the other sensors is quite good, particularly for the left wing sensors.

Phenomenology of Lightning Strikes to Aircraft

The phenomenology of an aircraft encountering a lightning event is complex and involves several parameters. These parameters include aircraft size and shape, altitude, static charge, ambient electric fields in which the aircraft is immersed, location of charge centers, and particle environment.

In order to discuss this phenomenology, it is convenient to categorize aircraft-lightning interaction events into three types: natural lightning, triggered lightning, and hybrid lightning. It is our intent in this section to define these concepts and to describe the basic phenomenologies associated with each category.

Natural Lightning

Natural lightning occurs without the presence of the aircraft. The presence of the aircraft is only incidental to the occurrence of natural lightning and is not contributory. An aircraft is subjected to this environment when, by chance, it is in the path of a naturally occurring lightning strike.

This phenomenon is further described with the help of figure 14. Figure 14(a) shows a stepped leader propagating from a cloud toward the Earth, and the aircraft happens to be in its path. Because the approaching leader induces large electric fields on the aircraft, arcs develop on the aircraft extremities, and these arcs propagate toward the leader and make contact, as shown in figure 14(b). The leader may then continue from the aircraft toward the ground, as in figure 14(c), or another branch of the channel may propagate toward the ground, as in figure 14(d). In either case, the important observation is that the lightning channel would have existed without the aircraft, and the aircraft's presence did not significantly influence the path of the channel.

The same scenario would apply to a natural intracloud event. It is believed that the F-106 has encountered very few natural lightning events.

Aircraft-Triggered Lightning

The focus of this paper is on aircraft-triggered lightning because most of the strikes to the F-106 are triggered events. This assessment is based largely on the observations in reference 26 describing the analysis of 49 radar returns of the F-106 being struck by lightning. In every case, the data in reference 26 indicate the channel begins at the aircraft and travels away from it. (It was later found that most, but not all, strikes were triggered (ref. 27).) This evidence prompted the development and application of nonlinear plasma physics air breakdown modeling of the aircraft triggering previously described which yields results in good agreement with measured data.

Aircraft-triggered lightning occurs because of the presence of an aircraft and would not otherwise exist. It occurs because the aircraft is able to sufficiently enhance the local electric field to cause air breakdown. The largest enhancements occur at the sharp points or edges, particularly if those points and edges are oriented in the direction of the ambient field. An aircraft in flight, such as the F-106, has many sharp points (e.g., the nose) and sharp edges (e.g., the wings and tail) around which the fields will be enhanced if the aircraft is immersed in a static electric field. These locally enhanced fields (within 0.5 m or so from the aircraft) are likely to be at least 10 times larger than the ambient field. Hence, it is considerably more likely that initial air breakdown and formation of a lightning channel will occur in the presence of the F-106 than in its absence. The requirements for triggered lightning are simply stated as follows. The static electric field which the aircraft experiences must be large enough and oriented properly so that the locally enhanced fields

at the extremes of the aircraft exceed the local air breakdown value. The ambient field must also be large enough to form and propagate a channel once a breakdown region has been established. A net charge on the aircraft also contributes to the local fields and can either suppress or enhance the breakdown, which may significantly change the requirements for the occurrence of triggered lightning. Also, the net charge can change the location of initial air breakdown by altering the local field distribution around the aircraft. Finally, one may conclude that triggered lightning *will* occur, if the proper conditions are satisfied. Essentially, the local field somewhere on the aircraft must exceed the air breakdown values of approximately 1.5 MV/m at 20 000 ft and 3.0 MV/m at sea level. In addition, triggered lightning will occur at the lowest possible field level. Hence, all the initial electromagnetic transients should be similar in amplitude depending on the location on the aircraft at which the initial breakdown occurs. A more detailed look at the environment required for triggered lightning is presented in the next section.

Triggered lightning environment. In order to discuss the triggered lightning environment, a typical thunderstorm is used as an example (ref. 28). The static electrical characteristics of this thunderstorm are a 40-C charge centered at 10 km above ground, a −40-C charge centered at 5 km, and a 10-C charge centered at 2 km, as shown in figure 15. The model of figure 15 is simplified slightly if the charges are assumed to be point charges located in a vertical line. For these simplifications, the static electric field can be analytically calculated as a function of space.

The calculation assumes that the Earth is a perfect ground plane, so it can be replaced by image charges. The results of the calculations are shown in figures 16(a) to 16(c). These figures show contours of a constant electric field as a function of space. The vertical scale is altitude and the horizontal scale is radial distance from the (assumed) vertical line of charges. Figure 16(a) shows contours of the radial component of the field, figure 16(b) shows the vertical component of the field, and figure 16(c) shows the total field magnitude. It should be remembered that the contours shown on the figures were calculated with the assumption of point charges, so the fields shown are actually upper limits on the actual field. If one of the contours is inside an extended charge cloud, the actual field is likely to be somewhat smaller at that point than the contour indicates.

Figure 16(a) is the most meaningful for the purposes of investigating triggered lightning on the F-106. If the aircraft is always in essentially level flight, the horizontal component of the field will be enhanced the most.

The triggered lightning response of the F-106 has been successfully modeled by the nonlinear approach previously described. Appendix A gives the air chemistry coefficient formulas used in the nonlinear model. Inherent to this approach is the calculation of the static field enhancements about the aircraft as shown in appendix B. Electrostatic field calculations done on the F-106 show that fields along the axis of the aircraft fuselage are enhanced by about a factor of 10 at the nose. Wing-wing ambient fields are enhanced by about a factor of seven at each wing tip. Vertical ambient fields are enhanced by about a factor of three at the tip of the vertical stabilizer. Hence, for level flight, vertical ambient fields are much less important than radial fields, unless the vertical ambient field is several times larger than the radial field.

Another factor that must be considered is that the minimum air breakdown field is larger at lower altitudes because of the increased air density there. A field which causes triggered lightning at a high altitude ($\approx$10 km) may not do so at lower altitudes because of the greater air density. The dashed lines in figures 16(a) and 16(b) illustrate this effect. They are the locus of points in space at which an electric field of breakdown strength can be reached on the aircraft with proper orientation. We assume, of course, that the net aircraft charge is zero. For a nonzero charge, the dashed lines could extend farther away from the charge centers. They also indicate the regions inside which triggered lightning can occur for the F-106 in level flight. Note that the volumes are much larger at high altitude, extending to almost 2 km from the charge center for the radial field case. At the very low altitudes ($\approx$2 km) the trigger region is only a few hundred meters across. In fact, because the charges are really extended and not point sources, it is possible that at these low altitudes no triggering region exists at all.

The response of aircraft to triggered lightning. In order to interpret direct-strike data acquired with the F-106, it is of some interest to investigate in a simple way the expected response of the aircraft. That is, given that triggered lightning occurs, what type of measured surface D-dot and B-dot records can be expected?

To begin, consider the situation shown in figure 17. This situation corresponds to the F-106 flying directly toward a positive charge center. The aircraft is polarized oppositely from the ambient field, resulting in a field at the D-dot sensor point (underneath the nose), which points toward the fuselage.

Presumably this field grows slowly over several seconds as the aircraft flies into a slowly increasing ambient field. This slow growth is far below the trigger level for the derivative sensors on the aircraft. For this geometry, the largest enhanced fields are at the nose of the aircraft, and eventually the enhanced field there becomes large enough to cause a corona. At that time electrons flow off the nose causing the field at the D-dot sensor location to become less negative. This happens very quickly and probably triggers the onboard instrumentation. As the air breaks down at the front of the F-106, the electric field increases at the aft end, possibly causing another breakdown there. That event is dependent on the characteristics of the breakdown at the nose. The corona at the nose effectively increases the length of the F-106 and therefore enhances the local field at the rear of the aircraft. Therefore, a large corona at the nose is more likely to cause a breakdown behind the aircraft.

Figure 17 also shows the expected behavior of the fields and their time derivatives at the D-dot forward and B-dot longitudinal sensor positions. The plots are simplified and ignore any behavior caused by the resonances of the aircraft. Actual records could be expected to look like those in figure 17 only with respect to general features. The pulses seen there could be separated by several hundred nanoseconds or longer, depending on the growth of the corona at the nose. It is significant that both single pulses and double pulses, as shown in figure 17, are seen in the measured data.

An example from the measured data that illustrates this behavior is shown in figure 18. Presented therein are two D-dot and B-dot events separated by about 170 μs. The waveforms behave similarly to the simplified waveforms shown in figure 17.

The case in which the ambient field is reversed in direction is similar. This reversal would occur if the aircraft were flying away from a positive charge center or toward a negative charge center. If one assumes once again that the initial breakdown is at the nose and a possible second breakdown occurs at the aft end, the expected field behavior is inverted from the previous case. The actual situation is somewhat different for the two cases, however. In the case shown in figure 17, a negative corona forms around the nose because the front of the aircraft is negatively charged. In the other case, a positive corona forms there. It is well-known that a negative corona requires a higher electric field to form than a positive corona, so the details of the two cases can be expected to differ somewhat (ref. 29). Intuitively, it seems reasonable that the smaller field required to initiate a positive corona would result in a slower and smaller measured D-dot response as the corona expands outward from the aircraft. The negative corona results in a faster breakdown when the required higher field is finally reached. This appears to be characteristic of the measured data, in that initially positive D-dot records (near the F-106 nose) tend to be larger and to have more high-frequency content than initially negative records.

This very simple model illustrates the environment for triggered lightning in the vicinity of a typical thunderstorm. In the discussion so far, three complicating factors have been omitted. First, in a real thunderstorm, the charge centers are not points but exist in extended regions. They also may be clumped into several smaller charge centers, around which locally high electric fields may exist. Second, in most thunderstorms there is a shear in the vertical direction, so that the charge centers are not in a vertical line. This destroys the cylindrical symmetry. Third, other thunderclouds in the vicinity alter the field distribution around any given cloud.

Fields required for triggering the F-106 at high (8230 m) and low (3050 m) altitudes have been calculated in a parameter study for various aircraft orientations and values of net charge on the aircraft. Lightning triggering conditions are determined by first computing the static fields on the aircraft caused by the net charge. The fields on the aircraft caused by the static ambient thunderstorm fields can be added through linear superposition to the fields caused by the net charge. The trigger level is then the ambient thunderstorm field magnitude, which causes the total field on the aircraft to exceed the corona level at at least one location. The procedure is to place the F-106, with a net charge on its surface, in a uniform electric field through the use of linearly derived initial conditions. The magnitudes of the field and the charge are chosen so that an air breakdown of the same order of magnitude as that seen in the measured data occurs (i.e., calculated and measured D-dot and B-dot responses on the aircraft are of similar magnitude). The location of this breakdown varies depending on the orientation of the field and the sign of the charge, but it generally occurs in one of three places: the nose, one of the wing tips, or the tip of the vertical stabilizer. Occasionally two locations are involved, as a breakdown at one location raises the local field at another location enough to cause a breakdown at the second location also.

The results of the triggering field calculations are summarized in table 1. Along the upper row of the headings in table 1 is shown the orientation of the ambient electric field for each of the parameter study elements in that column. The orientations are along the principal coordinate axes of the aircraft—longitudinal, horizontal, and vertical. Both positive

and negative fields are considered, because a negative corona air breakdown is different than a positive corona air breakdown. The aircraft charge Q_m is computed to be 1.79 mC and is the value for which a corona would form on the aircraft by virtue of only its net charge. The Q_m is thus the maximum charge the aircraft can hold. In the leftmost column is the net charge which was placed on the aircraft for each orientation. Five charge values were used: no charge (0), $\pm 0.5Q_m$, and $\pm Q_m$.

The field magnitudes for a given charge and orientation are given in the columns of values. Note that, as expected, the field magnitudes are much less for the cases having a charge, because the charge produces virtually all the local fields necessary to produce air breakdown. A word of explanation is necessary as to why these cases require any ambient field at all. Because Q_m was chosen to be large enough to cause breakdown by itself, it would seem that any field is superfluous. But this is not always the case; for example, a positive Q_m charge on the aircraft in the absence of a field induces air breakdown at the nose. However, if even a small ambient field oriented nose to tail is present, the breakdown at the nose is suppressed. For that field orientation and that net charge, the field magnitude must be increased until breakdown occurs at some point other than the nose. An example of the calculated sensor outputs for one element of the parameter study is shown in figure 19. This includes the outputs A to D. A typical nonlinear current (output E) is shown in figure 20.

There are six outputs from each element of the parameter study. The first is the electric field magnitude necessary to cause air breakdown for a given charge on the aircraft and a given orientation of the field (table 1). The other five outputs are responses of the aircraft to the initial conditions. These are listed below:

Designation	Output
A	*D*-dot forward
B	*D*-dot tail
C	*D*-dot left wing
D	*B*-dot longitudinal
E	Current at suspected air breakdown point

The locations of outputs A to D are shown on the finite-difference block model of the F-106 in figure 7. The location of output E was chosen by estimating where breakdown would occur. The estimate was made by locating the place on the model at which the largest electric field existed. This was the point of initial corona formation, but in some cases not the point where the largest current flowed at later times. Therefore, output E was not always useful.

In addition to the principal angles of electric field orientation with respect to the F-106 described above, the parameter study has been extended to intermediate angles between those shown in table 1. This was done for the higher flight altitude only. The results are similar to those already presented and are therefore omitted.

The effects of aircraft size and shape on trigger conditions. The overall objective of the F-106 direct-strike research program is to determine lightning environments for any size or type of aircraft. By necessity, nonlinear analysis in this program has concentrated on the F-106 itself. The thunderstorm environment necessary for a direct strike may be different, however, for different types of aircraft. That is, for an identical thunderstorm environment, one aircraft may encounter a direct strike, while a second differently shaped or sized aircraft may not. For this reason, it is desirable to look at the environment more generally. In this section, five different aircraft are placed in a thunderstorm environment (i.e., ambient electric field, charge on the aircraft, particular altitude, etc.) and the conditions necessary to produce a triggered lightning strike are determined.

The five aircraft investigated are listed below:

1. Half-size F-106
2. Double-size F-106
3. Normal-size F-106 with delta wings replaced with more conventional straight wings
4. Normal-size C-130
5. Normal-size F-106

The half- and double-size F-106 aircraft models afford a size range from approximately 9 to 36 m. Dimensional drawings of the scaled aircraft are shown in figures 21(a) to 21(e). Although the field enhancements around these two aircraft are, of course, the same, the effect of a given net charge on the aircraft is much different. Also, the responses of electromagnetic sensors on these aircraft are different because of the significantly different resonance characteristics.

The F-106 with the straight wings is used to evaluate the effect of the delta wing on field enhancements, resonant response, and charge storage properties. These are all expected to be changed. In particular, charge storage could be significantly affected, because the presence of the large, flat delta

wings allows the F-106 to hold more charge before breakdown field strengths are achieved.

The C-130 is included as a nonfighter type of aircraft. It has more rounded contours, particularly at the nose, and is representative of the shapes found in large passenger aircraft. It should give an idea of the environment necessary to generate triggered strikes on that type of aircraft. The normal-size F-106 is included for comparison purposes and for determination of relationships with actual flight data.

For each aircraft, two different environments were used. In both environments the net charge on the aircraft was fixed at $-0.5Q_m$, where Q_m is the maximum charge which can be on the airplane without causing immediate corona formation. It should be kept in mind that Q_m is different for each aircraft. Two separate ambient field orientations were used, one with the field oriented from nose to tail and the other oriented from top to bottom. For consistency, all computations were done at a simulated altitude of 8230 m (relative air density of 0.5) and with a water vapor percentage of zero.

The results are summarized in table 2. The field values E_{mag} represent the minimum field necessary to produce a triggered strike on the given aircraft model for the given orientation and Q_m. The Q_m is listed in millicoulombs and E_{mag} is in kilovolts per meter.

Several noteworthy items are apparent from table 2. First, aircraft size is the dominant determining factor for Q_m. For aircraft with similar shapes, one would expect Q_m to scale as the square of a typical dimension, along with the surface area. This is shown to be true, as Q_m varies by a factor of approximately 16 for the factor of 4 difference between the half-size and the double-size F-106. Second, the effect of the delta wing is shown in the table. The magnitude of Q_m for the normal-size F-106 with a delta wing is 1.79 mC versus a value of 2.00 mC for the F-106 with a straight wing. This is a somewhat surprising result, as one would expect that the large surface area of the delta wing would allow it to hold a large amount of charge. However, the presence of the delta wing changes the static electrical characteristics of the aircraft considerably. Because of the delta wing at the rear of the aircraft, field enhancements are significantly larger around the nose. In fact, a nose-to-tail oriented field has an enhancement factor of 6.3 for the aircraft with a straight wing and 7.4 for the aircraft with the delta wing. The same type of phenomenon occurs for a given net charge. That is, the charge arranges itself on the delta wing aircraft in such a way that it takes less charge to bring about corona formation.

Of importance also in table 2 is the magnitude of the field required for a lightning strike on the C-130. For the nose-tail field orientation the field magnitude is appreciably larger than that required for the F-106 models, which can be attributed to the bluntness of the nose of the C-130. In actual practice, the triggering field may differ by even more. The reason for this is that the C-130 is quite accurately represented near the nose by the finite-difference model, so its maximum enhancement should be correct. However, the sharp nose boom on the F-106 is less accurately represented, so actual enhancements on the F-106 are likely to be larger than the model predicts.

Hybrid Lightning

In addition to natural and aircraft-triggered lightning, a third type of strike to an aircraft is possible which will be called a "hybrid" strike. In this case, a natural leader channel is positioned somewhere near the aircraft, but not near enough for the aircraft field distortion to alter the channel course. The lightning leader leaves behind it in the channel a certain charge per unit length which produces, to the lowest order, a static field around the channel. This static field, at the location of the aircraft, may be large enough to cause a triggered streamer from the aircraft. The streamer would then certainly propagate to the natural channel, becoming a branch of the natural strike. It is unclear whether a strike of this kind would be more characteristic of a natural strike or a triggered strike.

A simple calculation can be done to get some idea of how near the aircraft a natural strike must be to cause a hybrid strike. For simplicity, one may assume that the natural channel is vertical and has a uniform charge density per unit length. Because only the orders of magnitude are desired, it is also assumed that the situation is quasi-steady state. That is, changes in the field distribution around the channel occur slowly and the static solution is approximately correct. The electric field E_r around a channel charge per unit length λ, which is effectively infinitely long, is radially directed and is given by

$$E_r = \frac{\lambda}{2\pi\varepsilon_o r} \tag{7}$$

Choosing an enhancement factor for the aircraft of about 10, which is typical around the nose of the aircraft, one finds that triggering occurs at a distance

$$r_{\text{trig}} = \frac{\lambda}{2\pi\varepsilon_o(E_b/10)} \tag{8}$$

where E_b represents the air breakdown field strength. A typical value for λ, calculated for a channel

having a charge of 5 C over a 3-km distance, is 1.667 C/km. The value E_b varies with altitude; at sea level it is about 3.0 MV/m and at 8230 m it is about 1.5 MV/m. Substituting these numbers into the above equations gives triggering distances of approximately 100 m at sea level and 200 m at an 8230-m altitude, resulting in a significantly greater distance than the distance at which the presence of the aircraft can directly alter the course of a natural lightning channel. Hence this hybrid strike is much more probable than a natural strike. It may even be that the natural strike as defined here does not exist, in that all strikes involving a natural lightning channel occur according to the hybrid scenario.

It is possible that the hybrid process could account for some of the variability in the measured data on the F-106. The reasoning behind this is the following. The normal triggered lightning model, which has the aircraft flying into a slowly increasing ambient electric field, requires that the triggering occur at the lowest possible threshold field level and results in aircraft responses which are very similar in amplitude and structure, because the only really significant adjustable parameters are the orientation of the field with respect to the aircraft and the net charge on the aircraft. This smallest field level is the electric field strength at which air breakdown occurs for any fixed altitude. Above this level air breakdown will always occur. Because an aircraft's motion through cloud fields is slow compared with electrodynamic relaxation time scales and air breakdown time scales, air breakdown must always occur at this threshold field level. However, in the hybrid model the natural channel can appear at any distance from the aircraft in a relatively short time, so triggering may occur at field levels which are significantly above the minimum level, resulting in aircraft responses which have much wider variety in both amplitude and structure.

Given the conditions under which natural and triggered lightning strikes occur, it appears far more likely that most strikes to the F-106 are triggered. Triggered lightning is *certain* to occur under the proper conditions, while natural lightning is probabilistic even under ideal conditions.

Nonparametric Maximum Likelihood Estimation of the Distributions of Peak Rates

The magnitudes of the voltages and currents induced in aircraft systems by lightning are proportional to the rates of change of the lightning electromagnetic fields. Information concerning the probabilities of peak rates (changes in current, electromagnetic flux density, and other quantities) exceeding various limits is necessary to provide the basis for determining the susceptibility to lightning of electronic systems aboard advanced aircraft and to guide the design of protection measures for these systems. Therefore, early attention was directed toward estimating percentiles of the underlying distributions of peak rates based on acquired F-106 time domain waveforms (ref. 30). Since then new recording instruments, called peak detectors, have been added to the experimental setup to increase the range of sensitivity and to provide new information concerning worst-case strikes. Measurements from the peak detector give information in the form (z_i, w_i) for $i = 1, 2, ..., n$, where n is the number of flights and each w_i is the largest of the peak rates w_{i1}, $w_{i2}, ...,$ w_{iz} that occurs as the result of $Z_i = z$ strikes during the ith flight.

If peak rates are assumed to be statistically independent and to have a common cumulative distribution function (e.g., $H(x)$), then

$$P(W_i \leq x | z_i) = [H(x)]^{z_i} \quad (i = 1, 2, ..., n) \qquad (9)$$

Although the individual peak rates are not observable, equation (9) directly links (z, w) with the underlying distribution. Upon observing a single pair (z, w) it is known that z observations from $H(x)$ fall within the range $(0, w)$ and that one or more of these is exactly equal to w. To restate this in a slightly different way, the data (z_1, w_1), $(z_2, w_2), ..., (z_n, w_n)$ provide the same information as is given by a series of largest order statistics in n independent samples of varying sizes.

The work presented herein addresses the problem of estimating $H(x)$ for the case in which the form of $H(x)$ is assumed unknown. Standard statistical techniques, such as relative frequency estimates, are not applicable because the maxima are not identically distributed. The classic approach (ref. 2) to the problem assumes that all realizations of Z_i are quite large and concentrates attention on certain limiting forms of the extreme value distributions as a basis for inference. The more recent theory of concomitants of order statistics (ref. 3) considers estimation when the members within independent pairs are linked by a linear regression model. To our knowledge, there are no published accounts which allow a general form of the underlying distribution as well as small numbers of observations from the underlying distribution which contribute to the maxima.

In a subsequent section we present maximum likelihood estimates of the probabilities that peak rates occur within certain intervals. These estimates are derived from a likelihood function which is based on equation (9) and the data (z_i, w_i) for $i = 1, 2, ..., n$. We refer to such estimates as

nonparametric maximum likelihood estimates because they can be calculated without assuming a particular form of $H(x)$.

In addition to providing a nonparametric approach to the analysis of data from the peak detector, the estimates might be used to judge the adequacy of various parametric models. They also permit calculation of estimates of the probability an aircraft encounters strikes of different levels of severity when exposed to the lightning environment for various time intervals.

A Grouped Data Likelihood Function

The estimation method to be considered assumes (Z_i, W_i) for $i = 1, 2, ..., n$ are statistically independent pairs and their link with $H(x)$ is as described in equation (9). Because $P(W_i = 0 | Z_i = 0) = 1$, the joint density of (Z_1, W_1), $(Z_2, W_2), ..., (Z_n, W_n)$ is

$$\prod_S z_i [H(w_i)]^{z_i - 1} h(w_i) \prod_{i=1}^{n} p_i(z_i) \qquad (10)$$

where $S = \{i : z_i \geq 1\}$ and $p_i(z)$ for $i = 1, 2, ..., n$ are probability mass functions of $Z_1, Z_2, ..., Z_n$. Since our main interest is $H(x)$ and the second factor $\prod p_i(z_i)$ does not depend on $H(x)$, we can limit our attention to the first factor $\prod z_i [H(w_i)]^{z_i - 1} h(w_i)$, which is the conditional density of $W_1, W_2, ..., W_n$ given $z_1, z_2, ..., z_n$.

The main reason for conditioning is to perform an analysis without introducing unnecessary assumptions concerning the form of the densities $p_i(z)$ for $i = 1, 2, ..., n$. If a maximum likelihood estimator of $H(x)$ were calculated from the full density in equation (10), it would not differ from the maximum likelihood estimator if calculated only from the first factor. Thus the actual benefit of conditioning is that the sampling distribution of the maximum likelihood estimator depends on the observed $z_1, z_2, ..., z_n$ rather than on the unknown nuisance parameters of the densities $p_i(z)$ for $i = 1, 2, ..., n$.

To estimate $H(x)$, consider grouping the maxima in a series of intervals having endpoints $0 = a_0 < a_1 < ... < a_k < a_{k+1} = \infty$, all intervals being of equal length except for (a_k, ∞). Let $\theta_j = H(a_j) - H(a_{j-1})$ be the probability of peak rates occurring within (a_{j-1}, a_j) for $j = 1, 2, ..., k$. Observations that exceed the full-scale limit of the peak detector are easily accounted for by choosing a_k equal to this upper limit. The probability of peak rates exceeding a_k is $\theta_{k+1} = 1 - (\theta_1 + \theta_2 + ... + \theta_k)$.

Let $\mathbf{v}_i = \left(v_{1i}, v_{2i}, ..., v_{(k+1)i}\right)$ be a vector of indicator variables which define the interval in which w_i happens to fall, so that $v_{ji} = 1$ if $a_{j-1} \leq w_i < a_j$ and $v_{ji} = 0$ otherwise for $j = 1, 2, ..., k+1$ and $i = 1, 2, ..., n$. The joint density of $\mathbf{V}$ given z is

$$f_i(\mathbf{v}|z, \theta) = \left(\theta_1^z\right)^{v_{1i}} \left[(\theta_1 + \theta_2)^z - \theta_1^z\right]^{v_{2i}} ... \left[(\theta_1 + \theta_2 + ... + \theta_k)^z - (\theta_1 + \theta_2 + ... + \theta_{k-1})^z\right]^{v_{ki}} \left[1 - (\theta_1 + \theta_2 + ... + \theta_k)^z\right]^{v_{(k+1)i}} \qquad (11)$$

This density assigns mass to the $k + 1$ dimensional unit vectors (1,0,...,0), (0,1,0,...,0), ..., (0,0,...,0,1).

The conditional density of $\mathbf{V}_1$, $\mathbf{V}_2$, ..., $\mathbf{V}_n$, given $z_1, z_2, ..., z_n$, is

$$\phi = \prod_{i=1}^{n} f_i(\mathbf{v}_i | z_i, \boldsymbol{\theta}) \qquad (12)$$

The grouped data maximum likelihood estimator of $\boldsymbol{\theta} = (\theta_1, \theta_2, ..., \theta_k)$ is the statistic $\hat{\boldsymbol{\theta}} = (\hat{\theta}_1, \hat{\theta}_2, ..., \hat{\theta}_k)$ which maximizes equation (12). Calculation of $\hat{\boldsymbol{\theta}}$ is discussed in the next section.

Maximum Likelihood Estimation

Consider reparameterization of equation (12) in terms of $\boldsymbol{\psi} = (\psi_1, \psi_2, ..., \psi_k)$ defined by

$$\theta_1 + \theta_2 + ... + \theta_j = \exp\left(-\sum_{l=j}^{k} \psi_l\right) \quad (j = 1, 2, ..., k) \qquad (13)$$

Substituting in equation (12) gives

$$\ln\phi = \sum_{i=1}^{n} (-z_i) \sum_{j=1}^{k} \psi_j \sum_{q=1}^{j} v_{qi} + \sum_{i=1}^{n} \sum_{j=1}^{k} v_{(j+1)i} \ln\left[1 - \exp\left(-z_i \psi_j\right)\right] \qquad (14)$$

The maximum likelihood estimator of $\boldsymbol{\psi}$ is the solution to $\partial \ln\phi / \partial \psi_j = 0$ for $j = 1, 2, ..., k$. The estimating equations are

$$\sum_{i=1}^{n} z_i \sum_{q=1}^{j} v_{qi} = \sum_{i=1}^{n} z_i v_{(j+1)i} \left[\exp(z_i \psi_j) - 1\right]^{-1} \quad (j = 1, 2, ..., k) \qquad (15)$$

The main advantage of the reparameterization defined in equation (13) is that the $\hat{\psi}_j$ can be calculated by solution of equations in equation (15) individually. The solution $\hat{\boldsymbol{\psi}}$ together with the transformation in equation (13) gives the maximum likelihood estimator of $\boldsymbol{\theta} = (\theta_1, \theta_2, ..., \theta_k)$. The solutions

to equation (15) give estimates of the conditional probabilities

$$\exp(-\psi_l) = H(a_l)/H(a_{l+1}) \ (l = 1, 2, ..., k)$$

which can be combined to give the product estimator

$$\hat{H}(a_j) = \exp\left(-\sum_{l=j}^{k} \hat{\psi}_l\right) \ (j = 1, 2, ..., k) \qquad (16)$$

This estimate exists and is unique, providing each of the grouping intervals (a_{i-1}, a_i) for $i = 1, 2, ..., k+1$ contains at least one w_i. This is because the expressions in equation (15) are then positive and finite for $\psi_j > 0$ and are decreasing functions of ψ_j for $j = 1, 2, ..., k$. Under this same condition,

$$-\partial^2 \ln\phi/\partial\psi_r \, \partial\psi_s \begin{cases} = 0 \ (r \neq s) \\ = \sum_{i=1}^{n} z_i^2 v_{(r+1)i} \exp(z_i\psi_r) \\ \times [\exp(z_i\psi_r) - 1]^{-2} \ (r = s = 1, 2, ..., k) \end{cases} \qquad (17)$$

defines a k by k diagonal matrix which is positive definite; thus, ϕ is concave in ψ and the solution to equation (15) maximizes ϕ.

Asymptotic Properties

For the independent and nonidentically distributed case, reference 31 gives general conditions under which a maximum likelihood estimator is consistent and asymptotically normal. For the estimators of the previous section, the conditions I(i), I(ii), II(ii), II(iii), and III of reference 31 are easy to check under the following simpler assumptions:

A. There exists an upper limit, for example, c, so that $1 \leq z_i \leq c$ for $i = 1, 2, ...$ with probability equal to 1.

B. Each θ_j for $j = 1, 2, ..., k+1$ lies interior to (0,1).

C. $J_{rs}(\psi) = \lim n^{-1} \sum_{i=1}^{n} -E(\partial^2 \ln f_i/\partial\psi_r \partial\psi_s)$ exists as $n \to \infty$ and $\mathbf{J} = (J_{rs}(\psi))$ is positive definite. The use of $E(\ )$ refers to an expected value obtained with reference to the conditional distribution in equation (12).

Condition A probably holds because the number of strikes that can be recorded over any bounded time interval is physically limited. Condition B does not differ from what is required for asymptotic normality in the standard situation of grouping the observations of a random sample.

Although condition C can hold if $Z_1, Z_2, ..., Z_n$ are not identically distributed, this is the only case we attempt to discuss. The expressions on the right-hand side of condition C define a diagonal matrix, $\mathbf{D} = (D_{rs}(\psi))$ where

$$D_{rs}(\psi) \begin{cases} = 0 \ (r \neq s) \\ = n^{-1} \sum_{i=1}^{n} z_i^2 \exp\left(-z_i \sum_{l=r+1}^{k} \psi_l\right) \\ \times [\exp(z_i\psi_r) - 1]^{-1} \ (r = s) \end{cases} \qquad (18)$$

The diagonal elements can be written

$$n^{-1} \sum_{i=1}^{n} g_r(Z_i)$$

where

$$g_r(z) = z^2 \exp\left(-z \sum_{l=r+1}^{k} \psi_l\right) [\exp(z\psi_r) - 1]^{-1} (z \geq 1) \qquad (19)$$

From the law of large numbers, $n^{-1} \sum_{i=1}^{n} g_r(Z_i)$ for $r = 1, 2, ..., k$ each converge (with probability equal to 1) to their expectations which exist (by condition A) and are positive (by condition B). This proves that condition C holds if $Z_1, Z_2, ..., Z_n$ are identically distributed.

Theorem II(iv) of reference 31 states that $n^{1/2}(\hat{\boldsymbol{\psi}} - \boldsymbol{\psi}_o)$ has a limiting ($n \to \infty$) normal distribution with mean vector 0 and covariance matrix $\mathbf{D}^{-1}$ where $\mathbf{D} = (D_{rs}(\boldsymbol{\psi}_o))$ is evaluated at the true parameter vector $\boldsymbol{\psi}_o$. A standard application of the delta method theorem (ref. 32) gives that $n^{1/2}(\hat{\boldsymbol{\theta}} - \boldsymbol{\theta}_o)$ also has an approximate normal distribution with covariance matrix Λ^{-1}, where $\Lambda = \mathbf{BDB}^T$. The elements of $\mathbf{B}$ are $B_{rs}(\boldsymbol{\theta}) = \partial\psi_s/\partial\theta_r$ for r and $s = 1, 2, ..., k$, as determined from equation (13).

Analysis of F-106 Peak Detector Data

Tables 3 and 4 summarize the largest peak readings of electromagnetic flux density D-dot and current I-dot as obtained during the 1983 to 1985 flights of the F-106 aircraft. On 6 of the first 20 flights, maxima of peak D-dot measurements exceeded the full-scale limit (48.7 A/m^2) of the peak detector. This limit was increased to 97.1 A/m^2 and was then exceeded only three times in the remaining flights. Cases which exceed the full-scale limits are noted in table 3. The number of strikes per flight varies from 1 to 72, and the typical number is less than 10. The largest peak I-dot rate observed in 60 flights is 380 kA/μs.

One way to analyze these data is to consider estimates of $P(W \leq x|z)$ for $z = 1, 2, ...$ obtained by grouping the maxima generated by common numbers of strikes. This permits weaker assumptions than

equation (3), but it greatly expands the dimension of the parameter space in that one must then estimate a different distribution for each row of tables 3 and 4. Further, there are too few observations over much of the range of z to give meaningful estimates of $P(W \leq x|z)$ in this way.

Following the method outlined in previous sections, maximum likelihood estimates of $\theta_j = H(a_j) - H(a_{j-1})$ for $j = 1, 2, ..., k$ were obtained and are given in tables 5 and 6. Standard deviations of the estimators are also given in these tables.

The plots of these estimates in figure 22 are not histograms in the usual sense because it is not possible to determine the actual percentages of peak readings which have occurred in various ranges. These plots suggest highly skewed distributions with slowly tapering tail areas.

Because of this feature, moderate increases in threshold specifications over much of the upper tail range ways by which electromag-
off in terms of decreasing the probabilities of exceeding such specifications. The asymptotic results of the previous section give 3.7 ± 1.0 as approximate 95-percent confidence limits for the percentage of peak D-dot rates which exceed 48 A/m^2. Similarly, approximate 95-percent confidence limits for the percentage of peak I-dot rates which exceed 250 kA/μs are 0.7 ± 0.2. Actual confidence levels might differ from 95 percent, depending upon the rate of convergence ($n \rightarrow \infty$) of the estimators to the limiting normal distribution.

Impact on Airworthiness Criteria

Although the F-106 research program is of much scientific interest, the motivation and objective of the research relate to identification and definition of lightning hazards to aircraft. These hazards are generally thought of as being of two types. The first, direct effects, refers to physical damage such as pitting, burning, magnetic deformation, and destruction of dielectric materials such as radomes. The second, indirect effects, refers to the hazards caused by electromagnetic coupling such as transient voltages and currents induced on antennas and cables connecting various electronic boxes. Transients can cause damage or upset of flight- and mission-critical electronic systems. Because the F-106 data are primarily useful for indirect effects, the scope of the remainder of this discussion is limited to this topic. In order to understand the impact of the lightning research program on airworthiness criteria, it is first necessary to discuss how energy couples into electronic systems.

Internal Coupling of Lightning-Induced Electromagnetic Fields

Electromagnetic coupling is best discussed in two parts: external and internal coupling. External coupling refers to the generation of surface currents and charges (or tangential magnetic fields and normal electric fields) by a lightning event. Internal coupling refers to the generation of electromagnetic fields, currents, and voltages on elements of the aircraft interior.

Conceptually, the two parts can be solved independently, with the external coupling solution defining the sources which then drive the internal response. This gives a good approximation if the internal coupling does not significantly "feed back" and thus alter the external coupling results. This exception occurs in instances involving large apertures such as an open weapons bay or wheel wells, large windows, and nonconducting panels.

There are three basic
netic energy penetrates an aircraft interior: apertures, exposed conductors, and diffusion. Apertures refer to openings in the aircraft skin and include such items as the cockpit, wheel wells, engine exhaust, seams on doors and panels, and areas covered by dielectrics. Exposed conductors include antennas of various kinds, airspeed probes, and some electrical or control cables. Exposed items may receive excitation either by lightning directly attaching to them or from induced fields when lightning is attached elsewhere on the aircraft. Diffusion is usually important only for carbon fiber composite (CFC) materials. Diffusion describes the process by which a surface current $J_s(\omega)$ induces an internal tangential electric field $E_s(\omega)$ by means of the surface transfer impedance $Z_t(\omega)$ according to

$$E_s(\omega) = Z_t(\omega) J_s(\omega) \tag{20}$$

where

$$Z(\omega) = \frac{\eta(\omega)}{\sinh\, k(\omega) d}$$

and ω is the angular frequency, d is the material thickness, and $\eta(\omega)$ and $k(\omega)$ are respectively the intrinsic impedance and the propagation constant of the surface material (e.g., CFC). At "late" times (or, alternatively, low frequencies), equation (20) reduces to the resistive voltage drop along the surface.

It is useful to summarize the parameters which are important to lightning coupling through these penetrations. In order to do so, a simple model of a cable is employed and is shown in figure 23. The cable is approximated by a transmission line of characteristic impedance Z_0 and having termination loads on each

end of impedances Z_1 and Z_2 as shown. The electromagnetic coupling sources are approximated in this illustration as point sources which include a series voltage source V_s and a shunt current source I_s as shown. In the figure, the transmission line is indicated schematically by its equivalent circuit model.

The figure includes a table which lists the penetrations of interest and the lightning coupling variable upon which the source V_s or I_s linearly depends. For example, the source V_s for an open hole aperture is a constant time B-dot. Contained in parentheses is the source variable which relates to the lightning environment (I-dot in this example).

It should also be pointed out that the table does not, by itself, give the entire picture with respect to what is important for coupling. For example, if Z_1 and Z_2 are small or zero and the cable is short with respect to wavelengths in the lightning pulse (which is often the case), then for aperture coupling dominated by the B field the current I_1 is proportional to B (or I, because I_1 for this situation is simply proportional to the time integral of V_s). Therefore, even though V_s is proportional to I-dot, I_1 is proportional to I. On the other hand, if Z_1 and Z_2 are large, then V_1 relates to I-dot and not to I.

In addition, in some cases where the transient responses of the cable are related to I, then the total waveform of I is important. This also requires quantification of the energy delivered to a load, which places a requirement on the action integral (ref. 33)

$$\int_0^\infty I^2 \, dt$$

This would be particularly important for damage of electronics as well as upset. Therefore, even for aperture coupling, I-dot, I, D-dot, and the action integral are important. For diffusion, only I and the action integral are important.

Certain other knowledge of lightning environments is required for system considerations. For example, upset of a digital system is determined by the amplitude of a pulse, the pulse width, and the repetition rate of pulses. Therefore, specifications on these parameters are also of interest.

An example of a comparison of a calculation and a measurement on an internal wire based on the model of figure 23 is shown in figure 24. The wire is inside the F-106 fuselage and is 9 m long, shorted to the structure on one end and terminated in a 50-Ω resistance on the other end. The wire passes within 0.61 m of some closed wheel well doors whose seams were modeled in the analysis as inductive seams because of their observable large gaps. The model for calculating the wire response is identical to that given in figure 23. The gap transfer inductance used in the model for the wheel well door gaps was chosen to be 6.45 nH-m. The lightning nose current I is given in figure 25. By inspection, it is clear that the large oscillations dominating the current response are related to the derivative of I. This is reasonable, since the wire inductance is 1.5 μH and the L/R time constant with the 50-Ω load is only 30 ns, which is much shorter than the period of oscillation (≈250 ns) of the cable current. In this frequency regime, the current response is limited by the 50-Ω load impedance, which is a large impedance compared with the cable inductance. Therefore, the current (or voltage) would be proportional to I, which it clearly is.

Note that this is an example of an internal wire response caused by a lightning event of low peak current and low I-dot (≈20 kA/μs peak). Even so, it produces an internal current pulse having frequencies related to aircraft and cable resonances. Aircraft external transient responses due to lightning have spectra with resonance peaks nominally in the range of 1 to 50 MHz, which will excite internal responses close to clock frequencies of aircraft computers (ref. 8).

Impact on Testing

The main issues of interest in testing include I-dot, D-dot, the temporal durations of I-dot and D-dot, and the late time currents, which are important for diffusion through CFC structures. By "late" time current we mean times exceeding a diffusion time constant. For times shorter than this time constant, a composite behaves similarly to a metal. For later times, current redistribution and diffusion through the composite structure is observed. Approaches which have been used to increase both I-dot and D-dot capabilities of generators for aircraft testing include the use of discrete peaking capacitors (refs. 34 to 36), distributed peaking capacitors (ref. 37), high-voltage oil-filled low-inductance Marx generators (refs. 38 and 39), and the so-called shock excitation techniques (ref. 40). In order to increase late time currents, a crowbar switch is used to provide for an exponential decay of a Marx generator as opposed to the normal damped sinusoid (ref. 41). It is clear that there is no consensus yet on the best way to accomplish these types of tests.

The maximum F-106 peak recordings of current and current rate of change are shown in table 7 along with a summary of the recent past criteria and new criteria established in the joint Atmospheric Electricity Hazard Protection Program for Aircraft (AEHP) (ref. 42). (The AEHP is a multiagency program managed by Wright Aeronautical Laboratories to develop and demonstrate lightning protection technology for digital systems onboard composite

aircraft.) Note that the absolute largest F-106 current rise rate measurement of 380 kA/μs is considerably greater than the old or new criteria for current rate of change. The approximate 95-percent confidence limits for the percentage of peak I-dot rates which exceed 250 kA/μs are 0.7 ± 0.2, as shown in figure 22. Considering that criteria are usually established at about the 99th quantile, 200 kA/μs as used in the AEHP program is appropriate.

The impact of the new criteria on testing for I-dot, D-dot, and their temporal durations is not fully known, but some general observations can be made. In order to increase I-dot or D-dot and to lengthen their duration, either peaking capacitors with high-inductance Marx generators or with low-inductance oil-filled Marx generators should be used. A low-voltage capacitor bank can possibly also be used but the transmission line return conductor system must be carefully designed and must be very close to the aircraft under test (ref. 43). The relative expense of providing large values of these parameters increases greatly as the size of the test object increases. For example, testing a vehicle the size of a Boeing 747 at I-dot = 200 kA/μs is not within the state of the art, but this type of test can be done on a small fighter-size aircraft.

Concluding Remarks

This research effort has resulted in the first statistical quantification of the electromagnetic threat to aircraft based on in situ measurements. Previous estimates of the in-flight lightning hazard to aircraft were inferred from ground-based measurements. The electromagnetic measurements made on the F-106 aircraft during these strikes have established a statistical basis for determination of quantiles and "worst-case" amplitudes of electromagnetic parameters of rate of change of current and the rate of change of electric flux density. The 99.3 percentile of the peak rate of change of current on the F-106 aircraft struck by lightning is about two and a half times that of previously accepted airworthiness criteria. The findings are at present being included in new criteria concerning protection of aircraft electrical and electronic systems against lightning. Since there are at present no criteria on the rate of change of electric flux density, the new data can be used as the basis for new criteria on the electric characteristics of lightning-aircraft electrodynamics. In addition to there being no criteria on the rate of change of electric flux density, there are also no criteria on the temporal durations of this rate of change or rate of change of electric current exceeding a prescribed value. Results on pulse characteristics presented herein can provide the basis for this development. The newly proposed lightning criteria and standards are the first which reflect actual aircraft responses to lightning measured at flight altitudes.

The focus of the discussion on phenomenology and modeling of lightning strikes centers on triggered lightning, since most of the strikes to the F-106 are triggered events. In every case of 49 ultrahigh frequency radar observations of the F-106 being struck by lightning, the data indicate that the channel begins at the aircraft and travels away from it. This evidence prompted the development and application of nonlinear air breakdown modeling of the aircraft triggering which gives results in good agreement with measured data. (Subsequently it was found that most, but not all, of the F-106 strikes were triggered.) Given information on lightning attachment location, the injected current waveform, etc., the linear modeling technique developed provides results for sensor responses over the surface of the aircraft which are in excellent agreement with the measured data. This technique is appropriate as a first step in the complex problem of prediction of internal induced effects in arbitrary aircraft types.

The discussion on maximum likelihood estimation of the distribution of peak rates of current and electromagnetic flux density on the basis of the F-106 peak detector data is the first known attempt to estimate a general form of underlying distribution on the basis of observing only the maxima of random variables. The main thing that this analysis provides is estimates of the probabilities that peak rates occur in various ranges. These estimates suggest highly skewed distributions with slowly tapering tail areas, which are of much interest in evaluating the lightning threat to aircraft.

Finally, the research reported herein has contributed to basic scientific knowledge by establishing new methods and results quantifying the electromagnetic interaction of lightning with aircraft. It must be recognized, however, that these results were obtained at altitudes ranging from 15 000 ft (4570 m) to about 40 000 ft (12 190 m), where strikes are quite obtainable. Since lower altitude strikes are much more difficult to obtain, much work remains to quantify low-altitude lightning-aircraft electrodynamics.

NASA Langley Research Center
Hampton, Virginia 23665-5225
April 27, 1987

Appendix A

Air Chemistry Coefficient Formulas (Ref. 44)

Calculation of E_{rel}:

$$E_{rel} = \frac{E_{mag}}{\rho_r} \frac{1}{(1 + 2.457P^{0.834})} \left(\frac{E_{mag}}{\rho_r} < 0.07853\left(1 + 2.457P^{0.834}\right)\right) \quad \text{(A1)}$$

$$E_{rel} = \frac{E_{mag}}{\rho_r}\left(-1.195P^{0.834}\right) \left(\frac{E_{mag}}{\rho_r} > 3.015 + 1.195P^{0.834}\right) \quad \text{(A2)}$$

$$E_{rel} = \left\{\left[\frac{E_{mag'}}{\rho_r} + \left(\frac{0.6884P^{0.834}}{2}\right)^2\right]^{1/2} - \frac{0.688P^{0.834}}{2}\right\}^2 \left(\text{all other } \frac{E_{mag}}{\rho_r}\right) \quad \text{(A3)}$$

where P is the percent water vapor, ρ_r is the relative air density, and E_{mag} is in electrostatic units (ESU).

Calculation of electron attachment rate α_e:

$$\alpha_e = \frac{100 - P}{100}\left[\alpha_3(1 + 0.344P) + \alpha_2\right]$$

where

$$\alpha_2 = 1.22 \times 10^8 \rho_r \exp\left(-21.15/E_{rel}\right)$$

$$\alpha_3 = \rho_r^2\left(6.2 \times 10^7 + 8.0 \times 10^{10}E_{rel}^2\right) / \left\{1 + 10^3 E_{rel}^2\left[E_{rel}(1 + 0.03E_{rel}^2\right]^{1/3}\right\}$$

Calculation of avalanche rate G:

$$G = 5.7 \times 10^8 \rho_r Y^5/(1 + 0.3Y^{2.5})$$

where $Y = E_{rel}/100$.

Calculation of electron-ion recombination coefficient β and ion-ion neutralization coefficient δ:

$$\beta = 2 \times 10^{-13} + 2.8 \times 10^{-12}(P)^{1/3}\text{m}^3/\text{s}$$

$$\delta = 2 \times 10^{-13} + \rho_r 2.1 \times 10^{-12}\text{m}^3/\text{s}$$

Calculation of electron mobility μ_e:

$$\mu_e = \frac{100\mu_a}{100 - P + PR}$$

where

$$R = 1.55 + 210/(1 + 11.8E_{rel} + 7.2E_{rel}^2)(\text{m/s})/(\text{V/m})$$

and

$$\mu_a = \left\{[(16.8 + E_{rel})/(0.63 + 26.7E_{rel})]^{0.6}\right\}/3\rho_r$$

Calculation of ion mobility μ_i:

$$\mu_i = \frac{2.5 \times 10^{-4}}{\rho_r}(\text{m/s})/(\text{V/m})$$

Appendix B

Aircraft Enhancement Factors

One of the uses of modeling is to determine the enhancement factors of the metallic F-106 aircraft if it is placed in a static electric field or has a net charge on its surface. These enhancement factors can be defined as the ratio of the local electric field at any location on the aircraft to the ambient field magnitude in the absence of the aircraft. Of course, for the case of a net charge on the aircraft, the enhancement factor must be defined as the ratio of the local electric field to the net charge.

The importance of enhancement factors is that they determine the conditions under which triggered lightning can occur. The local electric field at any point on or near the aircraft must exceed the value necessary for air breakdown in order for this to happen. Therefore, the enhancement factors can be used to find the minimum ambient field for which triggering will occur at a given altitude.

The calculated enhancement factors at selected locations on the block model of the F-106 are shown in figure 26 for three directions of ambient electric field and a net positive charge on the plane. The fields in figure 26 are in volts per meter for an ambient field of 1 V/m or in volts per meter for a 1-μC net charge.

The calculated fields are not the largest fields that would be seen on the actual F-106. Because of the finite spatial resolution of the model, details such as the nose boom are impossible to resolve. Hence, the large fields around the tip of structures such as this are not seen in the model. However, these large fields exist only in a very small volume, and whether or not they are the controlling factor in triggering lightning is unknown. A large volume of smaller fields with a higher total energy may be necessary for triggering to occur.

References

1. Rasch, Nickolus O.; Glynn, Michael S.; and Plumer, J. Anderson: Lightning Interaction With Commercial Air Carrier Type Aircraft. *International Aerospace and Ground Conference on Lightning and Static Electricity, 1984—Technical Papers,* National Interagency Coordination Group, 1984, pp. 21-1–21-11.
2. Gumbel, E. J.: *Statistics of Extremes.* Columbia Univ. Press, 1958.
3. David, H. A.: *Order Statistics,* Second ed. John Wiley & Sons, Inc., 1981.
4. Pitts, F. L.; Thomas, M. E.; Campbell, R. E.; Thomas, R. M.; and Zaepfel, K. P.: Inflight Lightning Characteristics Measurement System. *Federal Aviation Administration—Florida Institute of Technology Workshop on Grounding and Lightning Technology,* Rep. No. FAA-RD-79-6, 1979, pp. 105–111.
5. Pitts, Felix L.: Electromagnetic Measurement of Lightning Strikes to Aircraft. *J. Aircr.*, vol. 19, no. 3, Mar. 1982, pp. 246–250. (Available as AIAA-81-0083R.)
6. Thomas, M. E.: Direct Strike Lightning Measurement System. AIAA-81-2513, Nov. 1981.
7. Trost, Thomas F.; and Zaepfel, Klaus P.: Broadband Electromagnetic Sensors for Aircraft Lightning Research. *Lightning Technology,* NASA CP-2128, FAA-RD-80-30, 1980, pp. 131–152.
8. Trost, Thomas F.; and Pitts, Felix L.: Analysis of Electromagnetic Fields on an F-106B Aircraft During Lightning Strikes. *Proceedings of the International Aerospace Conference on Lightning and Static Electricity,* Volume 1, Culham Lab. (Abingdon, Oxon, England), 1982, pp. B3-1–B3-11.
9. Rustan, P. L., Jr.; and Moreau, J. P.: Aircraft Lightning Attachment at Low Altitudes. *10th International Aerospace and Ground Conference on Lightning and Static Electricity,* Association Aéronautique et Astronautique de France, 1985, pp. 259–265.
10. Moreau, J. P.; and Alliot, J. C.: E and H Fields Measurements on the Transall C160 Aircraft During Lightning Flashes. *10th International Aerospace and Ground Conference on Lightning and Static Electricity,* Association Aéronautique et Astronautique de France, 1985, pp. 281–287.
11. Thomas, Robert M., Jr.: Expanded Interleaved Solid-State Memory for a Wide Bandwidth Transient Waveform Recorder. *Lightning Technology,* NASA CP-2128, FAA-RD-80-30, 1980, pp. 119–129.
12. Pitts, Felix L.; and Thomas, Mitchel E.: *1980 Direct Strike Lightning Data.* NASA TM-81946, 1981.
13. Pitts, Felix L.; and Thomas, Mitchel E.: *1981 Direct Strike Lightning Data.* NASA TM-83273, 1982.
14. Thomas, Mitchel E.; and Pitts, Felix L.: *1982 Direct Strike Lightning Data.* NASA TM-84626, 1983.
15. Thomas, Mitchel E.: *1983 Direct Strike Lightning Data.* NASA TM-86426, Parts 1 to 3, 1985.
16. Thomas, Mitchel E.; and Carney, Harold K.: *1984 Direct Strike Lightning Data.* NASA TM-87690, Parts 1 to 3, 1986.
17. Zaepfel, Klaus P.; Fisher, Bruce D.; and Ott, Merle S.: *Direct-Strike Lightning Photographs, Swept-Flash Attachment Patterns, and Flight Conditions for Storm Hazards '82.* NASA TM-86347, 1985.
18. Fisher, B. D.; Brown, P. W.; and Plumer, J. A.: Research in Lightning Swept-Stroke Attachment Patterns and Flight Conditions With the NASA F-106B Airplane. *10th International Aerospace and Ground Conference on Lightning and Static Electricity,* Association Aéronautique et Astronautique de France, 1985, pp. 267–280.
19. Pitts, Felix L.; Finelli, George B.; Perala, Rodney A.; and Rudolph, Terence H.: F-106 Data Summary and Model Results Relative to Threat Criteria and Protection Design Analysis. *1986 International Aerospace and Ground Conference on Lightning and Static Electricity,* AFWAL-TR-86-3098, U.S. Air Force, Oct. 1986, pp. 5-1–5-20.
20. Yee, Kane S.: Numerical Solution of Initial Boundary Value Problems Involving Maxwell's Equations in Isotropic Media. *IEEE Trans. Antennas & Propag.*, vol. AP-14, no. 3, May 1966, pp. 302–307.
21. Merewether, David E.; and Fisher, Robert: *Finite Difference Solution of Maxwell's Equation for EMP Applications.* DNA 5301F (Contract No. DNA 001-78-C-0231), Electro Magnetic Applications, Inc., Apr. 22, 1980.
22. Rudolph, Terence; and Perala, Rodney A.: *Interpretation Methodology and Analysis of In-Flight Lightning Data.* NASA CR-3590, 1982.
23. Rudolph, T. H.; and Perala, R. A.: *Linear and Nonlinear Interpretation of the Direct Strike Lightning Response of the NASA F106B Thunderstorm Research Aircraft.* NASA CR-3746, 1983.
24. Rudolph, Terence H.; Perala, Rodney A.; McKenna, Paul M.; and Parker, Steven L.: *Investigations Into the Triggered Lightning Response of the F106B Thunderstorm Research Aircraft.* NASA CR-3902, 1985.
25. Rudolph, Terence; Perala, Rodney A.; Easterbrook, Calvin C.; and Parker, Steven L.: *Development and Application of Linear and Nonlinear Methods for Interpretation of Lightning Strikes to In-Flight Aircraft.* NASA CR-3974, 1986.
26. Mazur, Vladislav; Fisher, Bruce D.; and Gerlach, John C.: Conditions Conducive to Lightning Striking an Aircraft in a Thunderstorm. *8th International Aerospace and Ground Conference on Lightning and Static Electricity,* DOT/FAA/CT-83/25, Federal Aviation Administration, June 1983, pp. 90-1–90-7.
27. Mazur, Vladislav; Fisher, Bruce D.; and Gerlach, John C.: Lightning Strikes to a NASA Airplane Penetrating Thunderstorms at Low Altitudes. *J. Aircr.*, vol. 23, no. 6, June 1986, pp. 499–505.
28. Uman, Martin A.: *Lightning.* McGraw-Hill Book Co., c.1969.
29. Kuffel, E.; and Zaengl, W. S.: *High Voltage Engineering—Fundamentals.* Pergamon Press Inc., c.1984.
30. Lee, Larry D.; Finelli, George B.; Thomas, Mitchel E.; and Pitts, Felix L.: *Statistical Analysis of Direct-Strike Lightning Data (1980 to 1982).* NASA TP-2252, 1984.

31. Bradley, Ralph A.; and Gart, John J.: The Asymptotic Properties of ML Estimators When Sampling From Associated Populations. *Biometrika,* vol. 49, 1962, pp. 205–214.
32. Bishop, Yvonne M. M.; Fienberg, Stephen E.; and Holland, Paul W.: *Discrete Multivariate Analysis: Theory and Practice.* MIT Press, c.1975.
33. Fisher, Franklin A.; and Plumer, J. Anderson: *Lightning Protection of Aircraft.* NASA RP-1008, 1977.
34. Robb, J. D.; and Perala, R. A.: Experimental and Theoretical Evaluation of a Fast-Risetime, High Current Lightning Indirect Effects Simulator. *Proceedings of the International Aerospace Conference on Lightning and Static Electricity,* Volume 1, Culham Lab. (Abingdon, Oxon, England), 1982, pp. D3-0–D3-7.
35. Robb, J. D.; and Perala, R. A.: Measurements and Theoretical Analysis of a Full Scale NEMP Type Lightning Simulator for Aerospace Vehicles. *8th International Aerospace and Ground Conference on Lightning and Static Electricity,* DOT/FAA/CT-83/25, Federal Aviation Administration, June 1983, pp. 75-1–75-12.
36. Hebert, J. L.; Walko, L. C.; and Schneider, J. G.: Design of a Fast Risetime Lightning Generator. *10th International Aerospace and Ground Conference on Lightning and Static Electricity,* Association Aéronautique et Astronautique de France, 1985, pp. 115–119.
37. Perala, R. A.; Rudolph, T. H.; McKenna, P. M.; and Robb, J. D.: The Use of a Distributed Peaking Capacitor and Marx Generator for Increasing Current Rise Rates and the Electric Field for Lightning Simulation. *International Aerospace and Ground Conference on Lightning and Static Electricity, 1984—Technical Papers,* National Interagency Coordination Group, 1984, pp. 45-1–45-6.
38. Harrison, John L.; Chen, Y. G.; Galicki, Ed; and Richardson, William: A Threat-Level Lightning Simulator. *1986 International Aerospace and Ground Conference on Lightning and Static Electricity,* AFWAL-TR-86-3098, U.S. Air Force, Oct. 1986, p. 7-1.
39. White, Robert A.: Lightning Simulator Circuit Parameters and Performance for Severe-Threat, High-Action-Integral Testing. *International Aerospace and Ground Conference on Lightning and Static Electricity, 1984—Technical Papers,* National Interagency Coordination Group, 1984, pp. 40-1–40-14.
40. Butters, W. G.; Clifford, D. W.; Murphy, K. P.; Zeisel, K. S.; and Kuhlman, B. P.: Assessment of Lightning Simulation Test Techniques. *Proceedings of the International Aerospace Conference on Lightning and Static Electricity,* Volume 1, Culham Lab. (Abingdon, Oxon, England), 1982, pp. D13-0–D13-10.
41. Perala, R. A.; McKenna, P. M.; Rudolph, T. H.; and Robb, J. D.: Implementation of a Crowbar Switch in a Marx Generator/Peaking Capacitor Lightning Simulator System. *10th International Aerospace and Ground Conference on Lightning and Static Electricity,* Association Aéronautique et Astronautique de France, 1985, pp. 121–125.
42. Melander, B. G.; and Cooley, W. W.: *Atmospheric Electricity Hazards Threat Environment Definition.* AFWAL-TR-85-3052, U.S. Air Force, Aug. 1985. (Available from DTIC as AD A159 739.)
43. Burrows, B. J. C.; Luther, C.; and Pownall, P.: Induced Voltages in Full Size Aircraft at 10^{11}A/S. *1977 IEEE International Symposium on Electromagnetic Compatibility,* 77CH 1231-0 EMC, Inst. Electrical and Electronics Engineers, Inc., c.1977, pp. 207–214.
44. Radasky, William A.: *An Examination of the Adequacy of the Three-Species Air Chemistry Treatment for the Prediction of Surface-Burst EMP.* DNA 3880T (Contract No. DNA 001-75-C-0094), Mission Research Corp., Dec. 1975.

Table 1. Comparison of High- and Low-Altitude F-106 Triggering Fields as a Function of Charge and Orientation

Aircraft charge	Magnitude[a], kV/m, for electric field orientation of —					
	Back to front	Front to back	Right to left	Left to right	Bottom to top	Top to bottom
0	190 (250)	190 (250)	280 (380)	280 (380)	470 (590)	470 (590)
$0.5Q_m$	107 (140)	200 (230)	200 (210)	200 (210)	300 (350)	600 (660)
$-0.5Q_m$	273 (230)	150 (160)	200 (210)	160 (210)	640 (660)	300 (350)
Q_m	24 (34)	50 (60)	20 (40)	20 (40)	80 (120)	80 (160)
$-Q_m$	24 (60)	15 (34)	20 (40)	20 (40)	80 (160)	80 (120)

[a]Low-altitude field magnitude is in parentheses.

Table 2. Trigger Conditions for Aircraft of Various Sizes and Shapes

Aircraft	Field orientation	Q_m, mC	E_{mag}, kV/m
Half-size F-106	Nose to tail	0.45	100
	Top to bottom	.45	250
Double-size F-106	Nose to tail	7.16	100
	Top to bottom	7.16	250
Normal-size F-106 with straight wing	Nose to tail	2.00	120
	Top to bottom	2.00	240
Normal-size C-130	Nose to tail	6.90	190
	Top to bottom	6.90	210
Normal-size F-106	Nose to tail	1.79	100
	Top to bottom	1.79	250

Table 3. Largest Peak Rates of Change of Electric Flux Density for 62 Flights of the F-106 Aircraft

Number of strikes	Largest peak rates, A/m^2
1	4.5, 9.9, 15, 15, 17, 17, 17, 18, 20, 27, 43, 47, [a]48
2	7, 9.7, 15, 23, 24, 26, 29, 33, 39
3	12, 24, 26, 28, 28, 31, 40, [a]48
4	13, 39
5	17, 26, 28, 28, 28, 40, 75
6	16, 17, 37, 40, 78, [a]97
7	30, 37, 42, 42, [a]97
8	27, 30, [a]48
9	44, [a]48
11	32
12	31
14	36
19	39
20	[a]48
40	[a]48
72	[a]97

[a]Certain peak rates exceeded the full-scale limit of the peak rate detector. Initially this limit was 48.7 A/m^2 and was later increased to 97.1 A/m^2.

Table 4. Largest Peak Rates of Change of Current for 60 Flights of the F-106 Aircraft

Number of strikes	Largest peak rates, kA/μs
1	1.90, 7.6, 9.6, 10, 20, 20, 42, 54, 78, 82, 96, 134, 136
2	7.6, 11.4, 24, 28, 34, 40, 84, 88
3	1.91, 1.91, 20, 78, 88, 300
4	7.6, 42
5	5.8, 11.4, 44, 48, 60, 68, 198
6	3.8, 15.2, 22, 50, 110, 162
7	5.8, 22, 30, 76, 98
8	86, 134, 240
9	194, 380
11	44
12	42
14	86
19	17.2
20	260
27	174
40	240
72	54

Table 5. Maximum Likelihood Estimates of the Probabilities That Peak Rates[a] of Electric Flux Density Occur Within Selected Ranges

Lower grouping limit, A/m^2	Number of flights	Number of strikes	Estimate	Standard deviation
0	1	1	0.098	0.057
6	3	5	.197	.068
12	10	27	.314	.063
18	4	8	.070	.016
24	13	47	.162	.027
30	6	43	.048	.008
36	9	66	.051	.007
42	5	25	.023	.003
48	11	177	.037	.005

[a]For example, maxima of peak rates are counted in the range of 6 to 12 if they are less than 12 A/m^2 and are greater than or equal to 6 A/m^2.

Table 6. Maximum Likelihood Estimates of the Probabilities That Peak Rates[a] of Current Occur Within Selected Ranges

Lower limit, kA/μs	Number of flights	Number of strikes	Estimate	Standard deviation
0	30	135	0.876	0.012
50	15	133	.079	.011
100	5	21	.017	.002
150	4	47	.013	.002
200	3	50	.008	.001
250	3	32	.007	.001

[a]For example, maxima of peak rates are counted in the range 50 to 100 if they are less than 100 kA/μs and are greater than or equal to 50 kA/μs.

Table 7. Comparison of F-106 Data With Existing Criteria

Criteria	Peak current, kA	Maximum rise rate, kA/μs
Old[a]:		
NASA JSC-07636	200	100
Military Standard B-5087	200	100
SAE-AE-4L	200	100
NASA F-106 finding	54	380
New (AEHP):		
Cloud-ground—		
Severe	200	200
Moderate	20	50
Cloud-cloud—		
Severe	20	200
Moderate	5	50

[a] See reference 42.

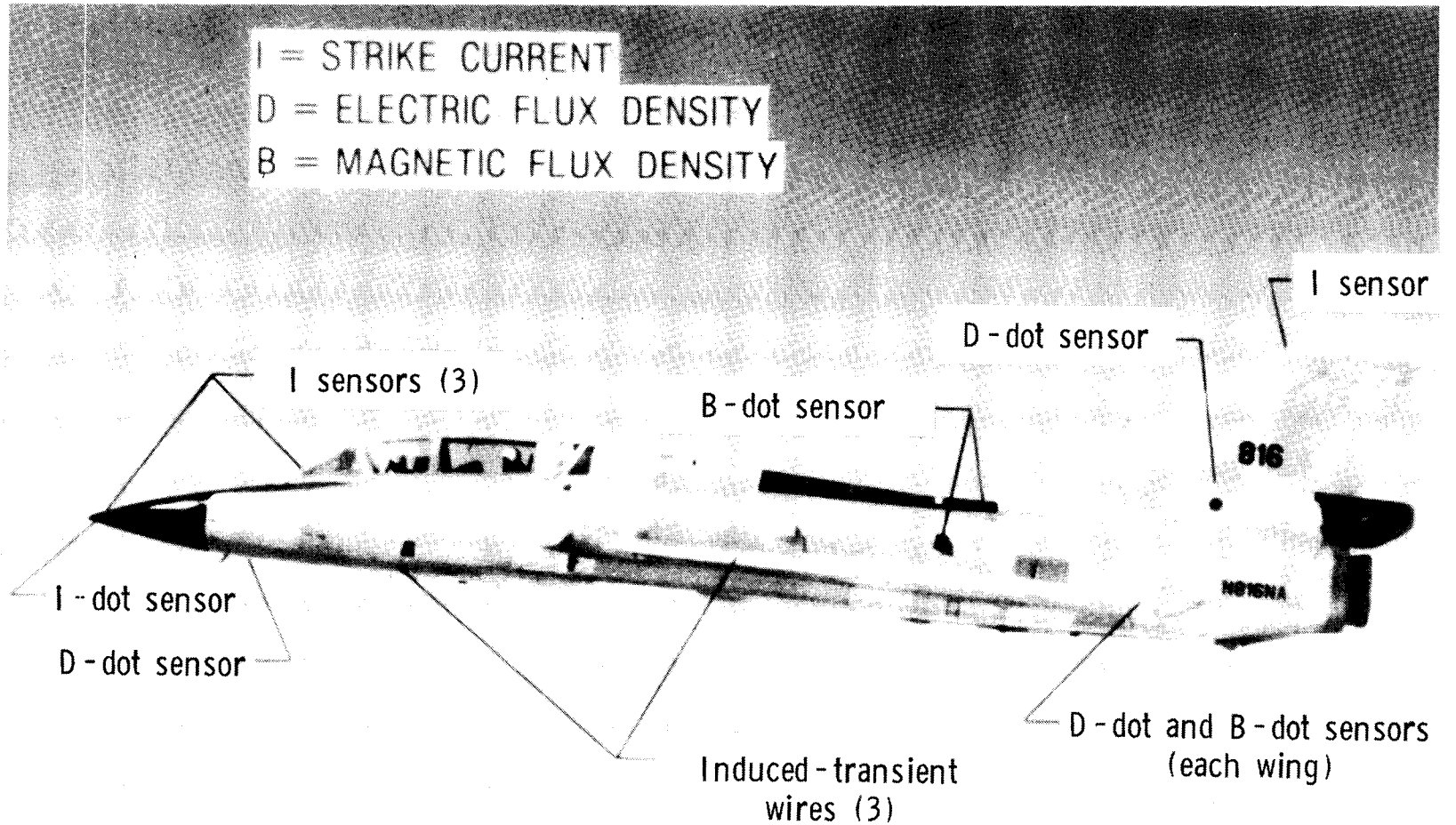

Figure 1. Location of electromagnetic sensors.

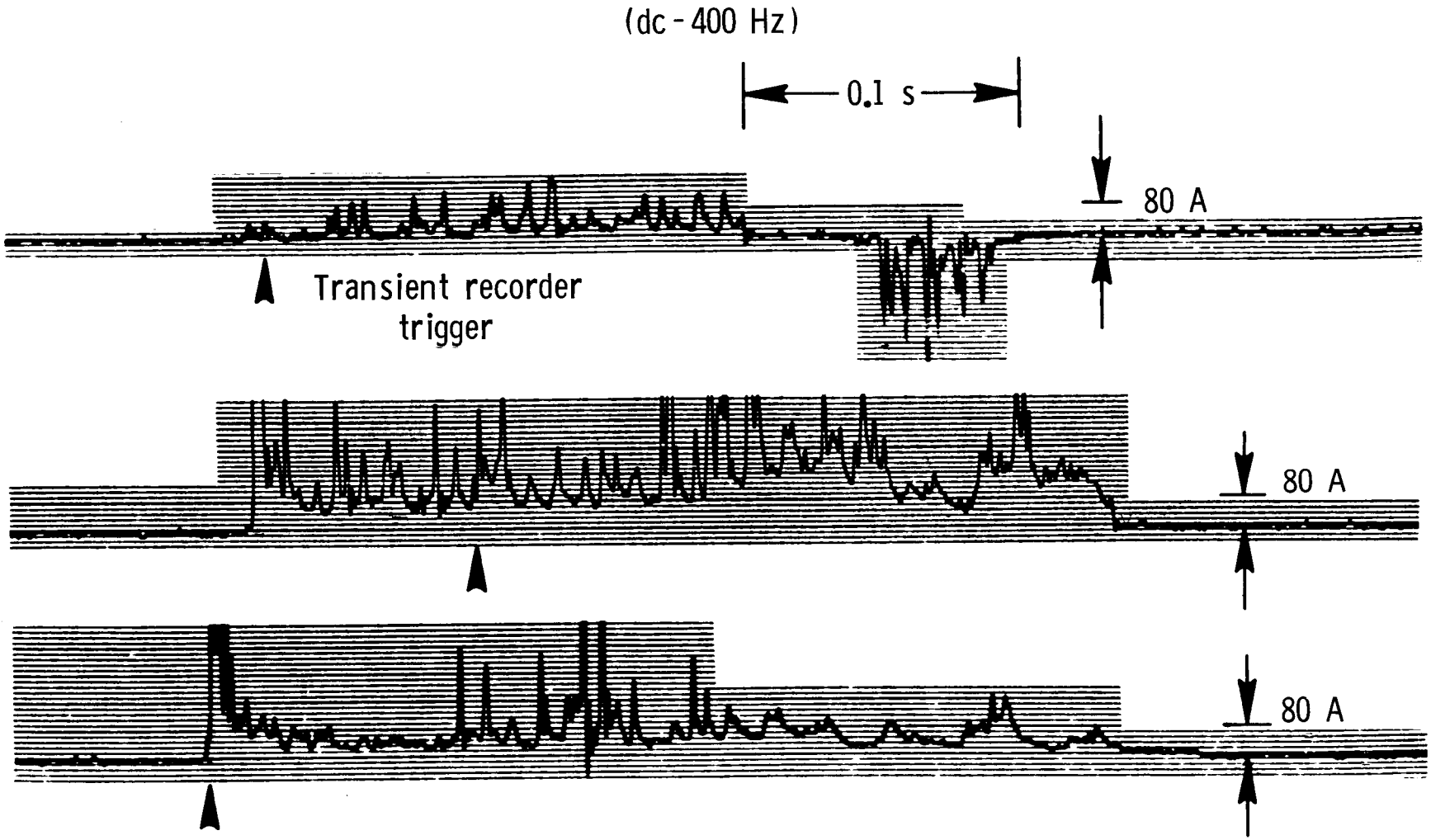

Figure 2. Vertical fin cap currents.

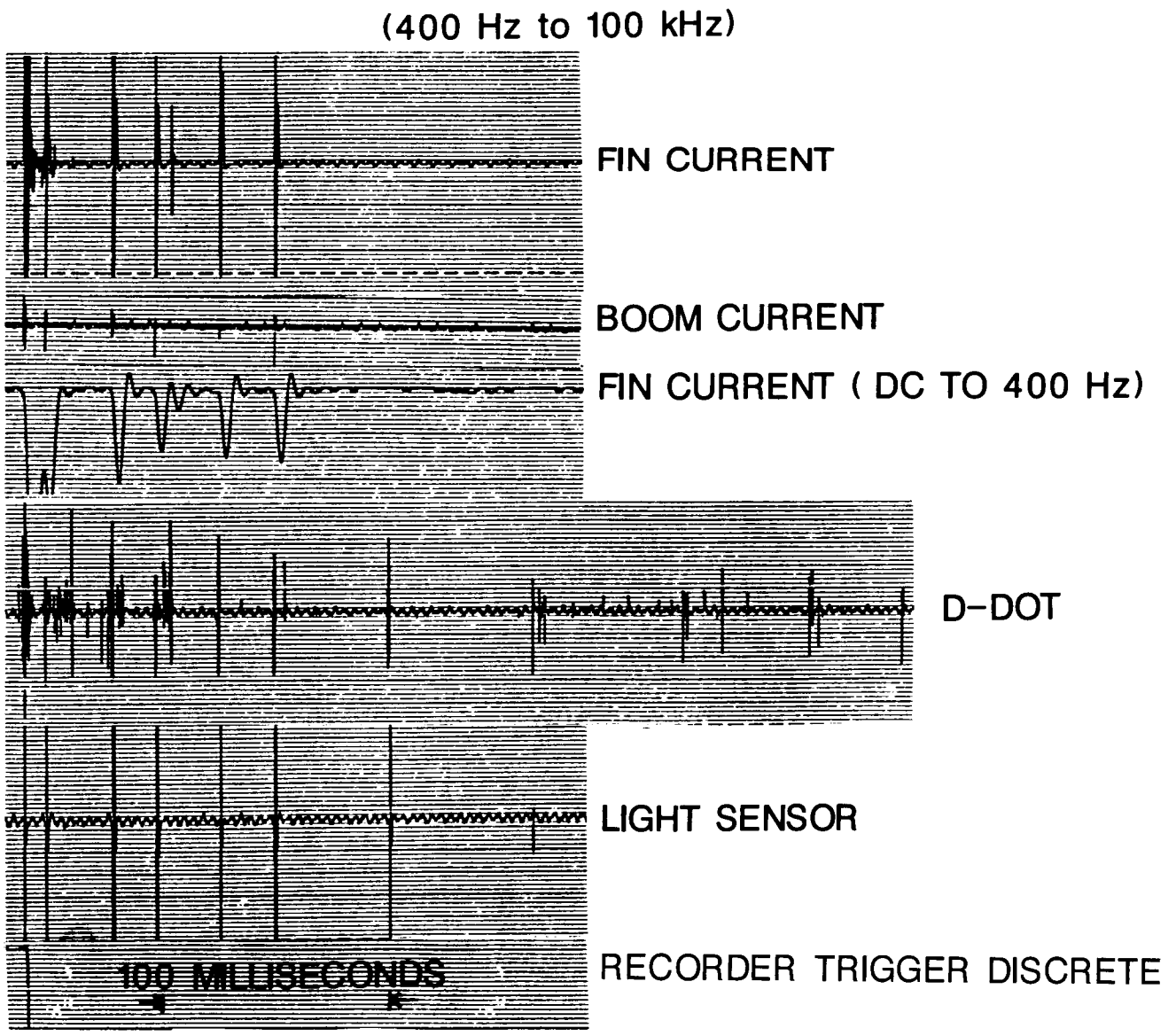

Figure 3. Temporal character of typical lightning strike.

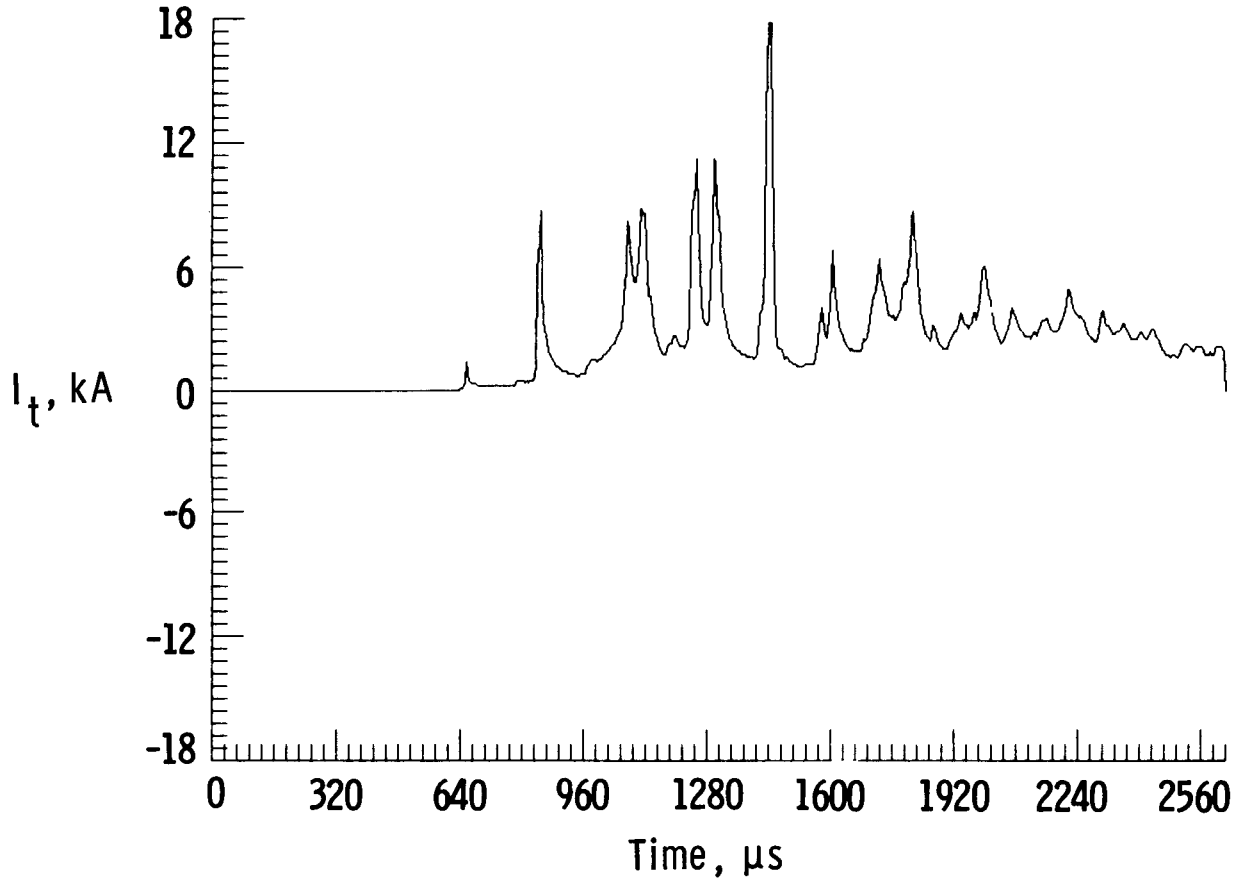

Figure 4. Vertical fin cap current corresponding to figure 3. (Recorded at 40-ns sample interval.)

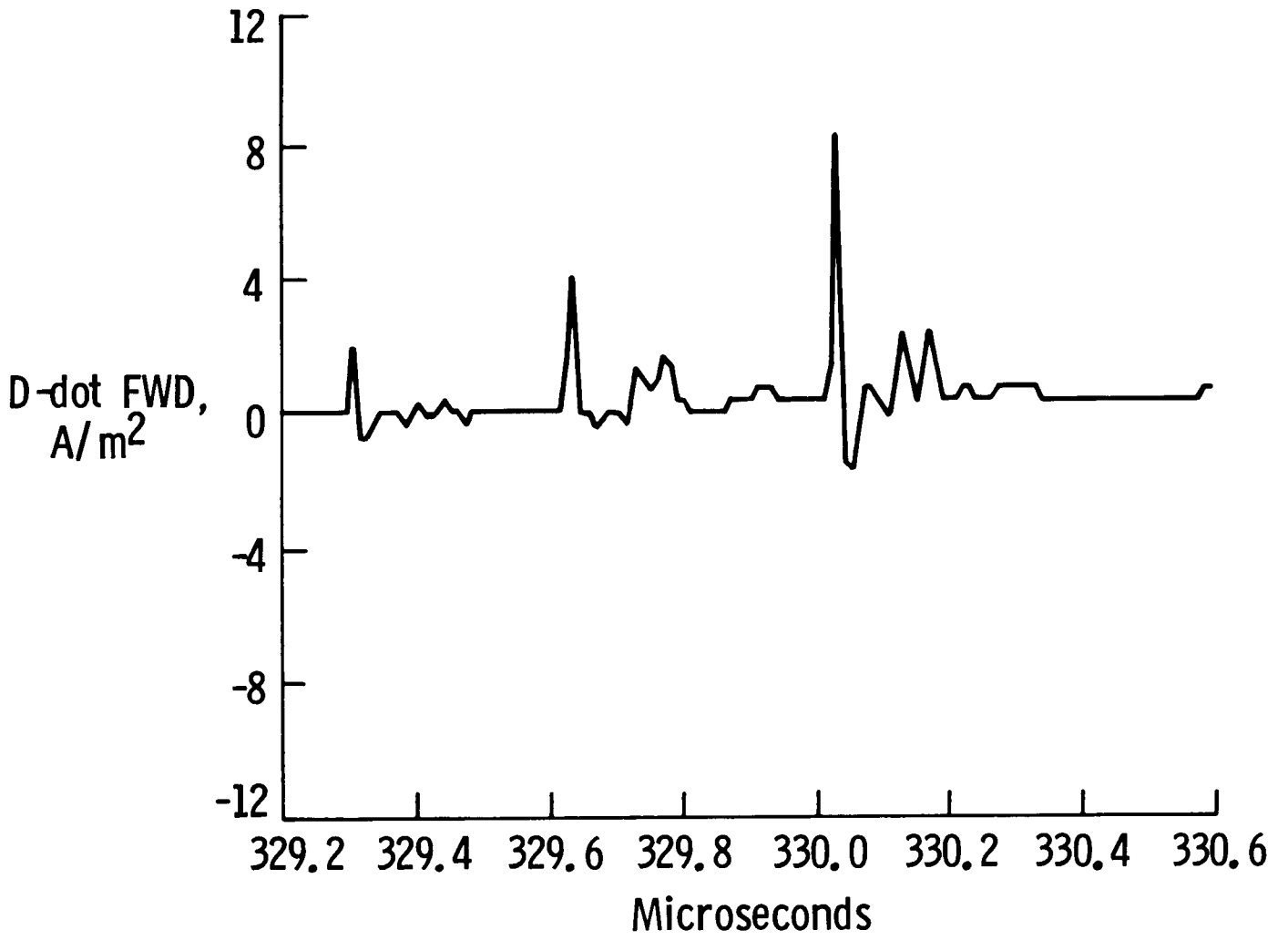

Figure 5. Rate of change of electric flux density from sensor located under forward fuselage. (Recorded at 10-ns sample interval.) Waveform recorded simultaneously with that in figure 6.

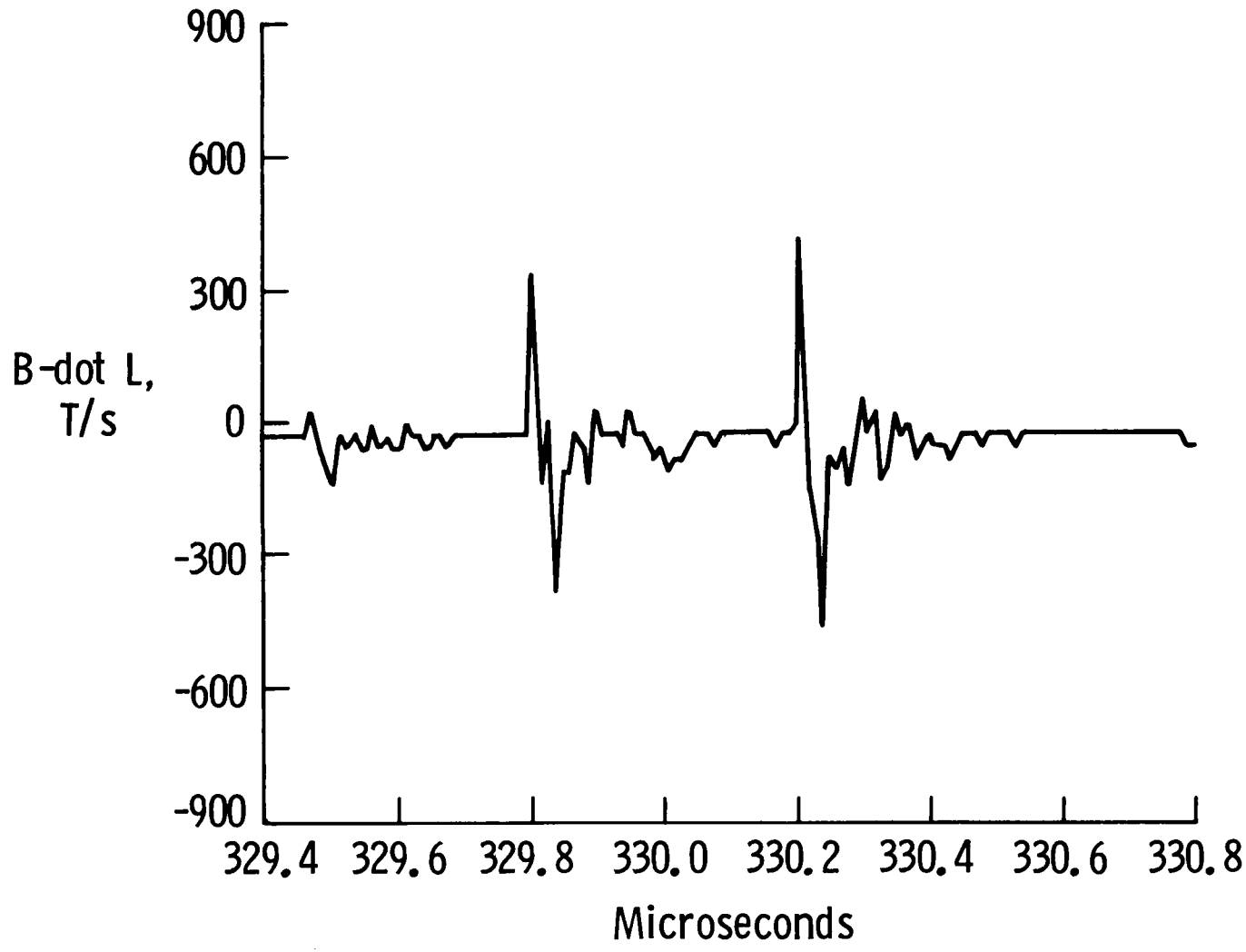

Figure 6. Rate of change of magnetic flux density from sensor located in port side of aft fuselage. (Recorded at 10-ns sample interval.) Waveform recorded simultaneously with that in figure 5.

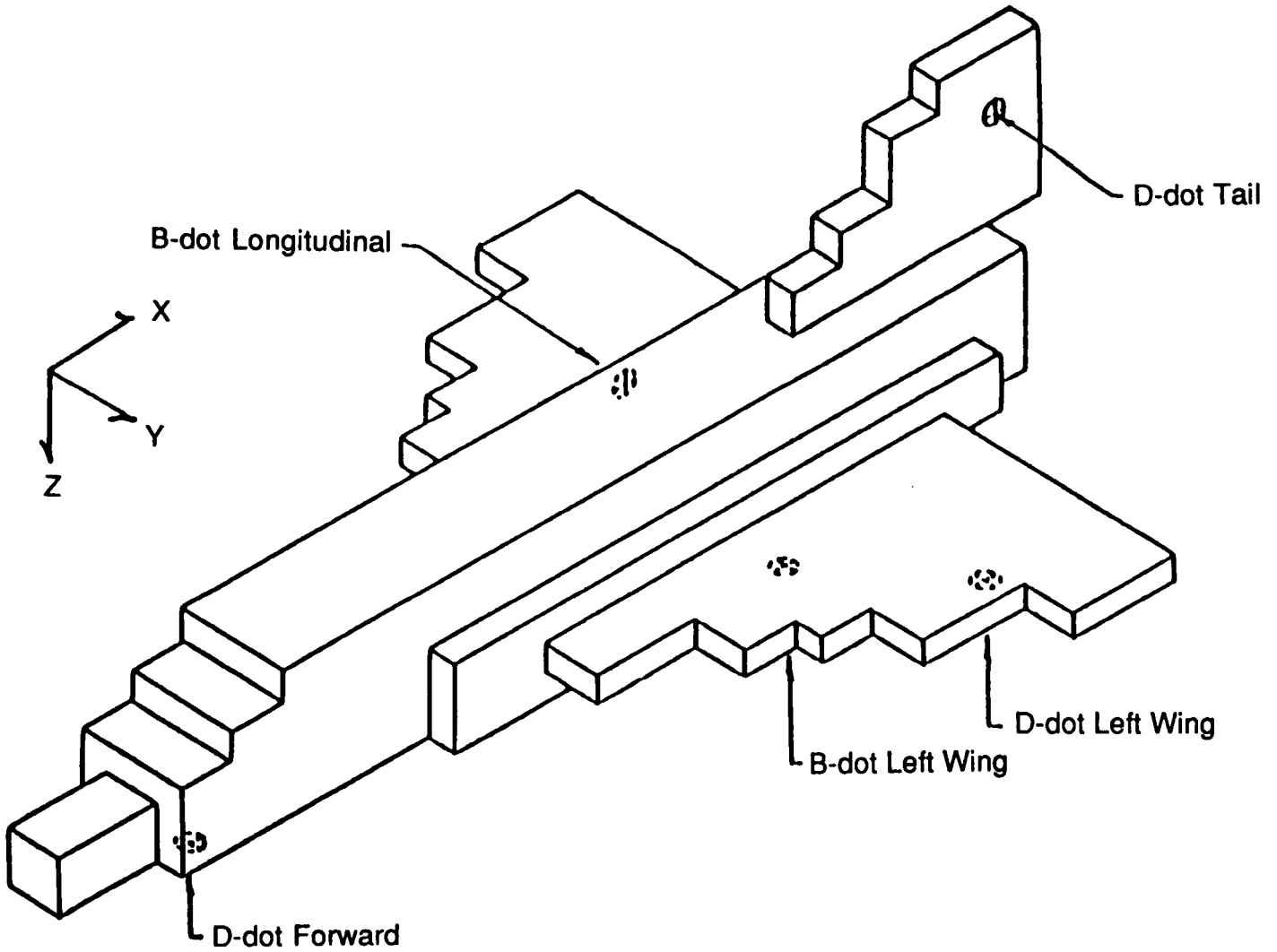

Figure 7. Model of F-106 used in finite-difference computer code.

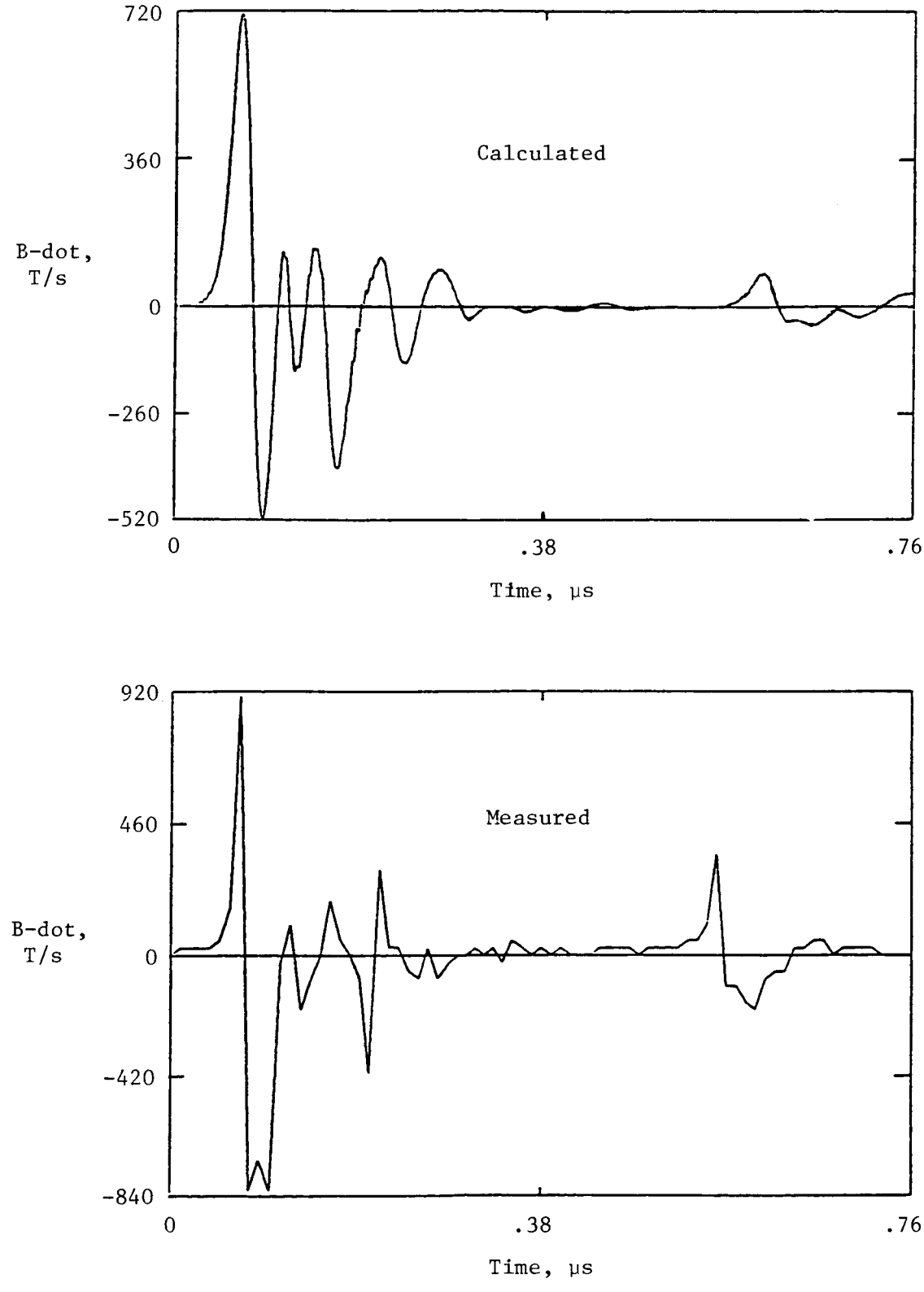

Figure 8. Comparison of nonlinear model calculated response (front to back, $E_{\text{mag}} = 0.20$ MV/m, $Q = Q_m/2$) with measured data for B-dot longitudinal sensor.

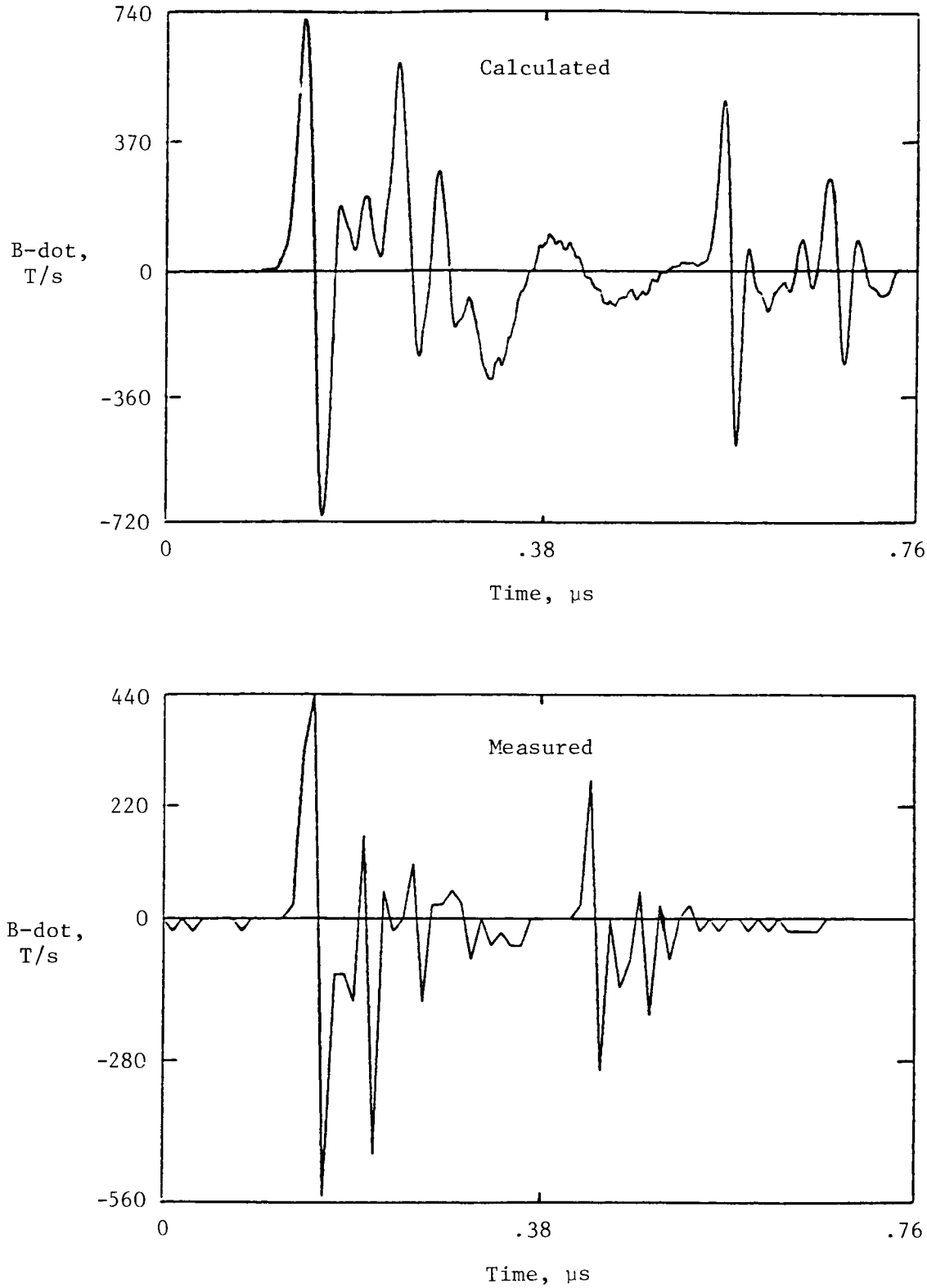

Figure 9. Comparison of nonlinear model calculated response (bottom to top, $E_{\text{mag}} = 0.64$ MV/m, $Q = -Q_m/2$) with measured data for B-dot longitudinal sensor.

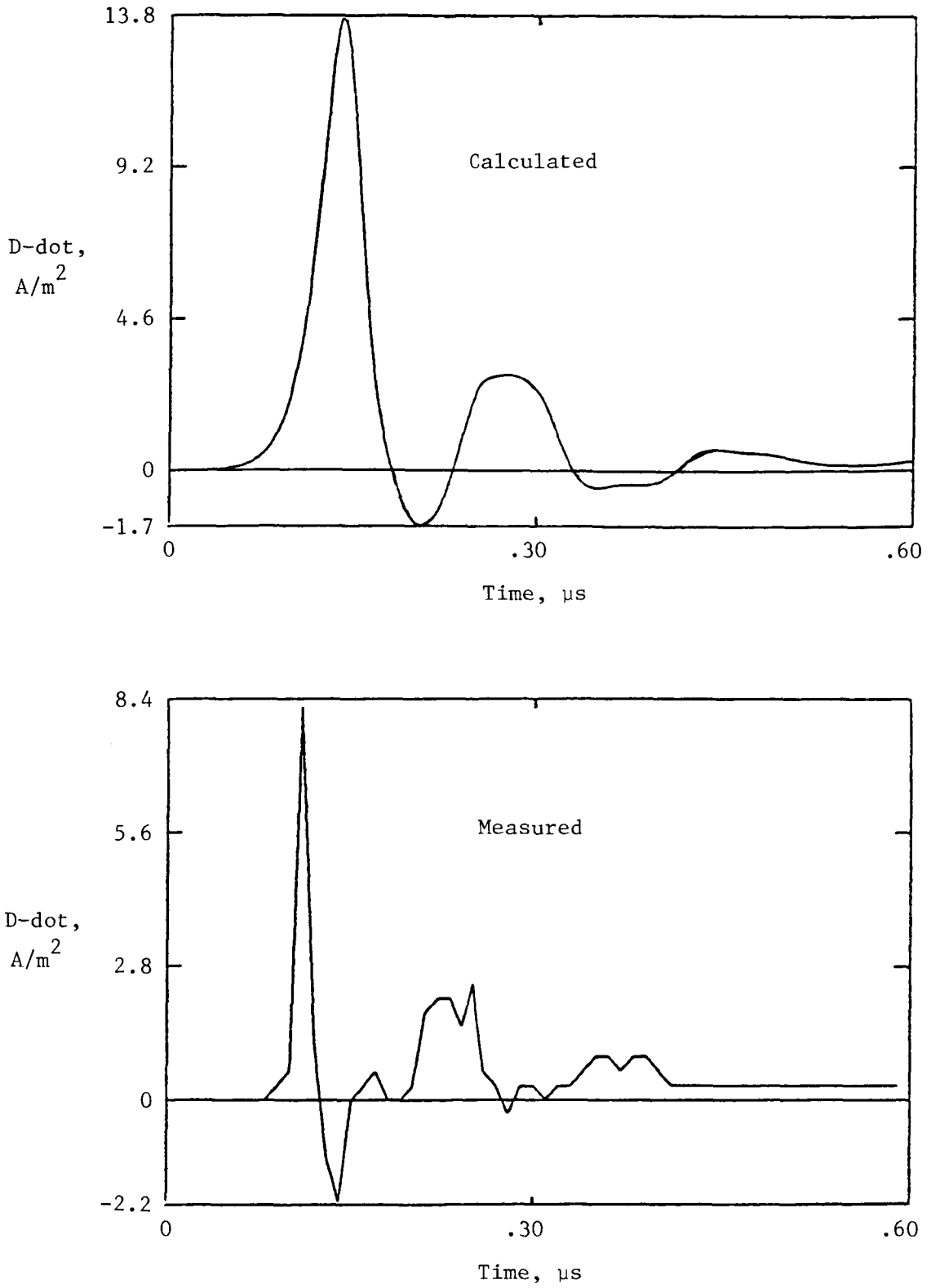

Figure 10. Comparison of nonlinear model calculated response (front to back, $E_{\text{mag}} = 0.19$ MV/m, $Q = 0$) with measured data for D-dot forward sensor.

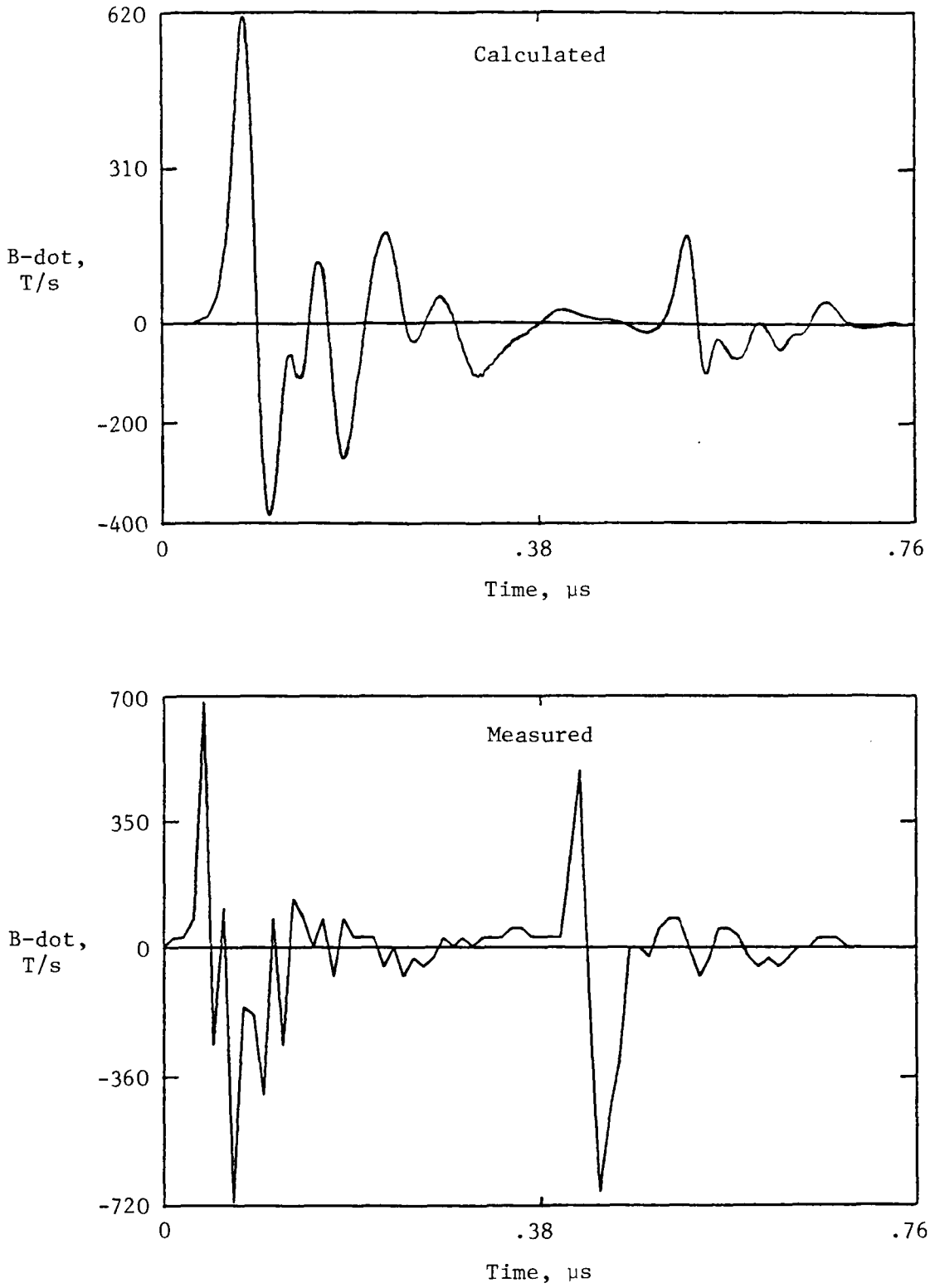

Figure 11. Comparison of nonlinear model calculated response (bottom to top, $E_{\text{mag}} = 0.64$ MV/m, $Q = Q_m/2$) with measured data for B-dot longitudinal sensor.

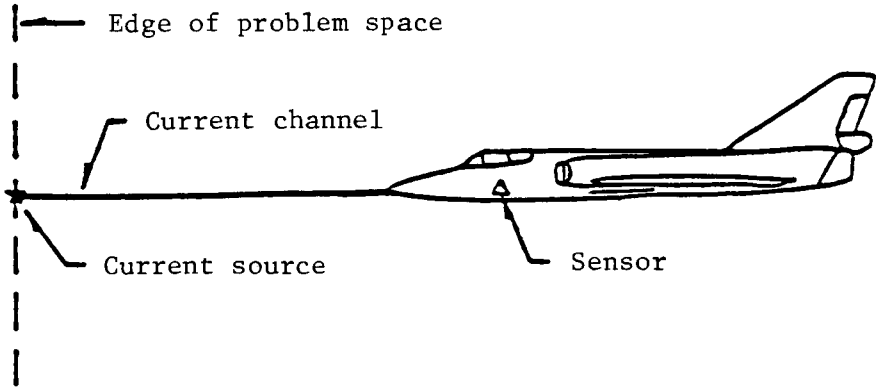

(a) Natural lightning.

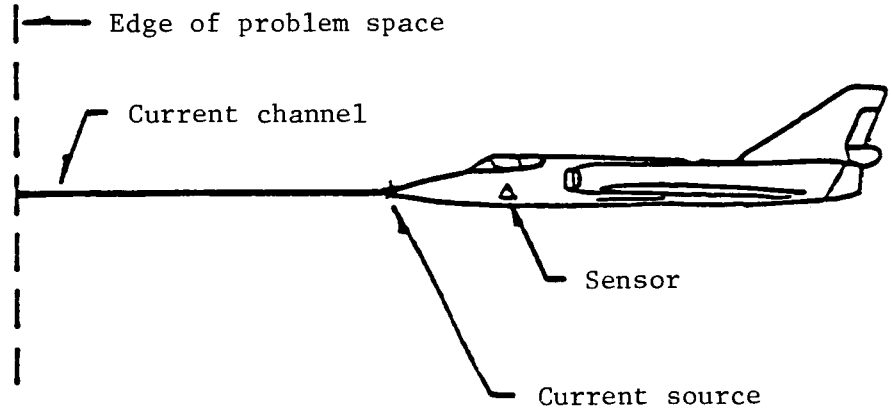

(b) Triggered lightning.

Figure 12. Model showing locations of current source used in computer code.

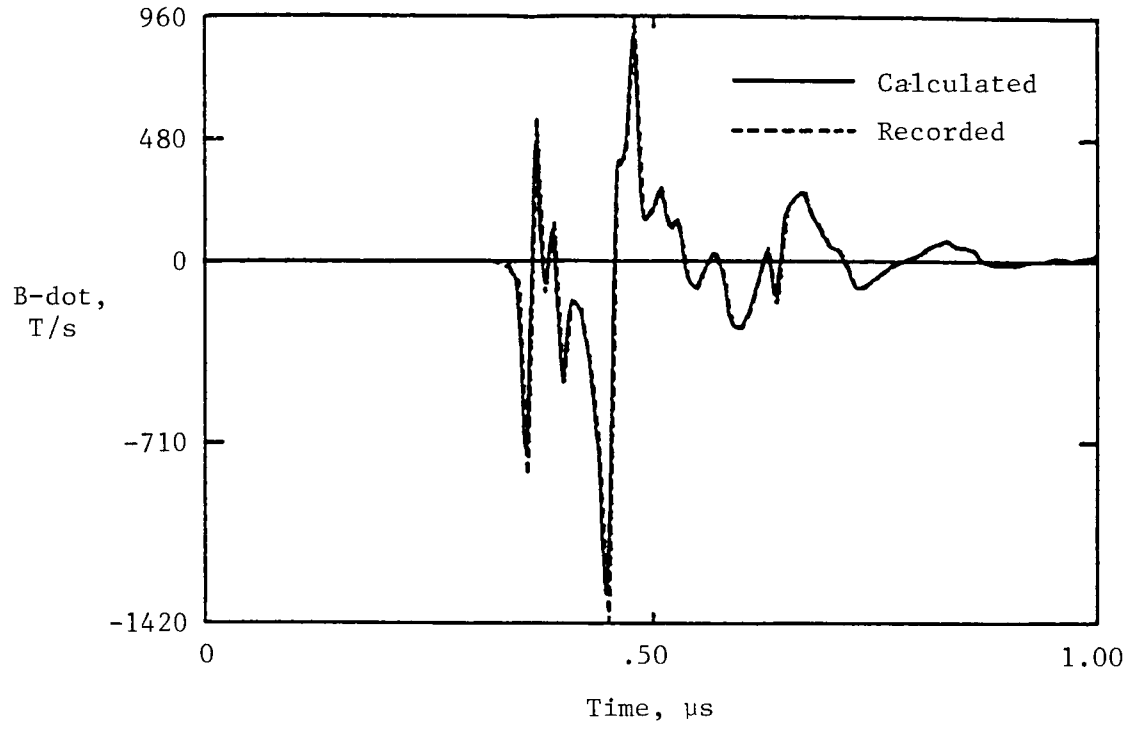

(a) *B*-dot longitudinal sensor.

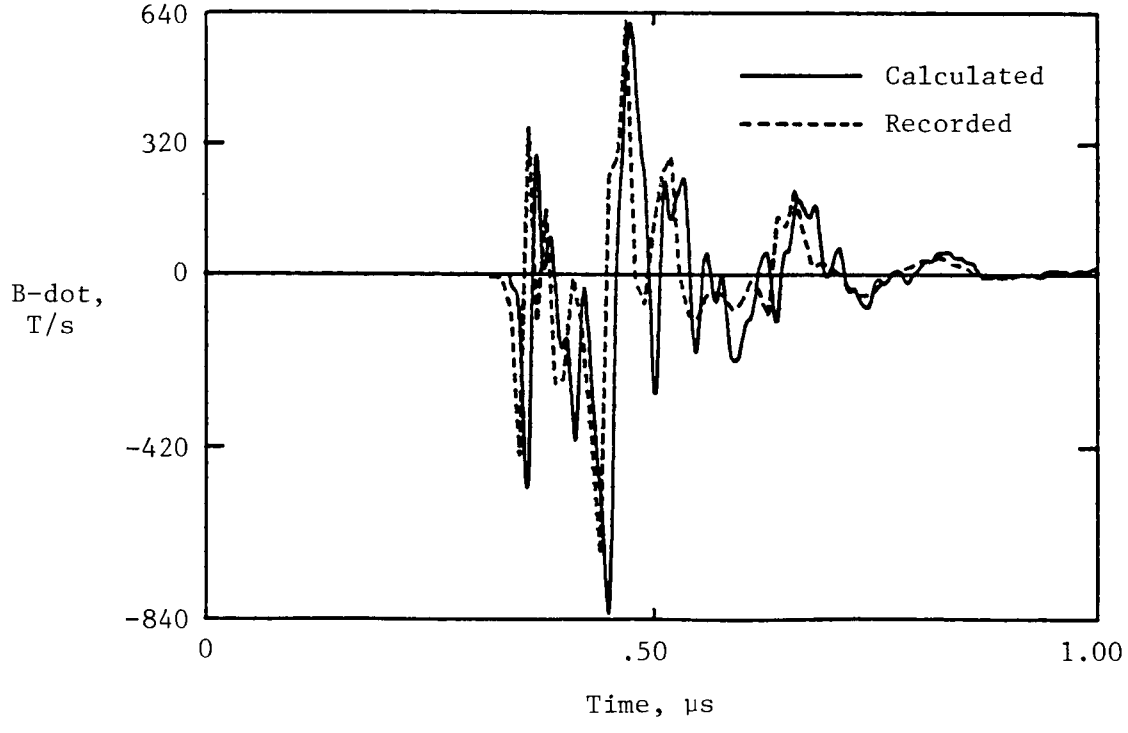

(b) *B*-dot left wing sensor.

Figure 13. Comparison of calculated linear model and recorded responses to triggered lightning.

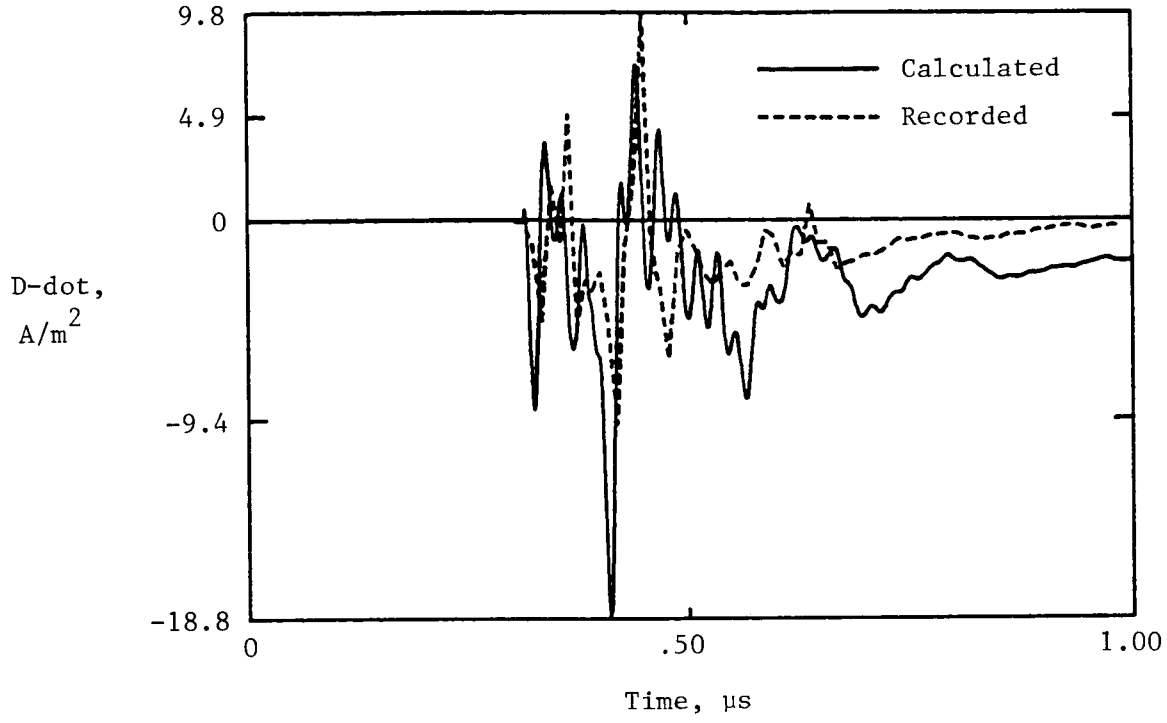

(c) *D*-dot forward sensor.

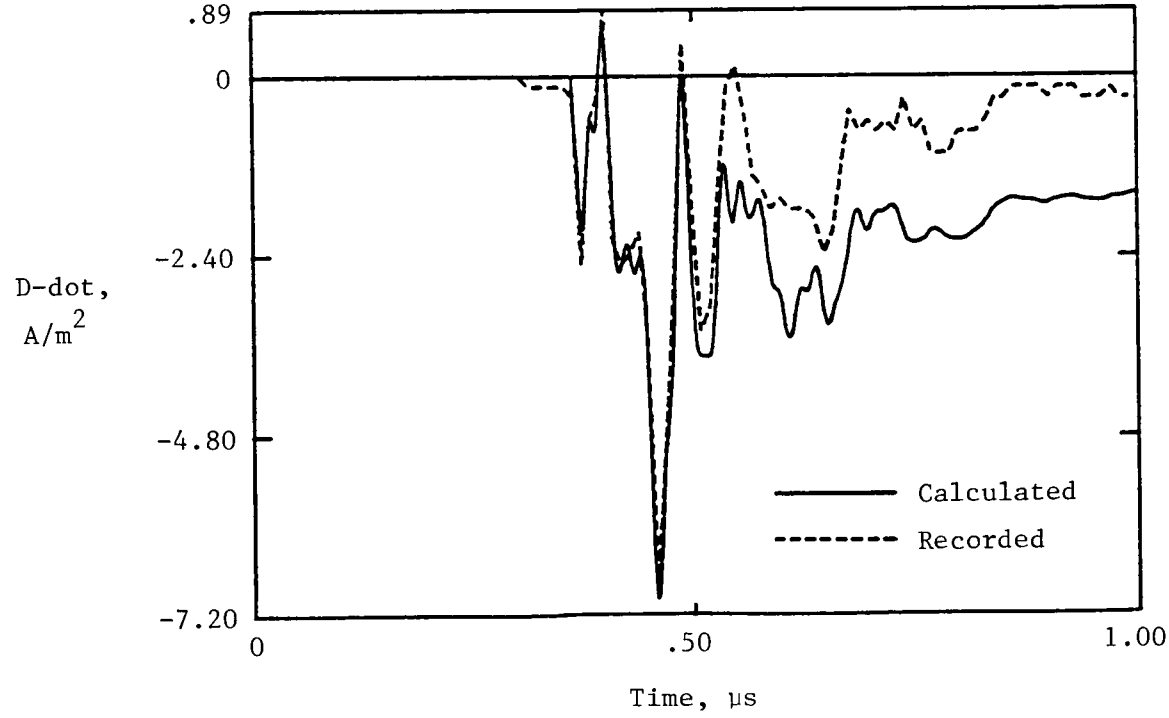

(d) *D*-dot left wing sensor.

Figure 13. Continued.

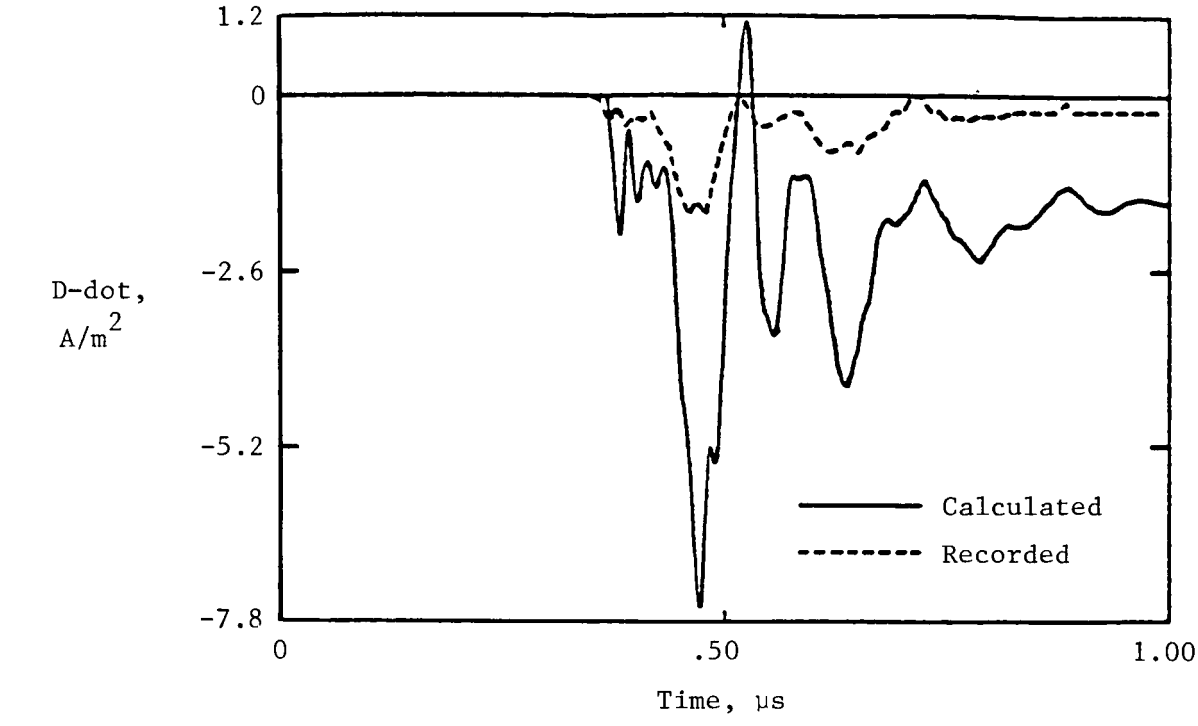

(e) *D*-dot vertical fin sensor.

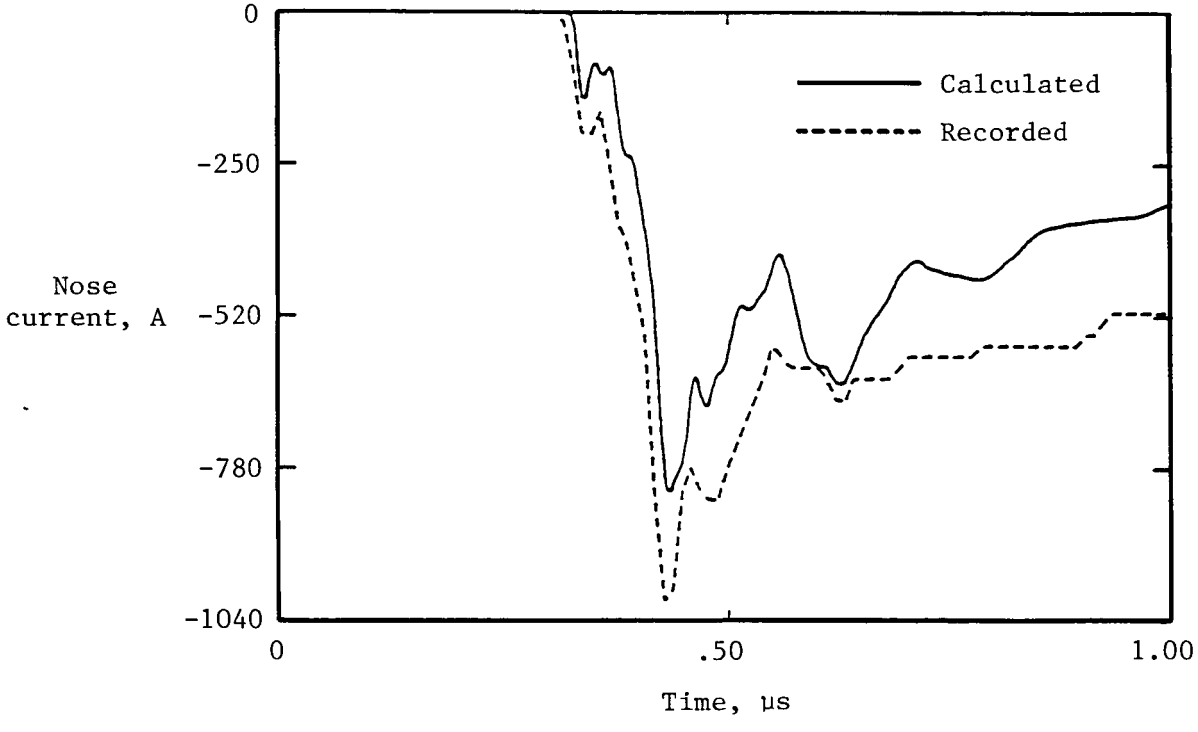

(f) Nose current.

Figure 13. Concluded.

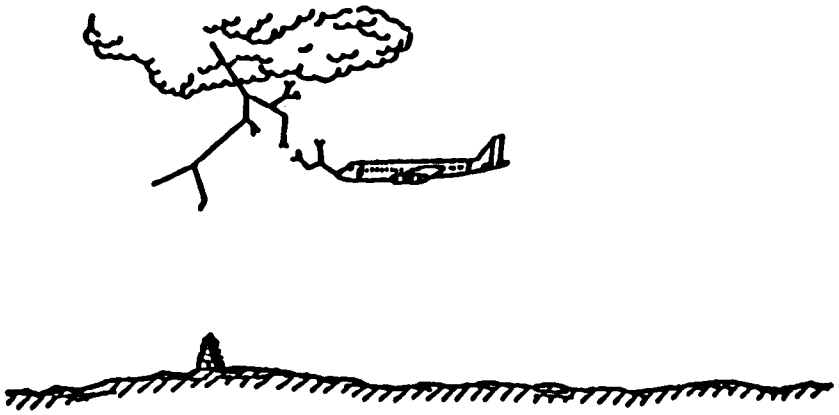

(a) Stepped leader propagating toward Earth.

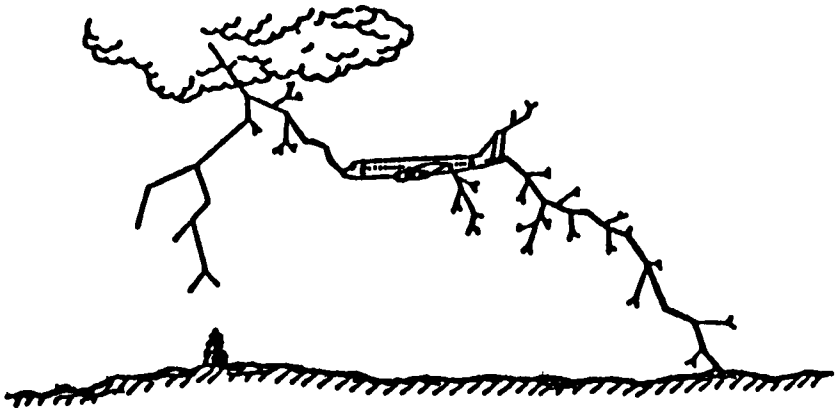

(b) Arcs from aircraft to leader.

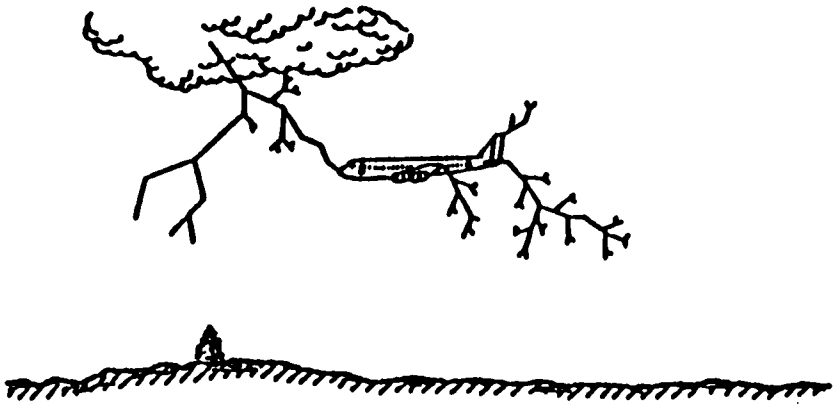

(c) Leader from aircraft to ground.

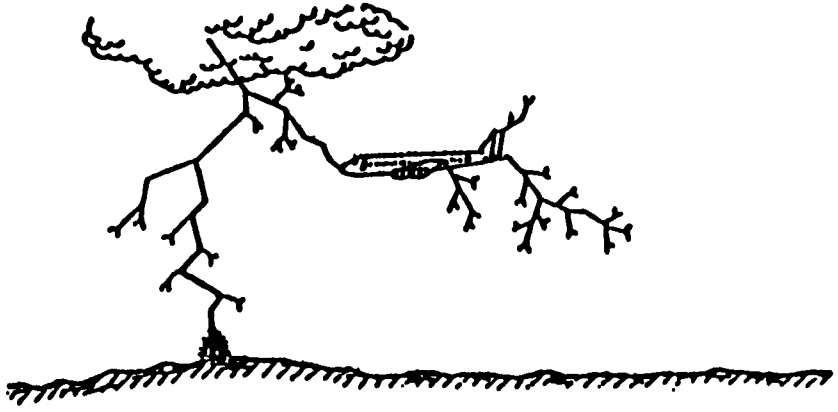

(d) Leader from source to ground.

Figure 14. Natural lightning strike to aircraft.

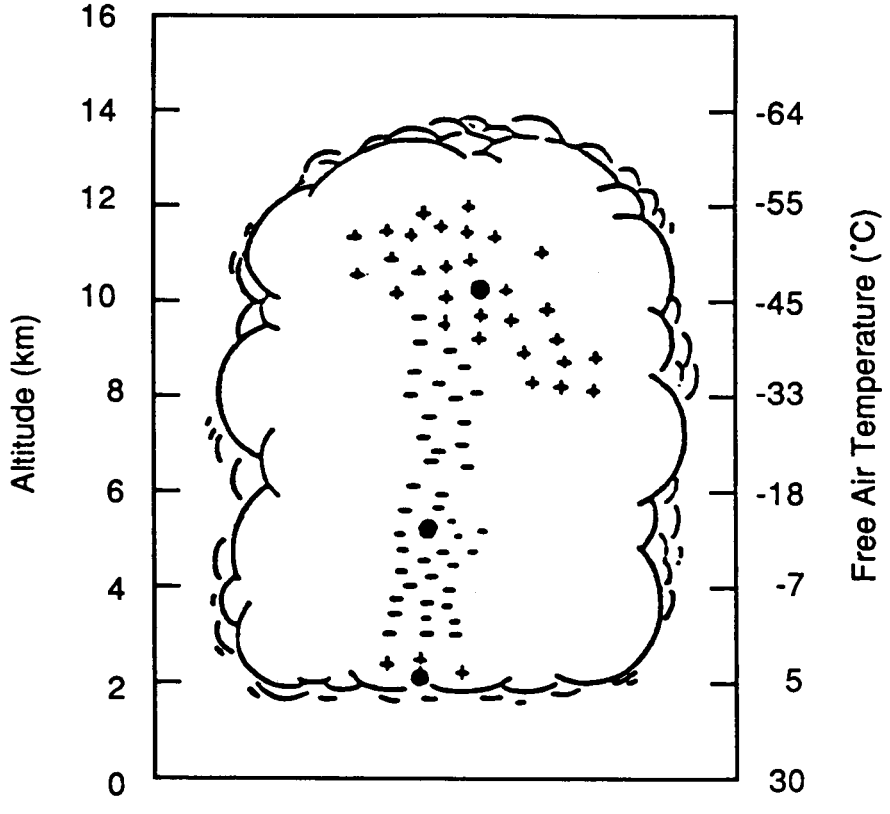

Figure 15. Thunderstorm charge separation model from reference 27.

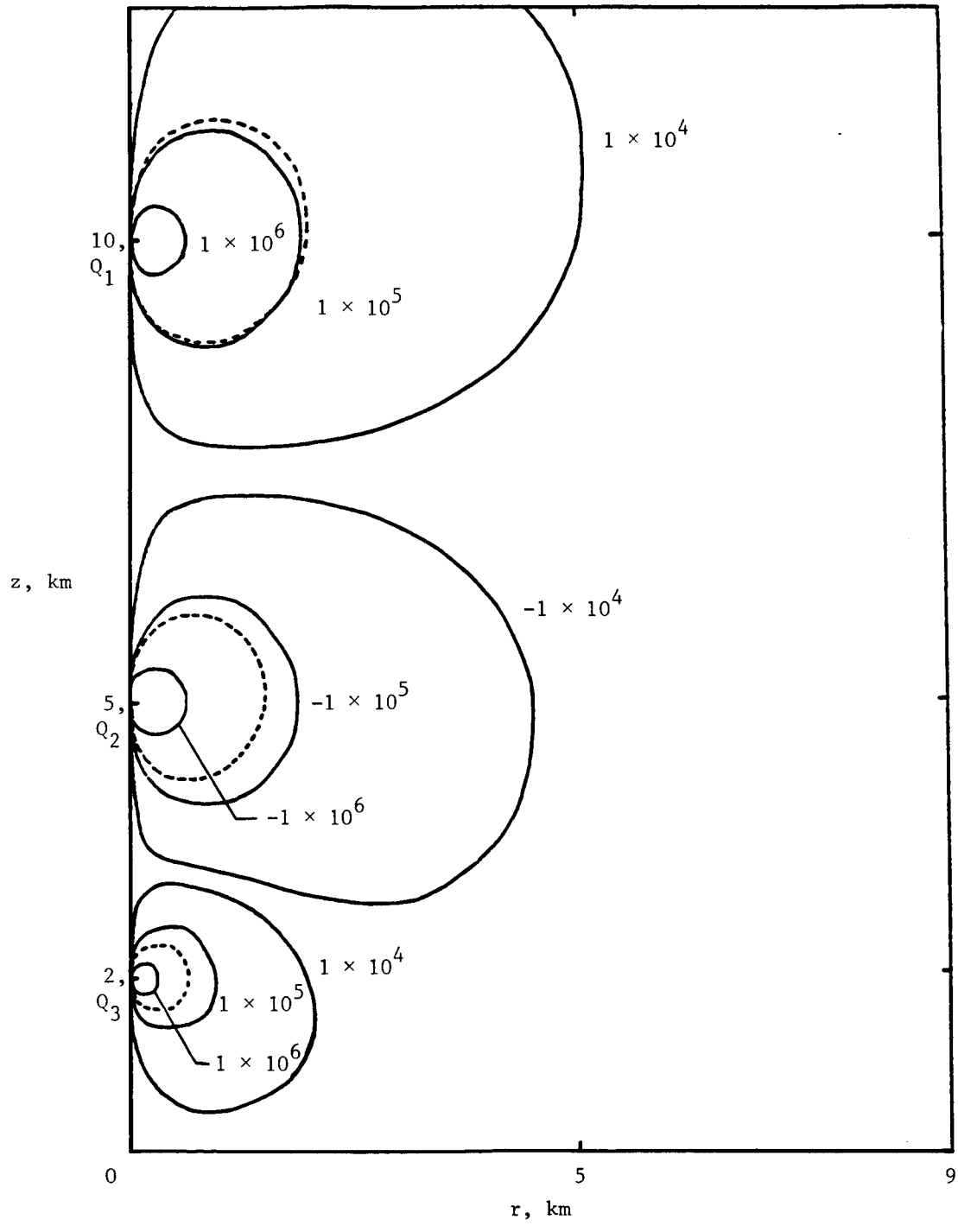

(a) Radial component.

Figure 16. Components of electric field for thunderstorm model. Dashed lines indicate minimum air breakdown field.

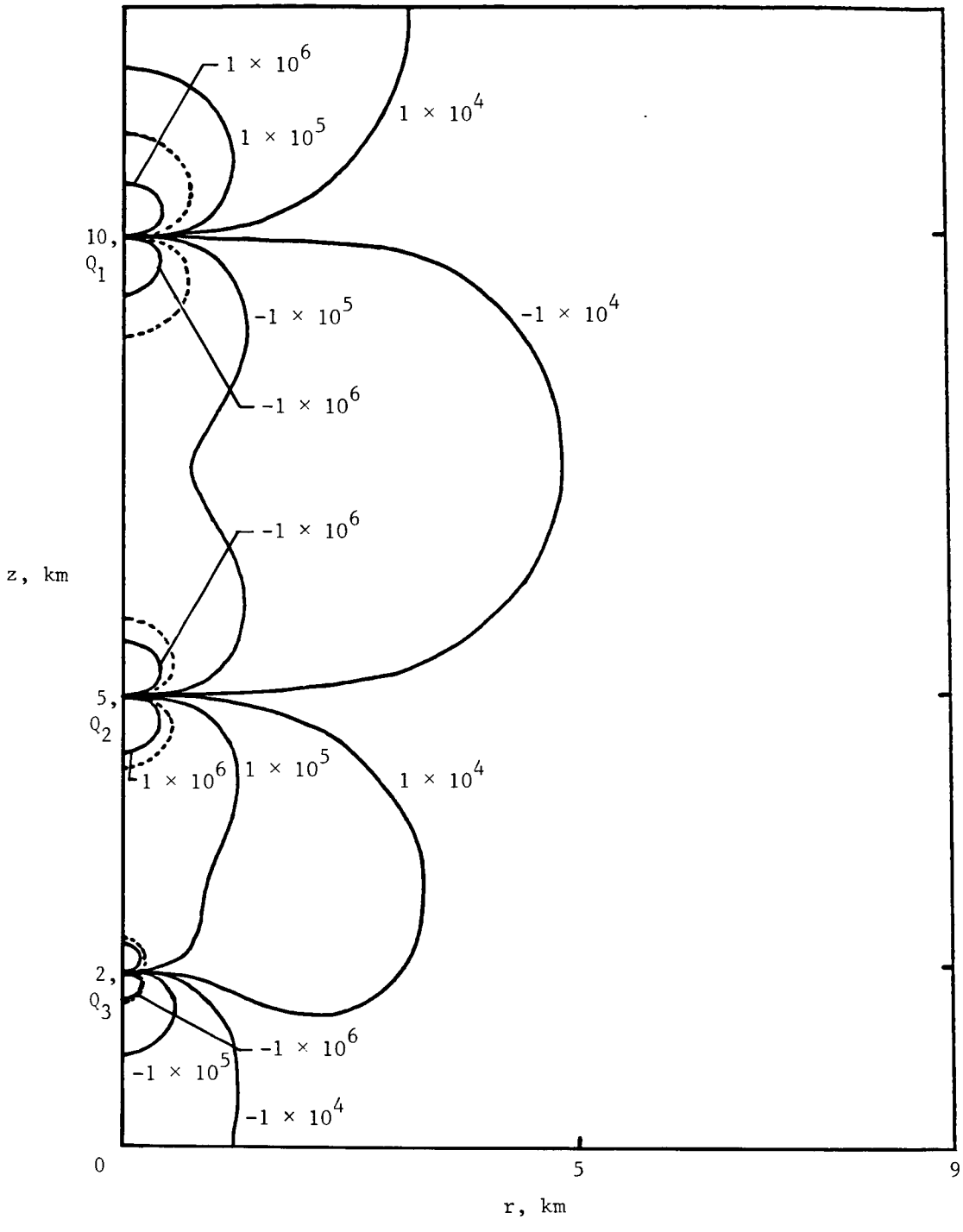

(b) Vertical component.

Figure 16. Continued.

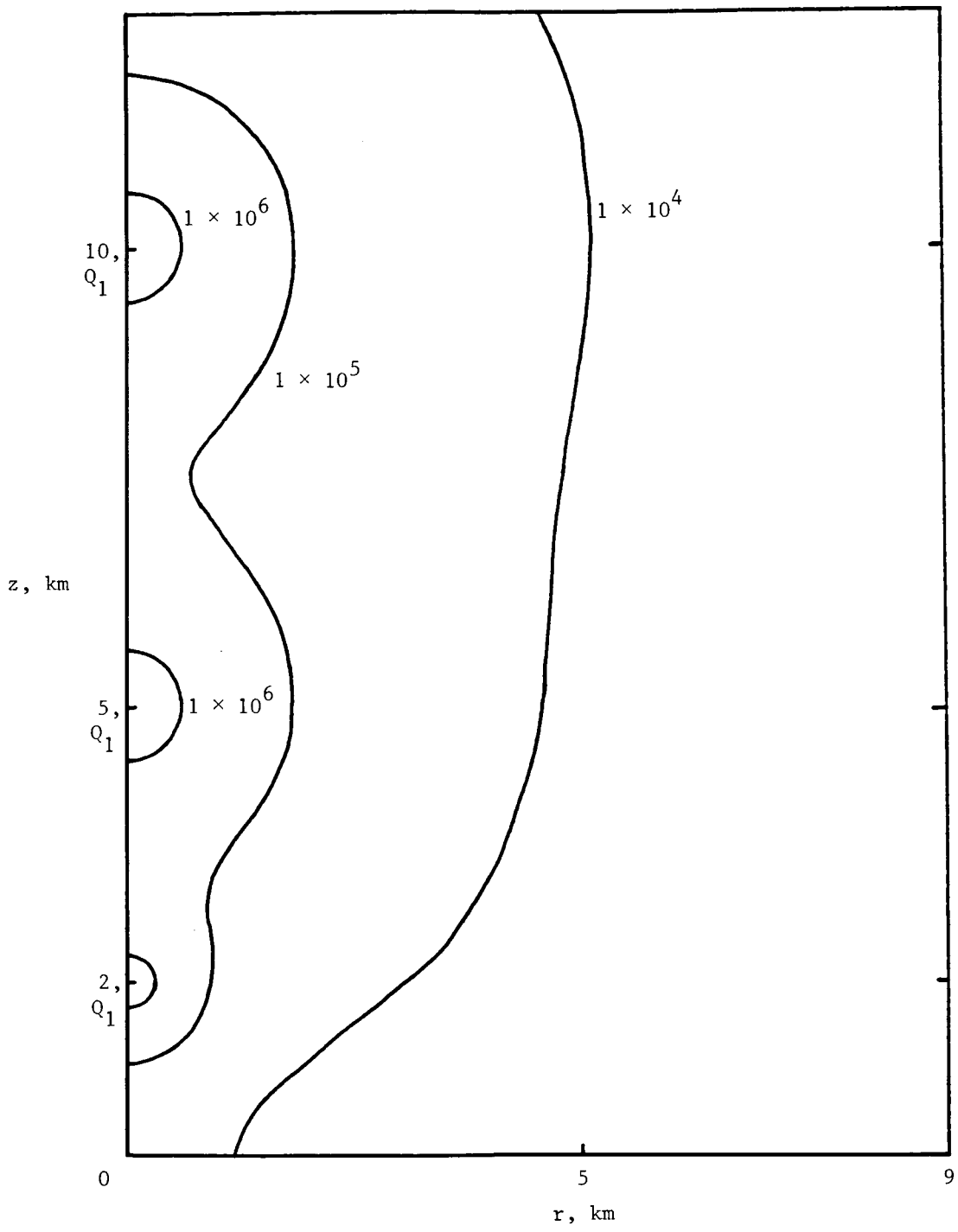

(c) Magnitude.

Figure 16. Concluded.

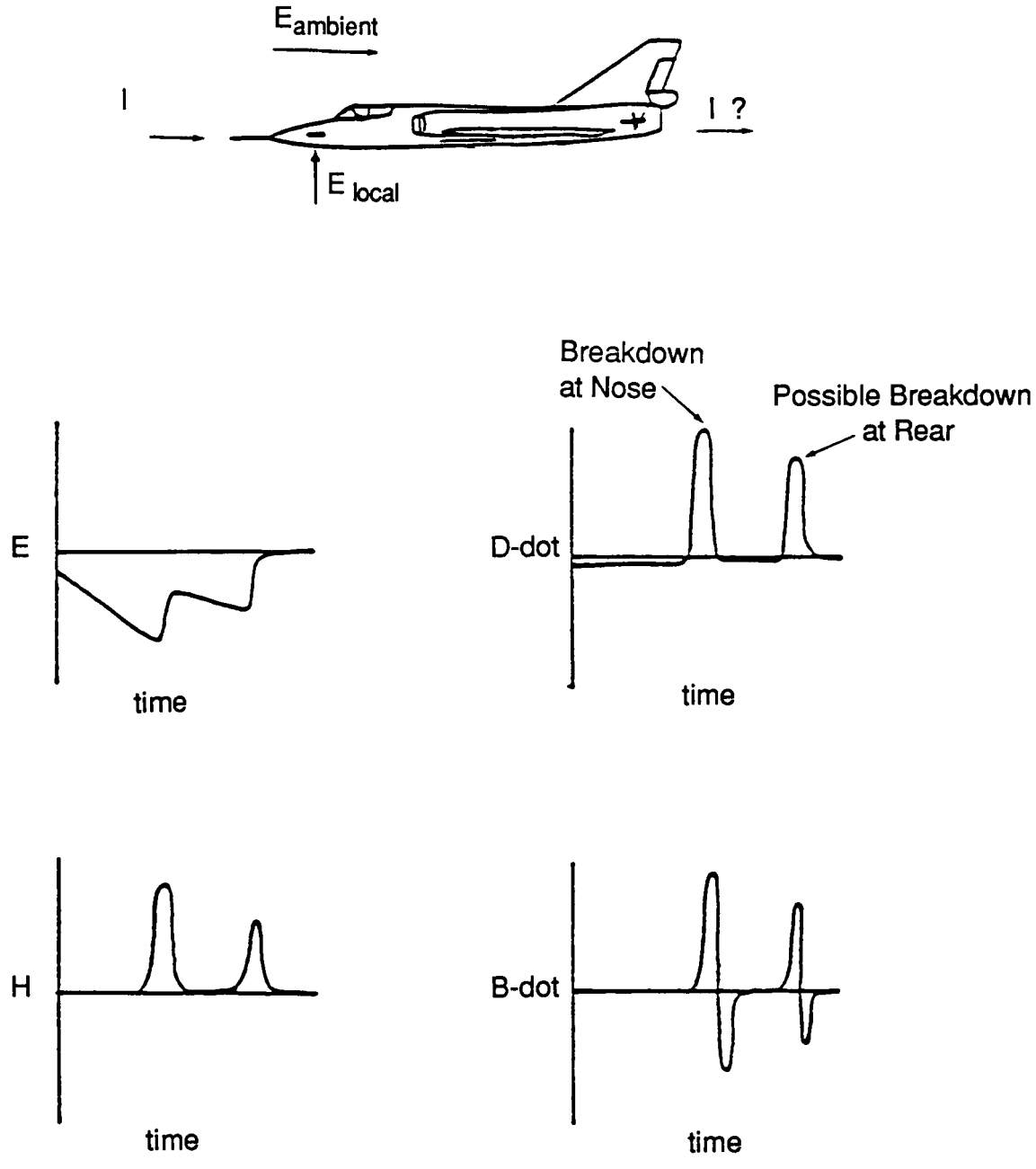

Figure 17. Expected behavior of triggered lightning for electric field oriented nose to tail.

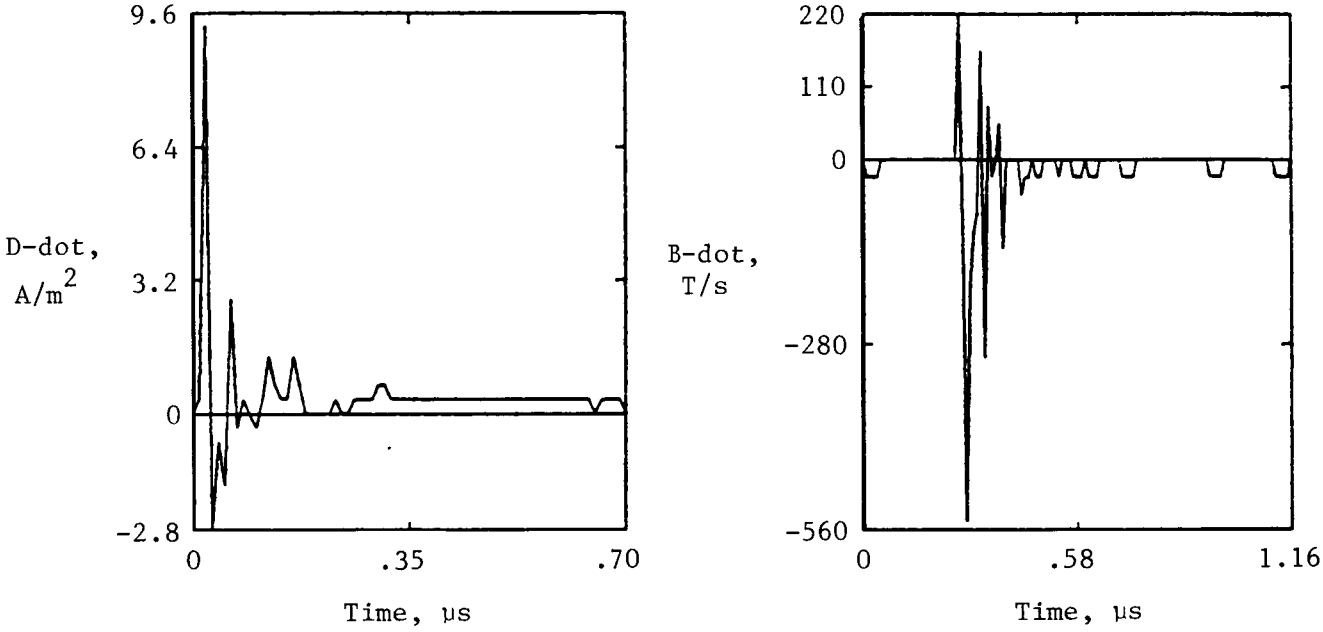

(a) First pulse.

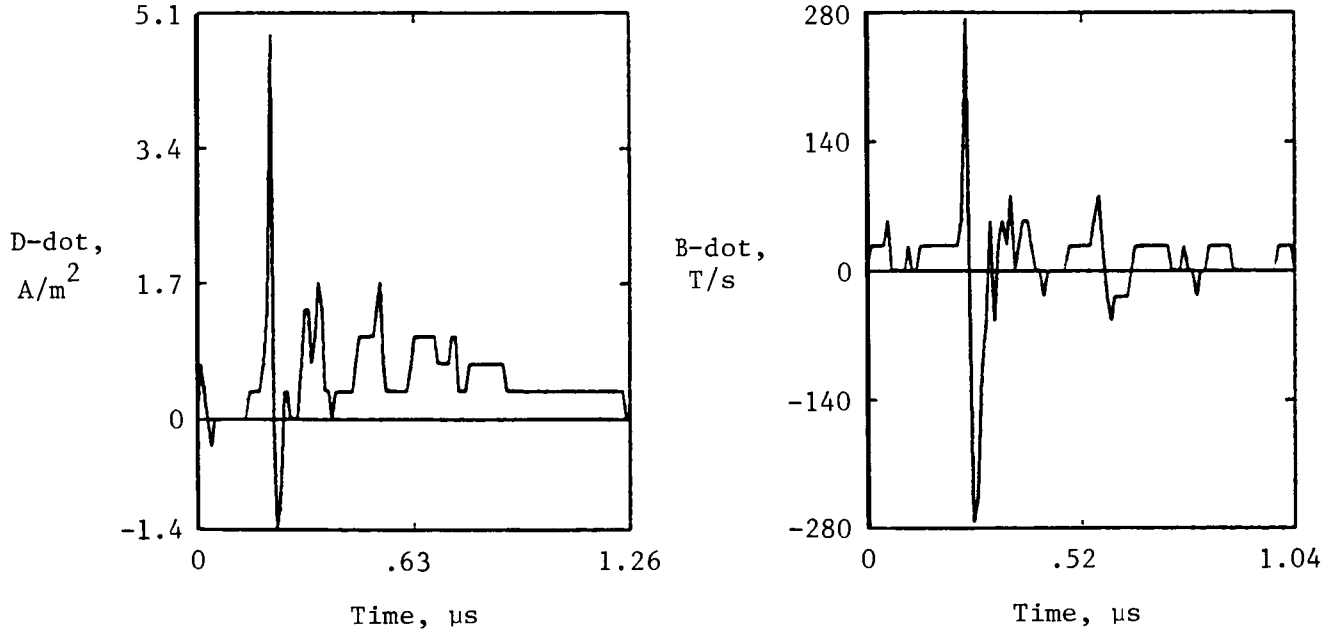

(b) Second pulse.

Figure 18. In-flight D-dot and B-dot strike data.

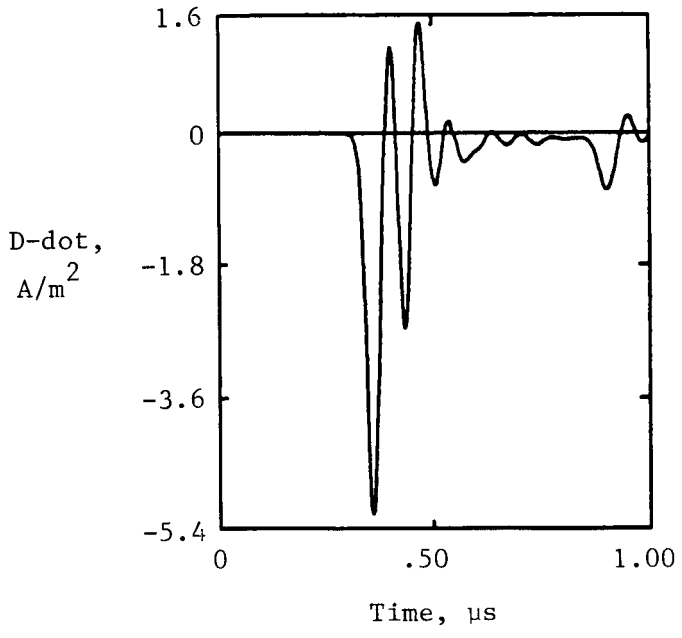

(a) Output A.

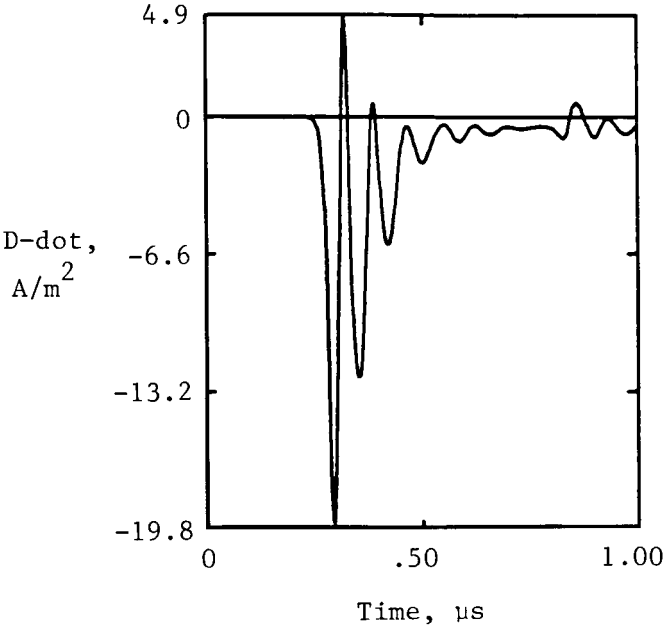

(b) Output B.

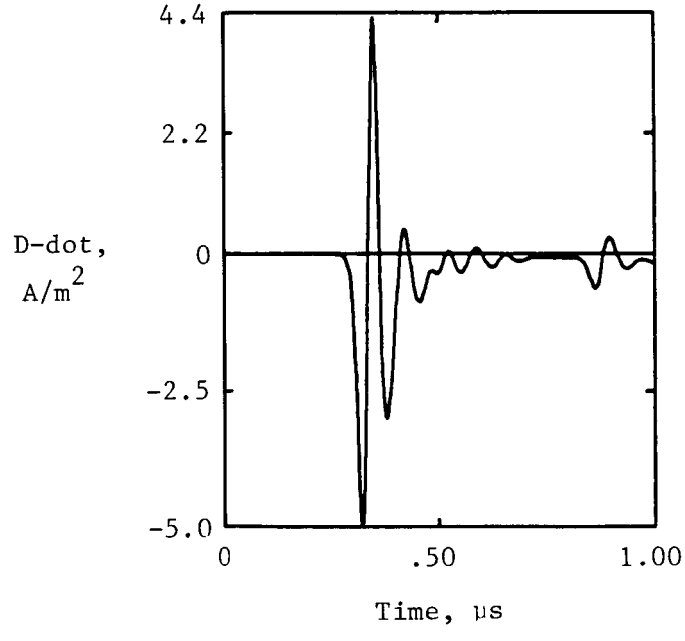

(c) Output C.

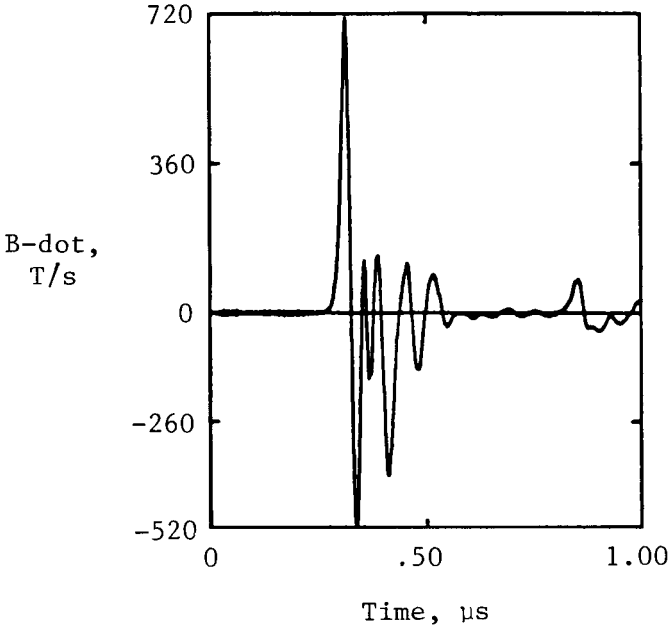

(d) Output D.

Figure 19. F-106 aircraft response from nonlinear lightning computer model.

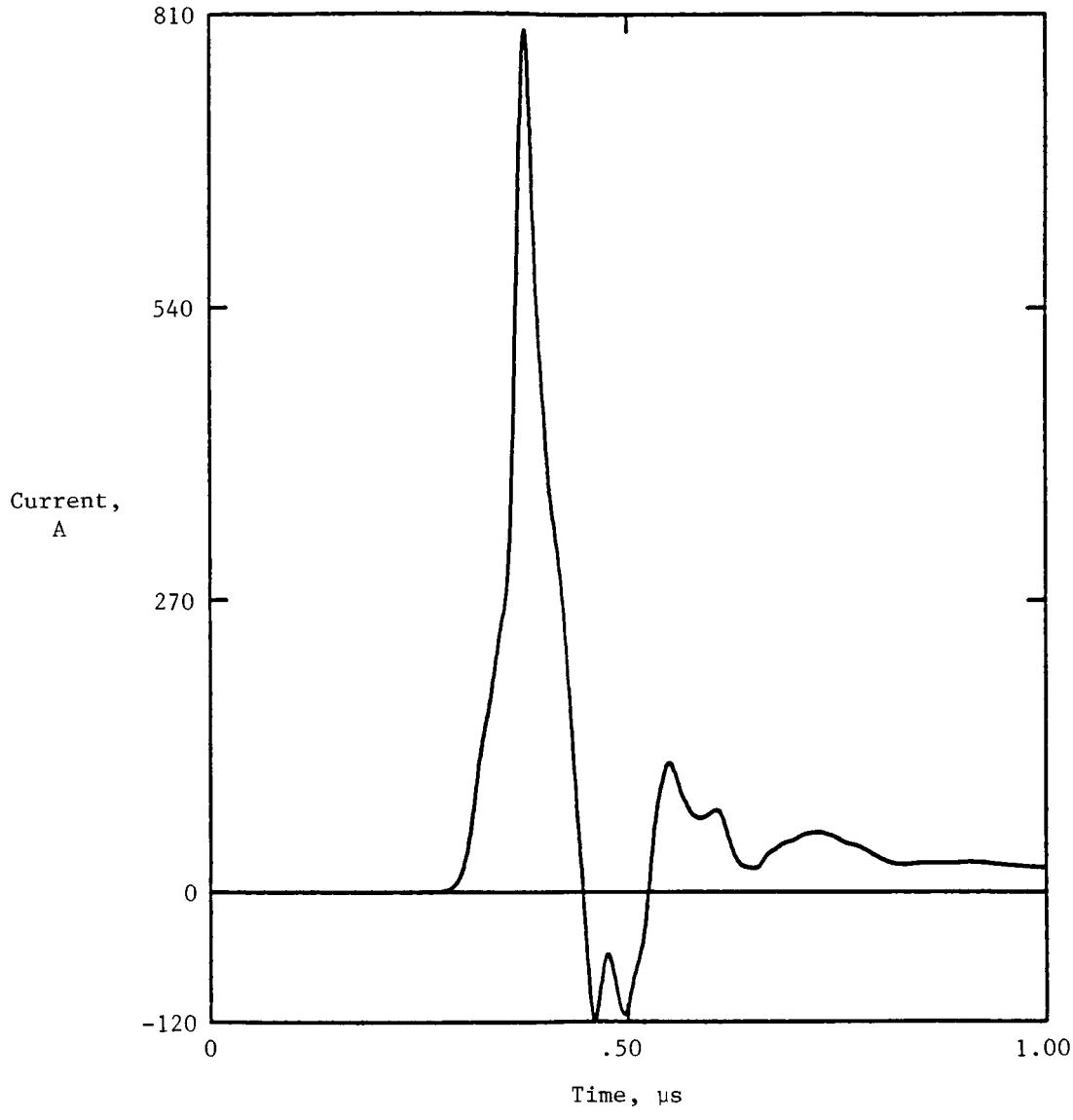

Figure 20. Nose boom current from nonlinear lightning computer model.

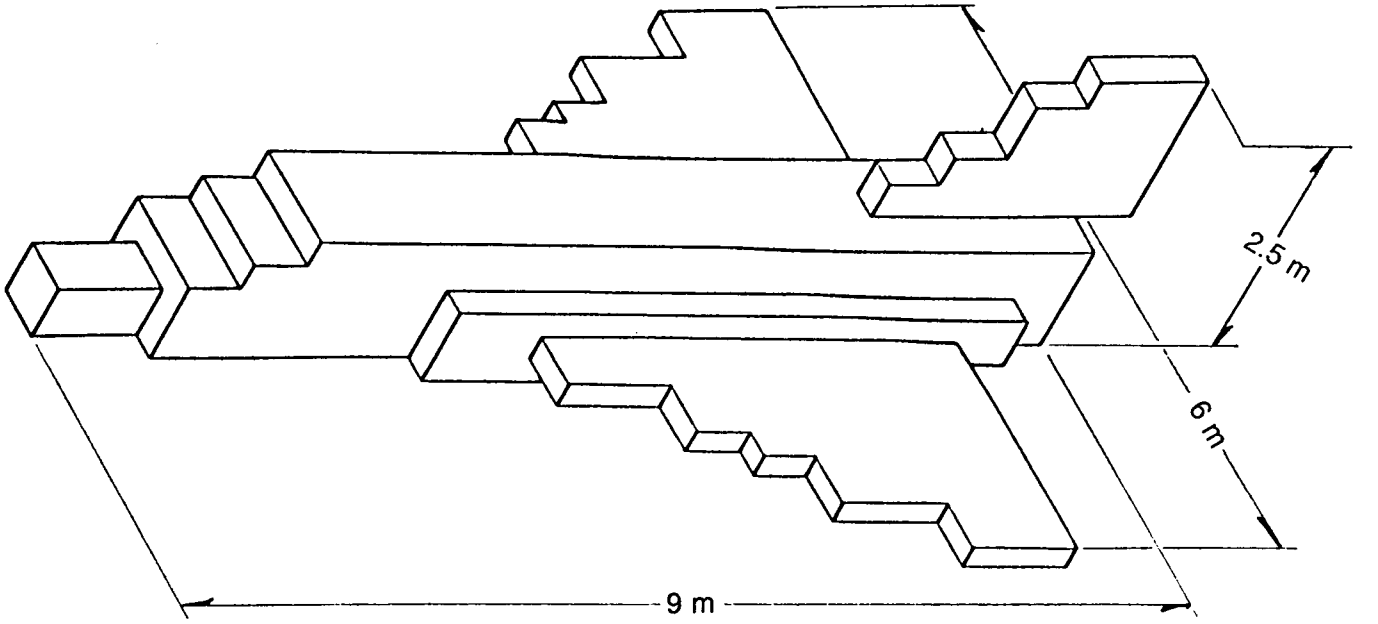

(a) Half-size F-106.

Figure 21. Dimensional drawings of scaled aircraft.

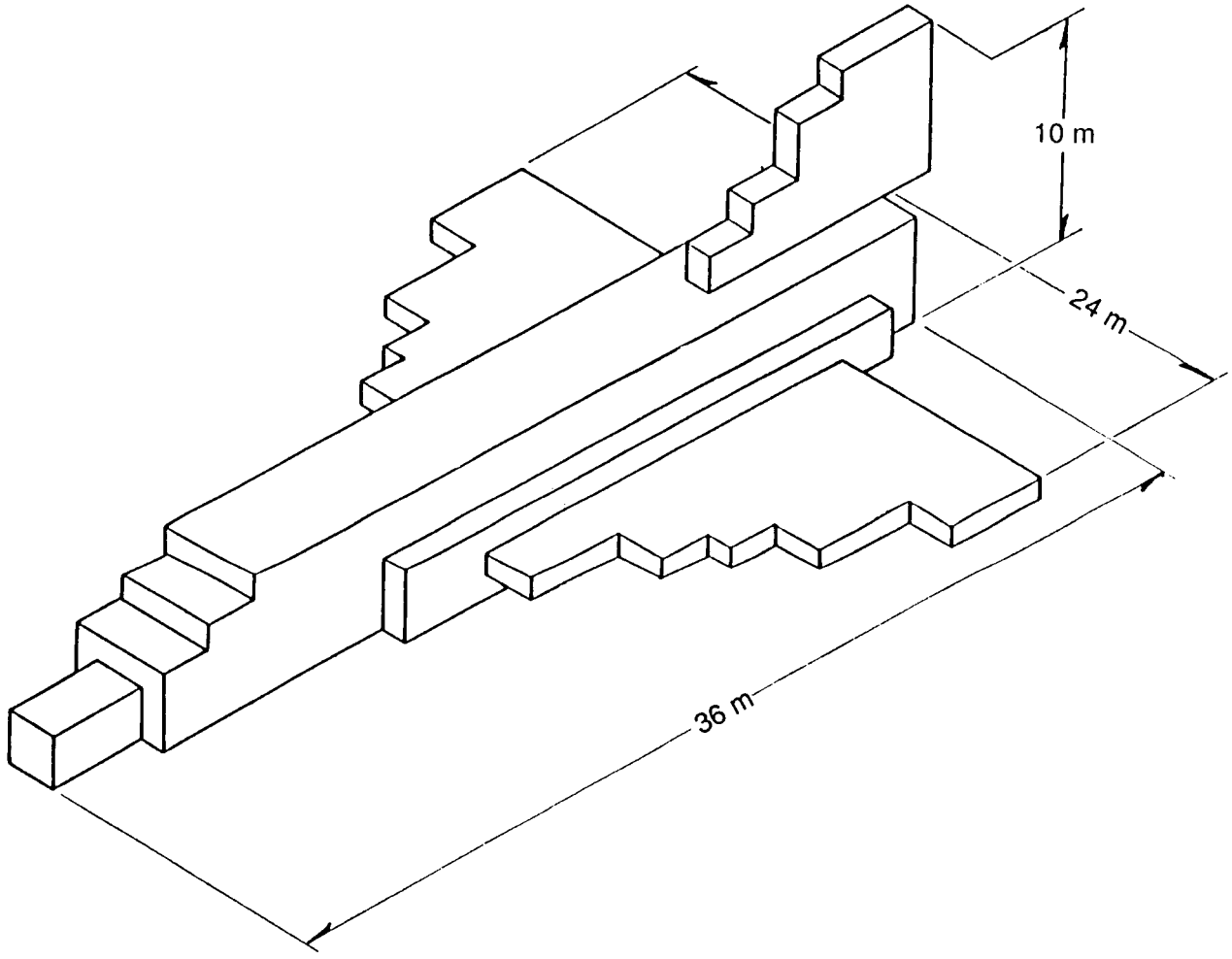

(b) Double-size F-106.

Figure 21. Continued.

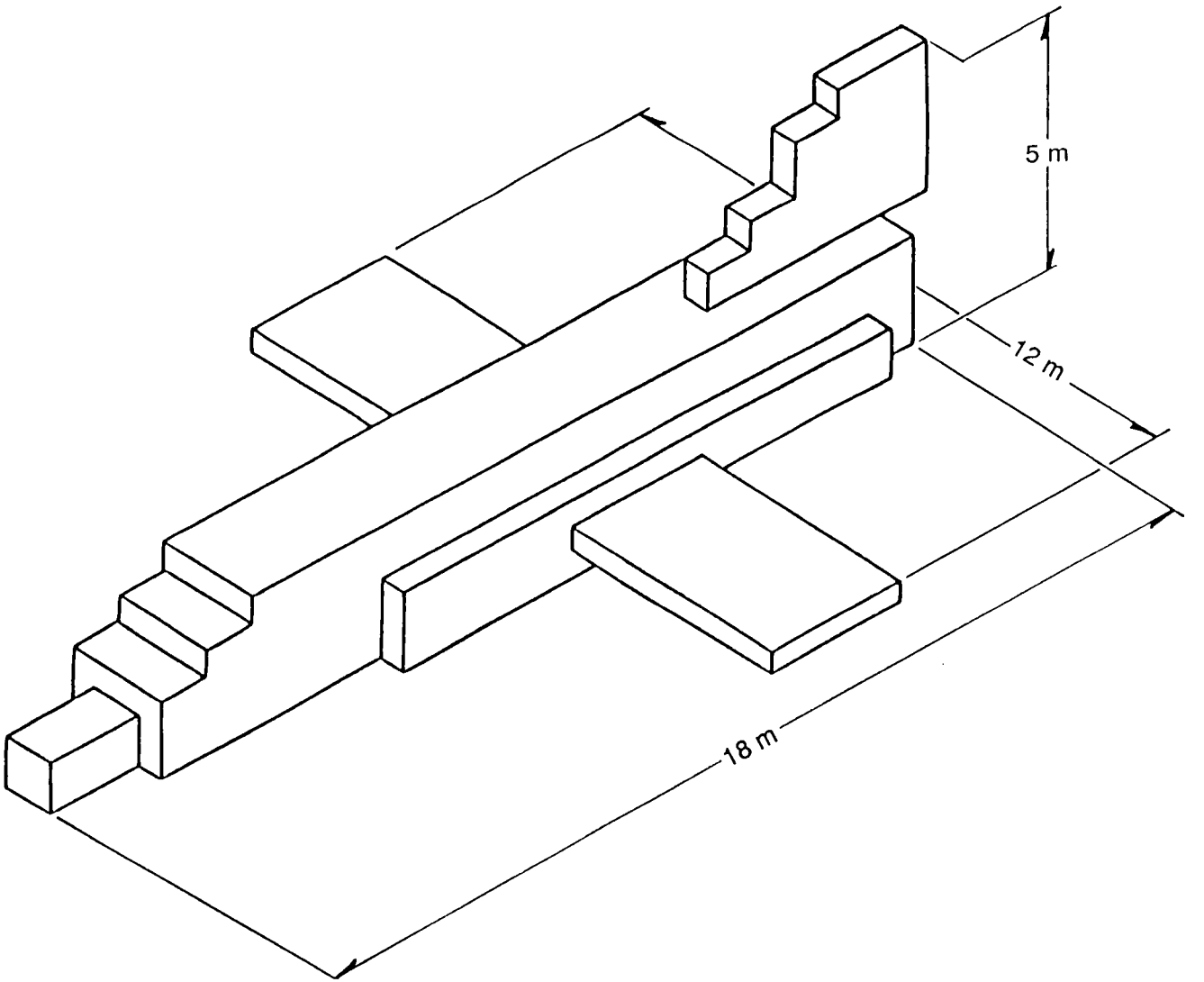

(c) Normal-size F-106 with conventional straight wings.

Figure 21. Continued.

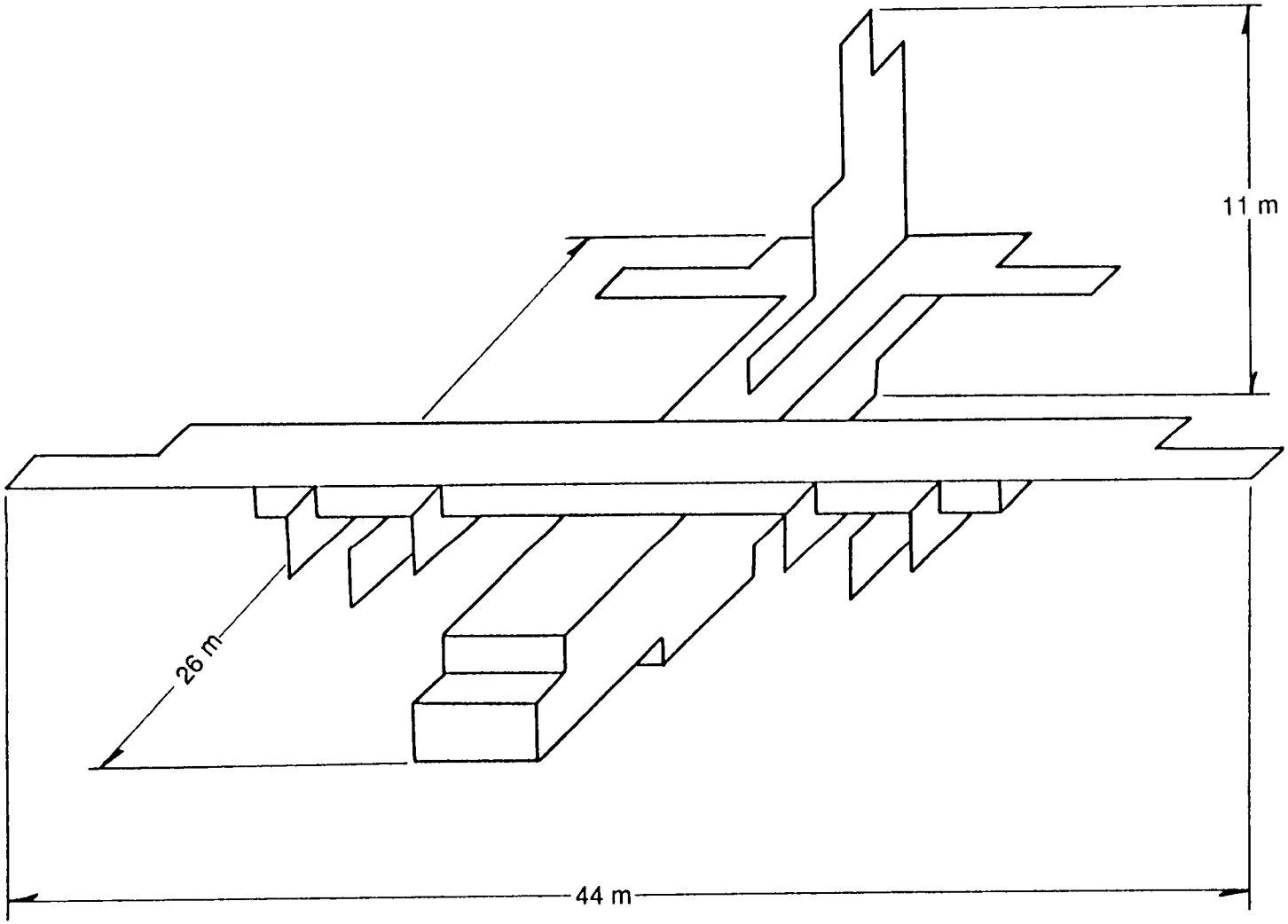

(d) Normal-size C-130.

Figure 21. Continued.

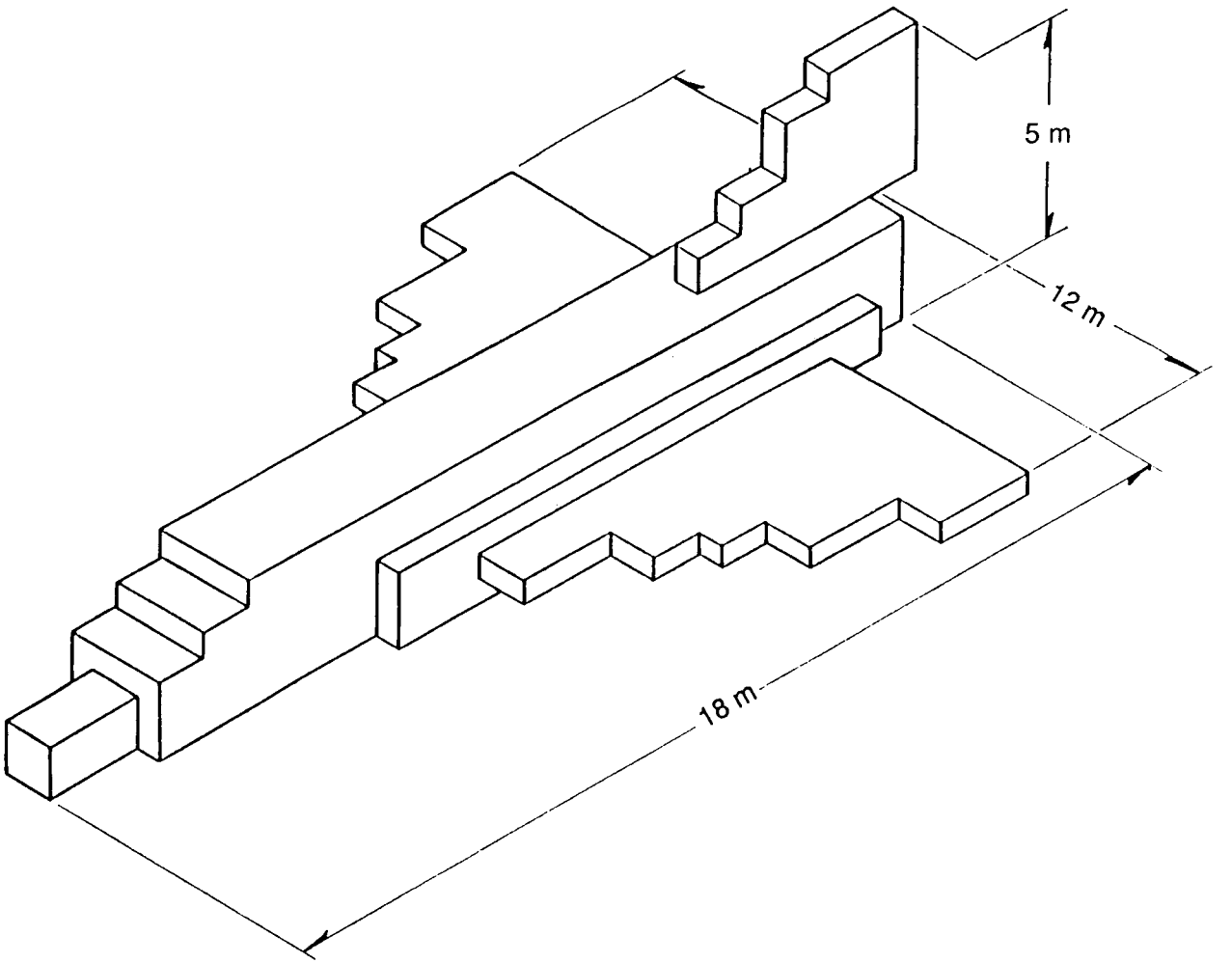

(e) Normal-size F-106.

Figure 21. Concluded.

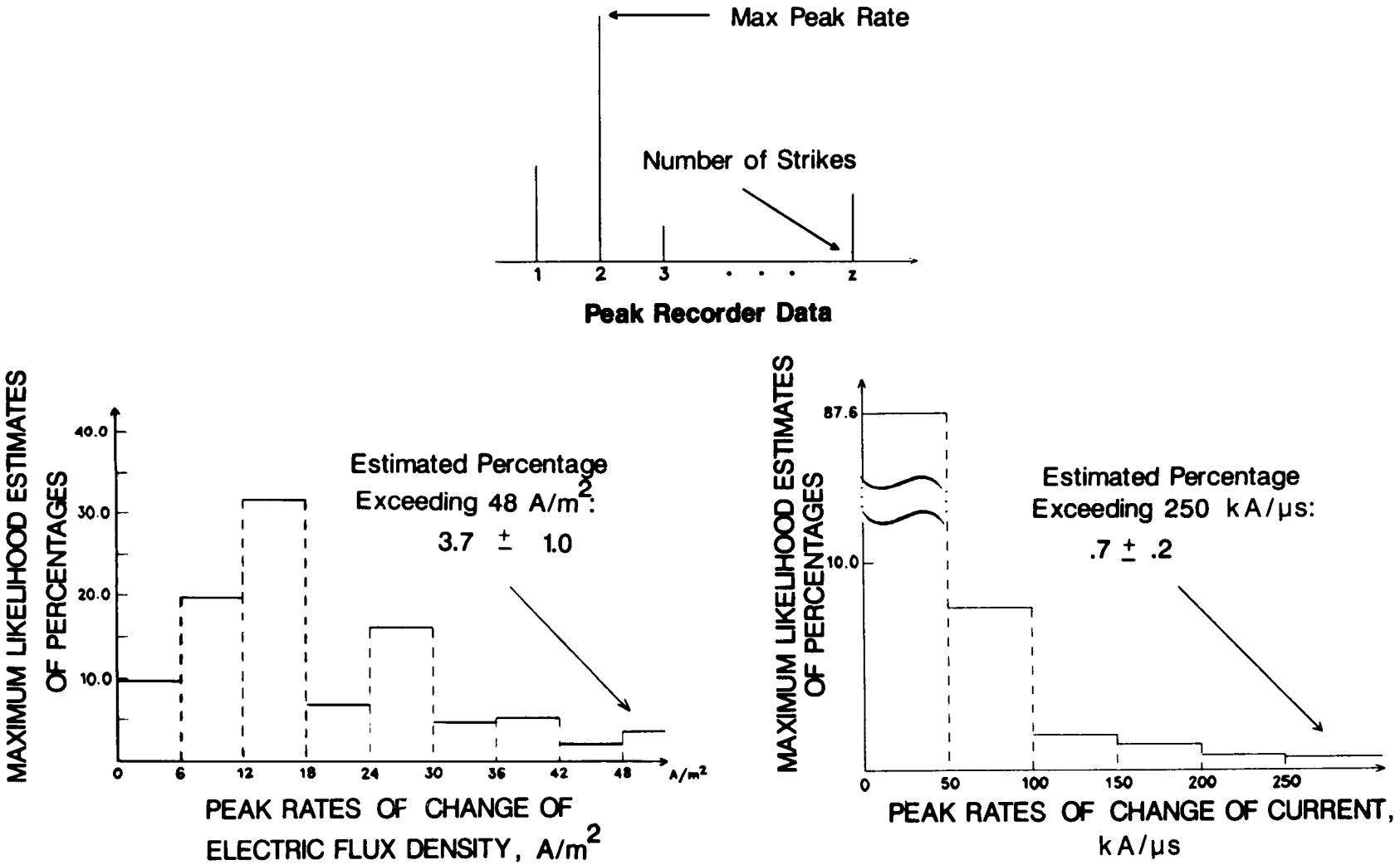

Figure 22. Distributions of peak D-dot and I-dot.

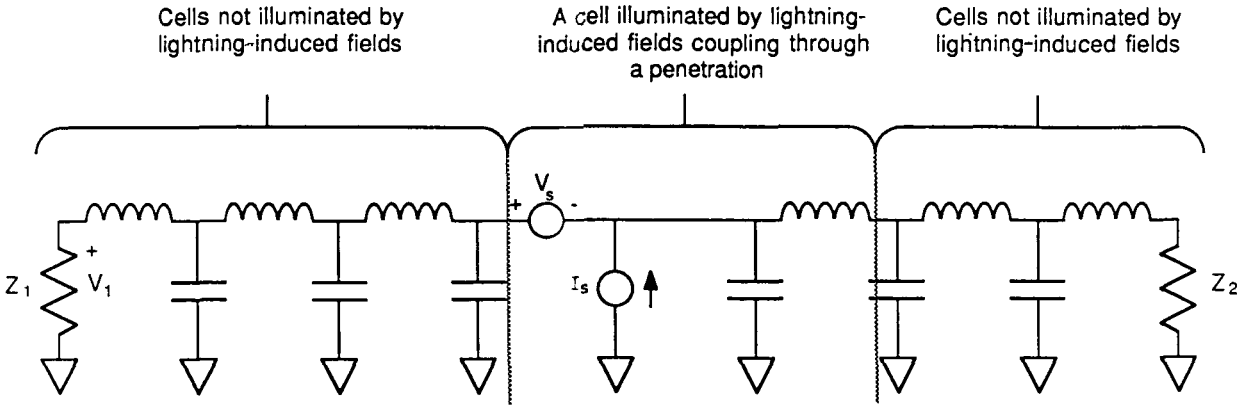

Lumped parameter model of a transmission line with characteristic impedance Z_0. Each cell exposed to lightning-induced fields has a voltage source V_s and a current source I_s. The sources are dependent upon the lightning environment as shown below for various penetrations.

	Source Relationship to Lightning Environment	
Penetration Type	V_s Proportional to	I_s Proportional to
Open hole aperture	B-dot (I-dot)	D-dot (I)
Resistive seam aperture	B (I)	negligible
Inductive seam aperture	B-dot (I-dot)	negligible
Diffusion through CFC	Z_t B (I)	negligible
Exposed conductor - Direct attachment	negligible	I
Exposed conductor - Lightning strikes aircraft nearby	B-dot (I-dot)	D-dot (I)

Figure 23. Transmission line model of lightning coupling to cable.

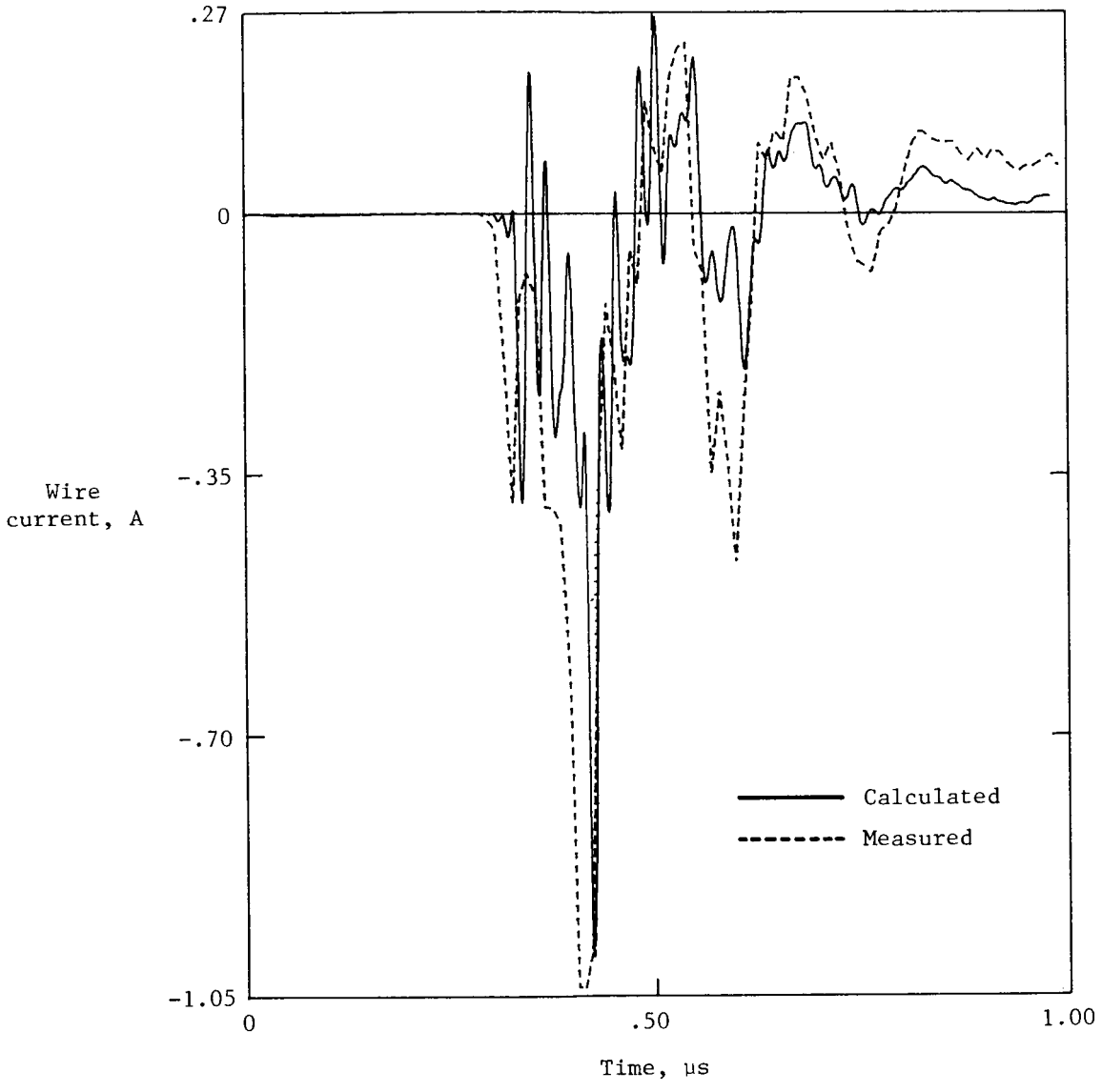

Figure 24. Comparison of calculated and measured current in internal wire.

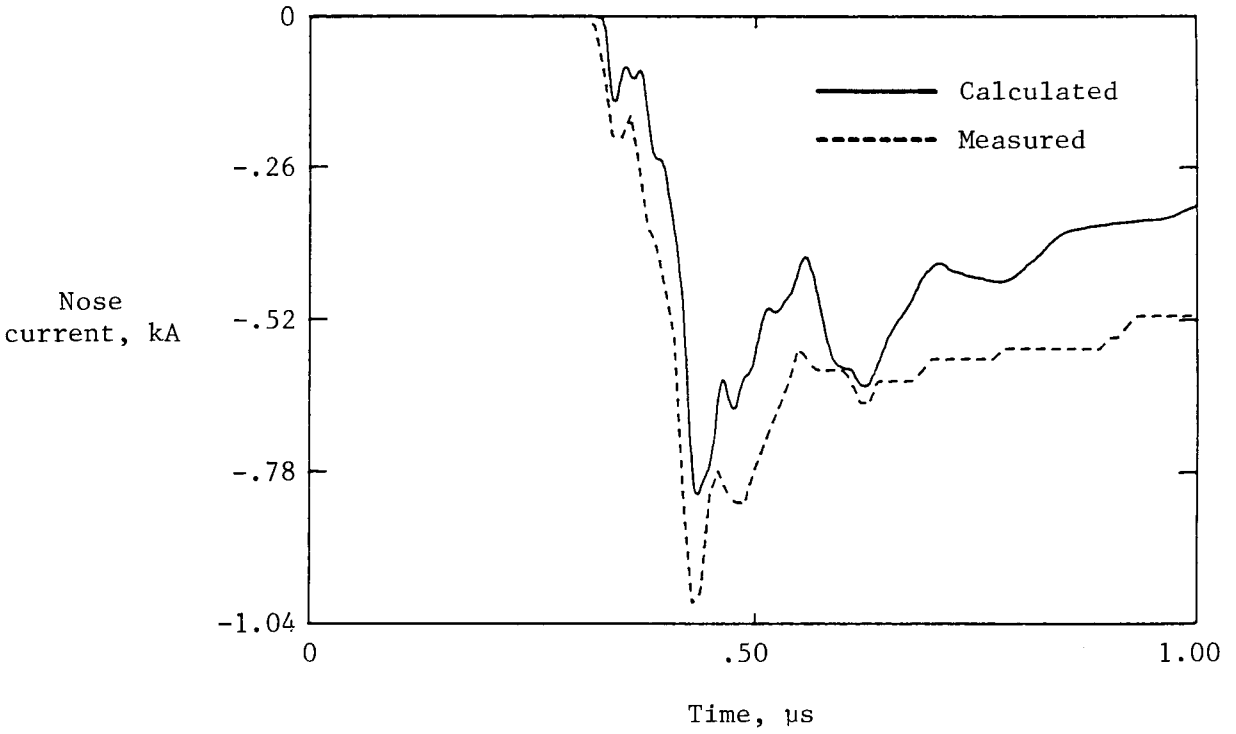

Figure 25. Concurrent calculated and measured nose boom current for internal wire response of figure 24.

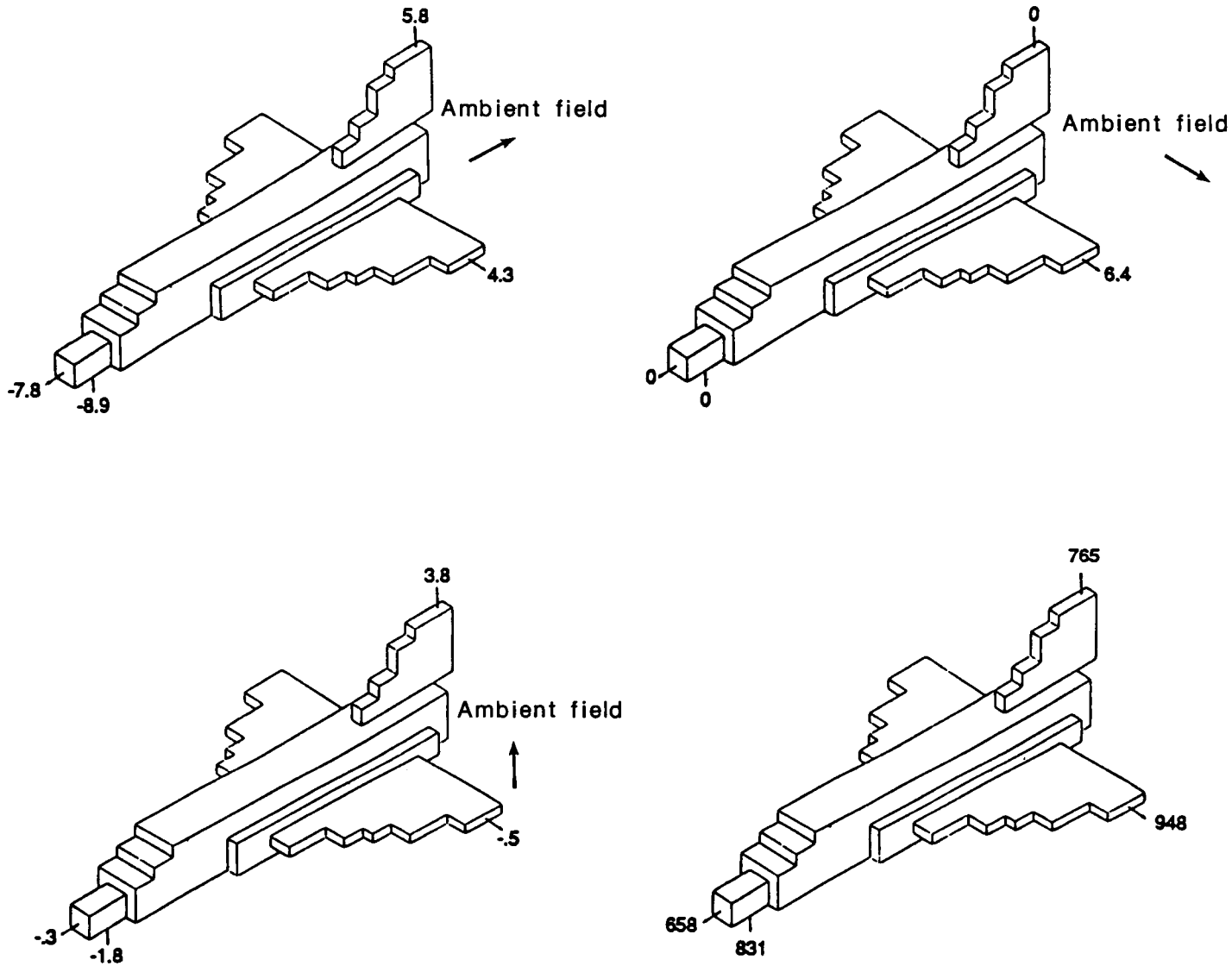

Figure 26. Calculated electric field enhancement factors for three field directions and for 1 μC aircraft charge. Values given are in volts per meter.

NASA
National Aeronautics and Space Administration

Report Documentation Page

1. Report No.	2. Government Accession No.	3. Recipient's Catalog No.
NASA TP-2737		

4. Title and Subtitle	5. Report Date
New Methods and Results for Quantification of Lightning-Aircraft Electrodynamics	June 1987
	6. Performing Organization Code
7. Author(s)	8. Performing Organization Report No.
Felix L. Pitts, Larry D. Lee, Rodney A. Perala, and Terence H. Rudolph	L-16281
9. Performing Organization Name and Address	10. Work Unit No.
NASA Langley Research Center Hampton, VA 23665-5225	505-66-21-04
	11. Contract or Grant No.
12. Sponsoring Agency Name and Address	13. Type of Report and Period Covered
National Aeronautics and Space Administration Washington, DC 20546-0001	Technical Paper
	14. Sponsoring Agency Code

15. Supplementary Notes

Felix L. Pitts: Langley Research Center, Hampton, Virginia.
Larry D. Lee: Old Dominion University, Norfolk, Virginia.
Rodney A. Perala and Terence H. Rudolph: Electro Magnetic Applications, Inc., Lakewood, Colorado.

16. Abstract

The NASA F-106 has acquired considerable data on the rates of change of electromagnetic parameters on the aircraft surface during over 700 direct lightning strikes while penetrating thunderstorms at altitudes from 15 000 to 40 000 ft (4570 to 12 190 m). These in situ measurements have provided the basis for the first statistical quantification of the lightning electromagnetic threat to aircraft appropriate for determining indirect lightning effects on aircraft. These data are presently being used in updating previous lightning criteria and standards developed over the years from ground-based measurements. The proposed lightning standards will be the first which reflect actual aircraft responses measured at flight altitudes. Nonparametric maximum likelihood estimates of the distribution of the peak electromagnetic rates of change for consideration in the new standards are obtained based on peak recorder data for flights which have multiple strikes. The linear and nonlinear modeling techniques developed provide means to interpret and understand the direct-strike electromagnetic data acquired on the F-106. The reasonable results obtained with the models, compared with measured responses, provide increased confidence that the models may be credibly applied to other aircraft types and used in the prediction of internal coupling effects in the design of lightning protection for new aircraft.

17. Key Words (Suggested by Authors(s))	18. Distribution Statement
Lightning Lightning aircraft Lightning criteria Lightning interaction	Unclassified – Unlimited Subject Category 47

19. Security Classif.(of this report)	20. Security Classif.(of this page)	21. No. of Pages	22. Price
Unclassified	Unclassified	66	A04

For sale by the National Technical Information Service, Springfield, Virginia 22161-2171